Title: Precision experiments with phonons, photons and spins to test Lorentz Invariance and to Detect Dark Matter and High Frequency Gravitational Waves

Date: Aug 23, 2017 02:00 PM

URL: http://pirsa.org/17080030

Abstract:

Frequency and Quantum Metrology Research Group

THE UNIVERSITY OF WESTERN AUSTRALIA

eQus
ARC CENTRE OF EXCELLENCE FOR ENGINEERED QUANTUM SYSTEMS

- **Core membership**
- Michael Tobar
- Eugene Ivanov
- John McFerran
- Alexey Veryaskin
- Sascha Schediwy
- Maxim Goryachev
- Nikita Kostylev
- Jeremy Bourhill

- **Research students**
- Natalia Carvalho
- Akhter Hoissan
- David Gozzard
- Ben McAllister
- Graeme Flower
- Scott Hardie

Research Programs

Precision Measurement with frequency, time or phase.

1) Clocks, Oscillators, low noise detection

2) ACES Mission

3) Fundamental Physics Tests

ARC Centre of Excellence in Engineered Quantum Systems

1) Spins in solids (dressed states of photons and spins)

2) Opto-Mechanics -> Macroscopic Mass at the quantum limit

3) Low noise quantum limited readouts

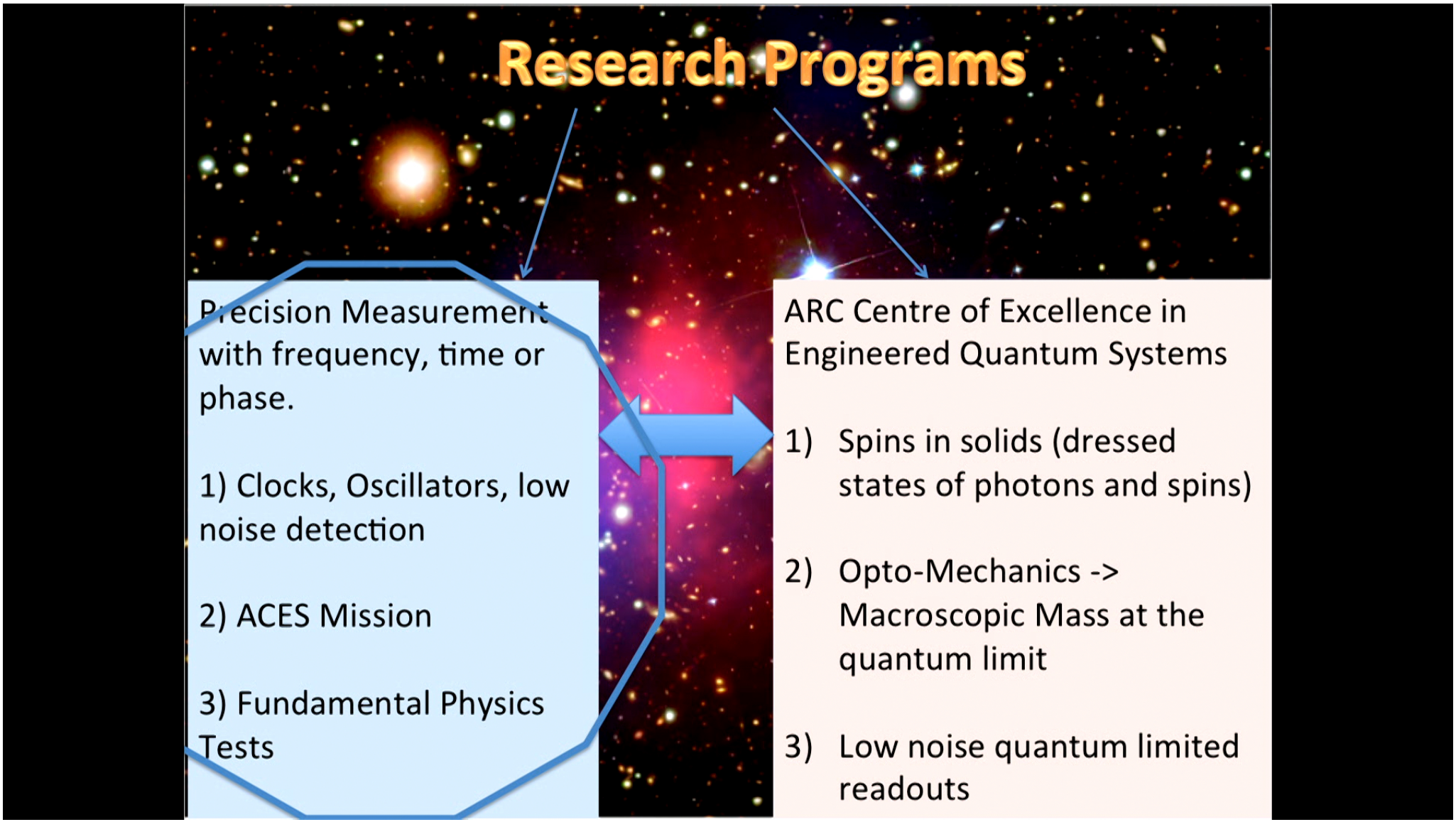
Research Programs
Precision Measurement with frequency, time or phase.
1) Clocks, Oscillators, low noise detection
2) ACES Mission
3) Fundamental Physics Tests
ARC Centre of Excellence in Engineered Quantum Systems
1) Spins in solids (dressed states of photons and spins)
2) Opto-Mechanics -> Macroscopic Mass at the quantum limit
3) Low noise quantum limited readouts

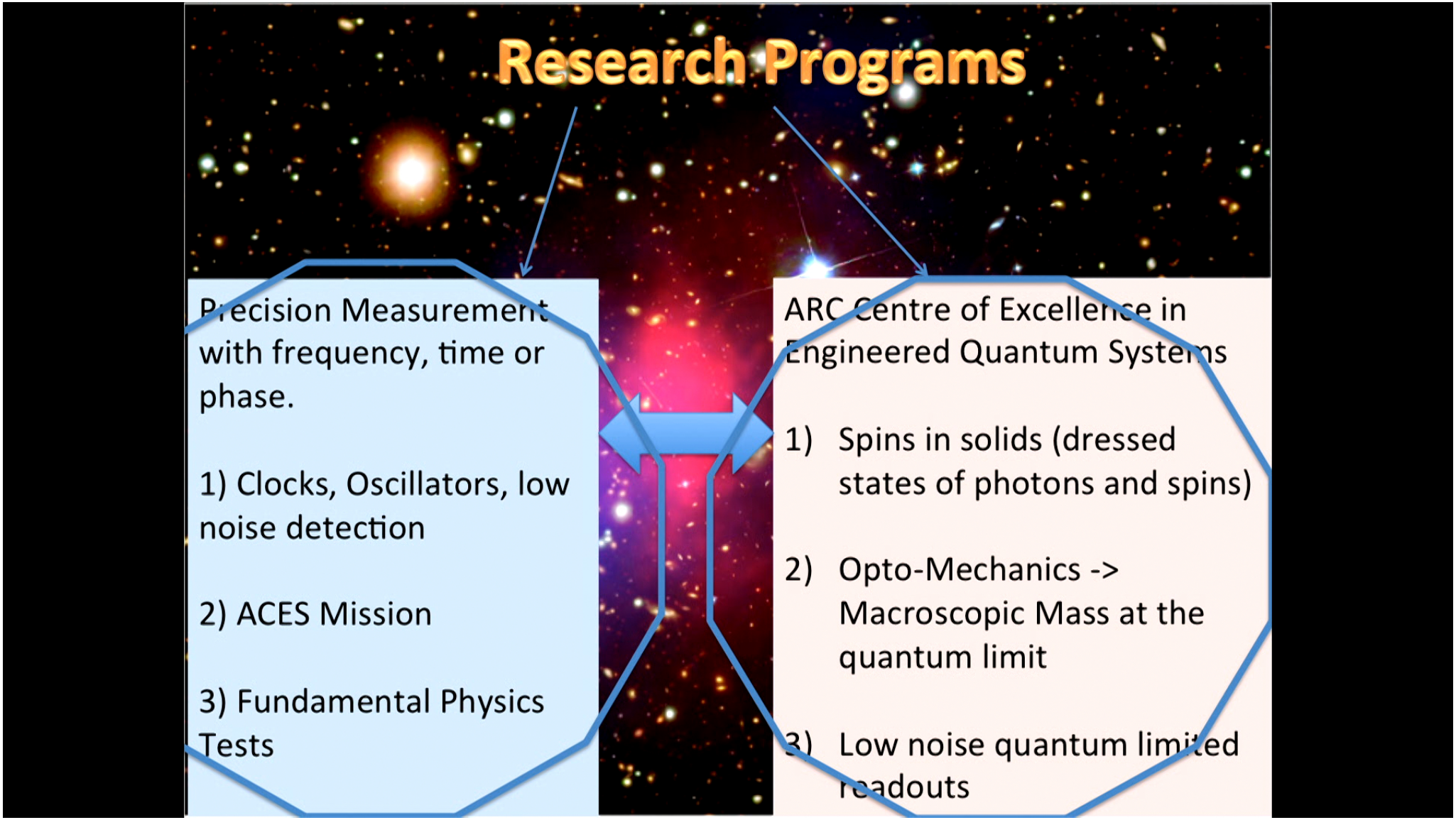
Research Programs
Precision Measurement with frequency, time or phase.
1) Clocks, Oscillators, low noise detection
2) ACES Mission
3) Fundamental Physics Tests
ARC Centre of Excellence in Engineered Quantum Systems
1) Spins in solids (dressed states of photons and spins)
2) Opto-Mechanics -> Macroscopic Mass at the quantum limit
3) Low noise quantum limited readouts

Current Projects in Time and Frequency and Fundamental Tests

- Key Technology
  - Yb Lattice Clock (ACES)
  - Cryogenic Sapphire Oscillator (CSO) -> 10^{-17}
  - Microwave Interferometry: Low Phase Noise Oscillators and Phase Detection
  - High-Q Cavities -> transducers -> Special designs -> Photon, Phonons, Spins (Hybrid systems)

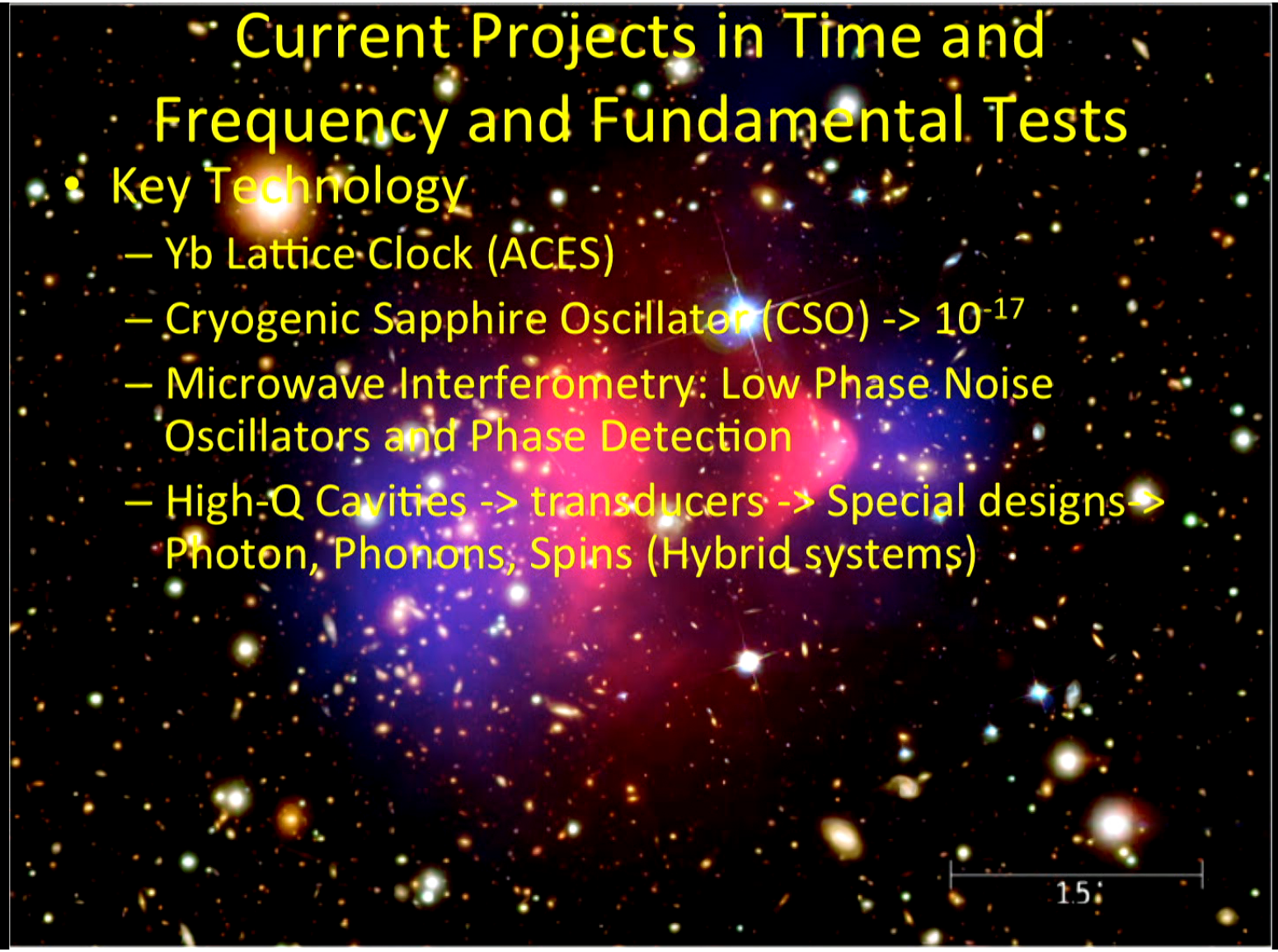

Current Projects in Time and Frequency and Fundamental Tests

- Key Technology
  - Yb Lattice Clock (ACES)
  - Cryogenic Sapphire Oscillator (CSO) -> 10^{-17}
  - Microwave Interferometry: Low Phase Noise Oscillators and Phase Detection
  - High-Q Cavities -> transducers -> Special designs -> Photon, Phonons, Spins (Hybrid systems)
- Test on Fundamental Physics
  - Lorentz Invariance (CSO, BAW, short range gravity)
  - Dark Sector Detection (Axion, Paraphoton)
  - Variation of Fundamental Constants
  - ACES laser ranging time transfer

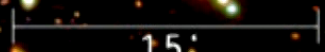

Precision experiments with phonons, photons and spins to test Lorentz Invariance and to Detect Dark Matter and High Frequency Gravitational Waves

1. Phonons
2. Photons
3. Spins (if time)

Cooling/Damping Massive Objects (phonons) to the Ground State (need high-Q)

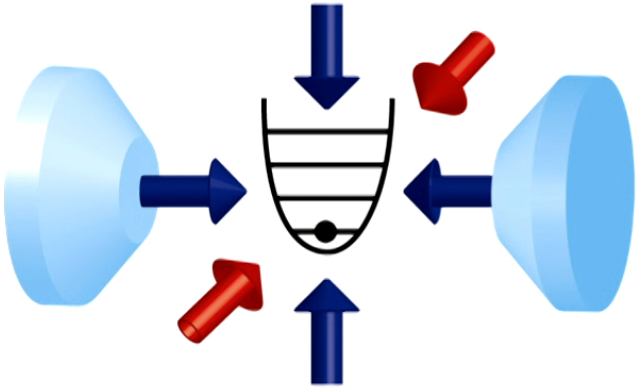

Cooling/Damping Massive Objects (phonons) to the Ground State (need high-Q)

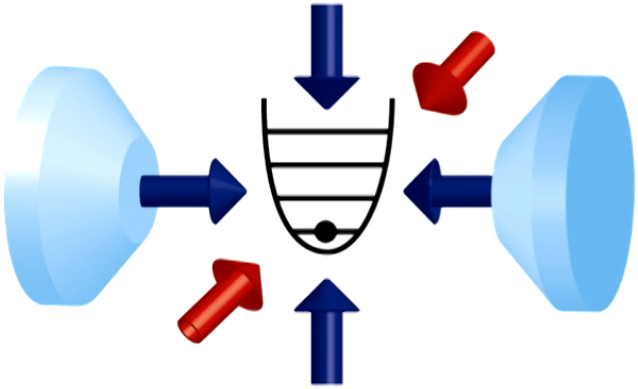

Cavities

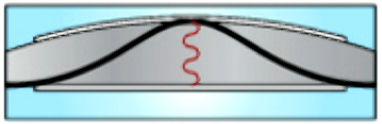

Quartz: Piezoelectric

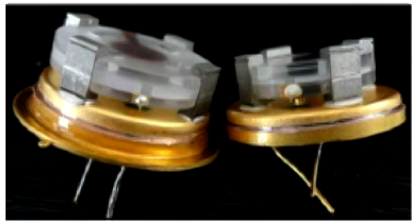

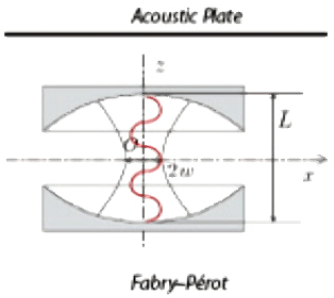

Fabry–Pérot

system with (quasi) unbounded dimention(s)

Cooling/Damping Massive Objects (phonons) to the Ground State (need high-Q)

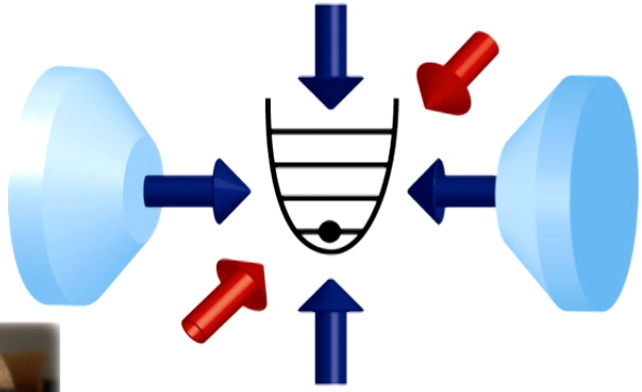

Sapphire: Parametric

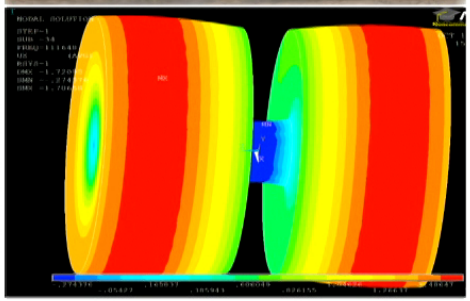

Cavities

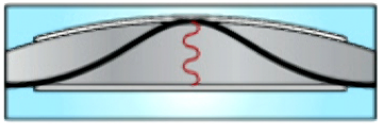

Quartz: Piezoelectric

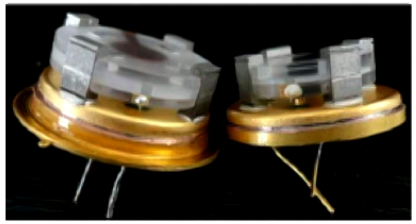

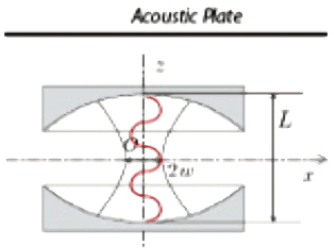

Fabry–Pérot

system with (quasi) unbounded dimention(s)

Quartz Phonon Trapping Technology

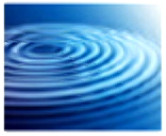

Tabletop experiment could detect gravitational waves

Oct 17, 2014 10 comments

Tiny device could beat LIGO to detecting ripples in space–time, say physicists

Acoustic analog of optical Fabry-Pérot:

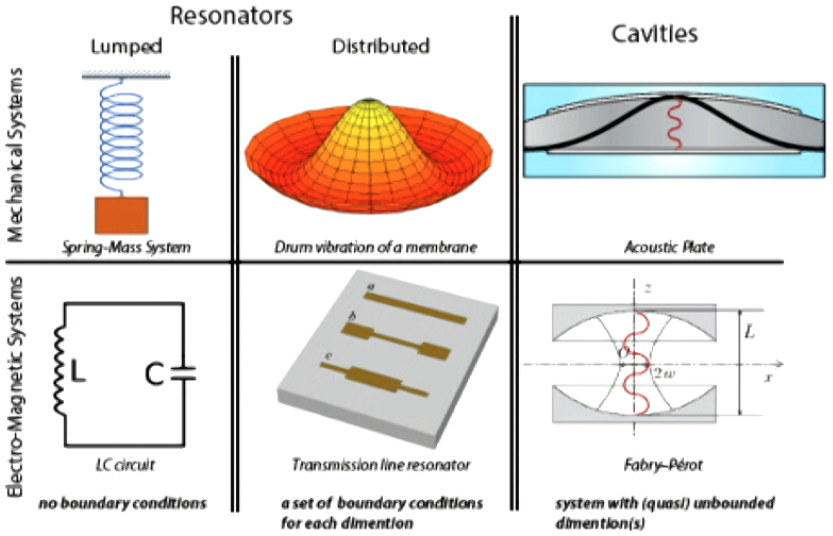

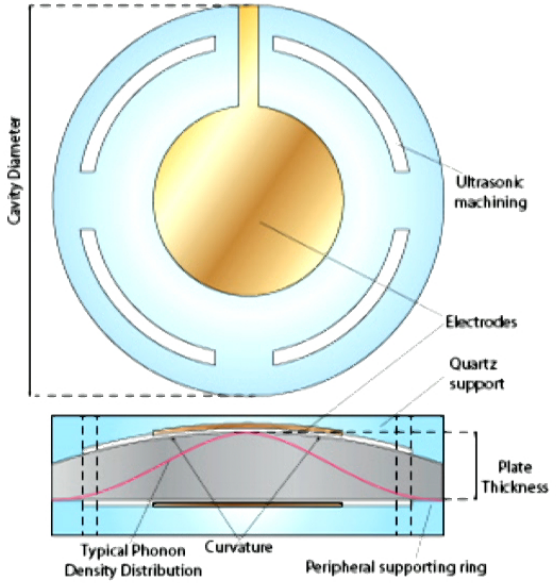

Features:

- phonon wavelengths $\sim 8 - 1000\ \mu$m ($f \to 1$ GHz),
- (quasi)-longitudinal and (quasi)-transverse polarizations,
- effective phonon trapping (BVA-technology),
- extremely long acoustic phonon life times ($Q \to 10^{10}$)...

Devices Under Test

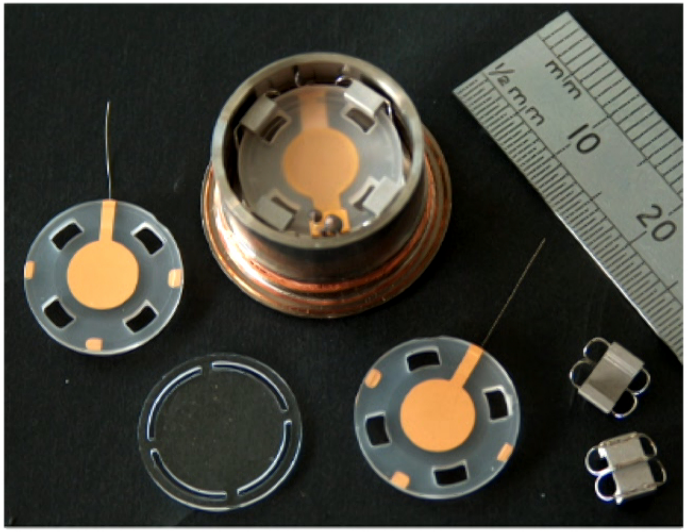

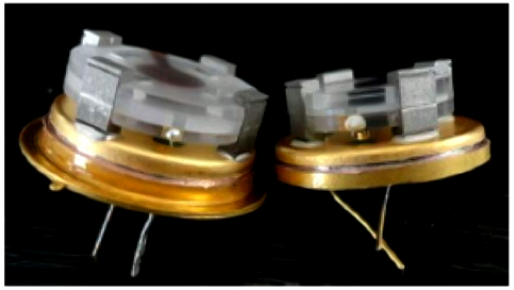

- Top High Quality α-quartz,
- BVA-technology,
- SC-cut,
- plano-covex...

Devices Under Test

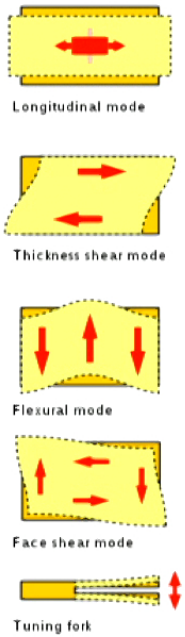

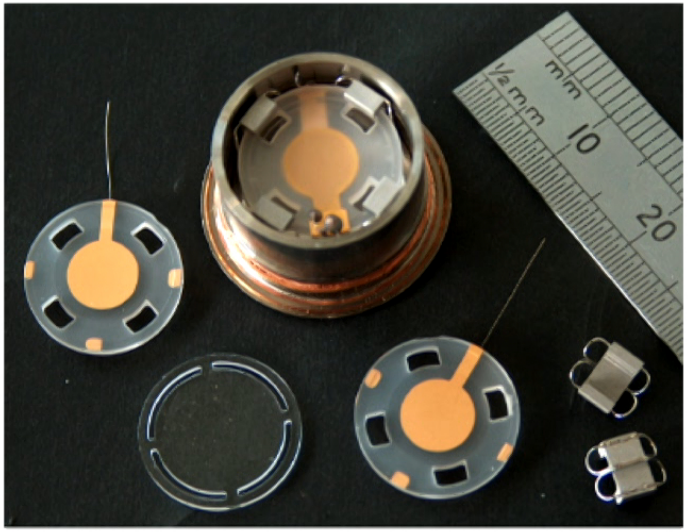

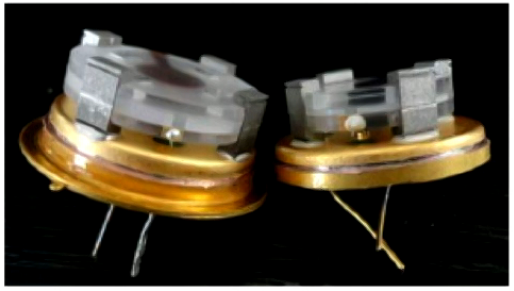

- Top High Quality α-quartz,
- BVA-technology,
- SC-cut,
- plano-covex...

Room temperature

A BAW quartz resonators optimized for the 5th overtone of the C-mode (slow shear) at $5-10$ MHz in the Akhiezer regime $(Q \times f = constant)$.

Cryogenic temperature

Acoustic cavity traps longitudinally polarised phonons (of up to 227th OT) in Landau-Rumer regime $(Q = constant)$.

Loss Mechanisms in Phonon-Trapping Acoustic Cavities[1,2,3]

APPLIED PHYSICS LETTERS **100**, 243504 (2012)

Extremely low-loss acoustic phonons in a quartz bulk acoustic wave resonator at millikelvin temperature

Maxim Goryachev,[1,2] Daniel L. Creedon,[1] Eugene N. Ivanov,[1] Serge Galliou,[2] Roger Bourquin,[2] and Michael E. Tobar[1,a)]
[1]*ARC Centre of Excellence for Engineered Quantum Systems, University of Western Australia, 35 Stirling Highway, Crawley WA 6009, Australia*
[2]*Department of Time and Frequency, FEMTO-ST Institute, ENSMM, 26 Chemin de l'Épitaphe, 25000, Besançon, France*

(Received 28 March 2012; accepted 27 May 2012; published online 13 June 2012)

Low-loss, high frequency acoustic resonators cooled to millikelvin temperatures are a topic of great interest for application to hybrid quantum systems. When cooled to 20 mK, we show that resonant acoustic phonon modes in a bulk acoustic wave quartz resonator demonstrate exceptionally low loss (with Q-factors of order billions) at frequencies of 15.6 and 65.4 MHz, with a maximum $f \cdot Q$ product of 7.8×10^{16} Hz. Given this result, we show that the Q-factor in such devices near the quantum ground state can be four orders of magnitude better than previously attained. Such resonators possess the low losses crucial for electromagnetic cooling to the phonon ground state, and the possibility of long coherence and interaction times of a few seconds, allowing multiple quantum gate operations. © *2012 American Institute of Physics*. [http://dx.doi.org/10.1063/1.4729292]

Loss Mechanisms in Phonon-Trapping Acoustic Cavities[1,2,3]

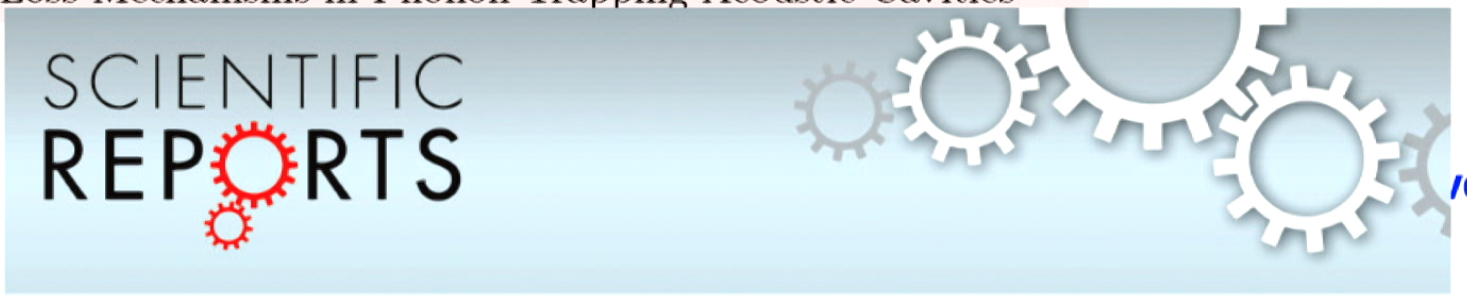

OPEN

SUBJECT AREAS:
APPLIED PHYSICS
OPTOMECHANICS
SENSORS AND BIOSENSORS
MECHANICAL PROPERTIES

Received
16 April 2013

Accepted
12 June 2013

Published
4 July 2013

Extremely Low Loss Phonon-Trapping Cryogenic Acoustic Cavities for Future Physical Experiments

Serge Galliou[1], Maxim Goryachev[2], Roger Bourquin[1], Philippe Abbé[1], Jean Pierre Aubry[3] & Michael E. Tobar[2]

[1]Department of Time and Frequency, FEMTO-ST Institute, ENSMM, 26 Chemin de l'Épitaphe, 25000, Besançon, France, [2]ARC Centre of Excellence for Engineered Quantum Systems, University of Western Australia, 35 Stirling Highway, Crawley WA 6009, Australia, [3]Oscilloquartz SA, Brévards 16, 2002 Neuchâtel, Switzerland.

Correspondence and

Low loss Bulk Acoustic Wave devices are considered from the point of view of the solid state approach as phonon-confining cavities. We demonstrate effective design of such acoustic cavities with phonon-trapping techniques exhibiting extremely high quality factors for trapped longitudinally polarized phonons of various wavelengths. Quality factors of observed modes exceed 1 billion, with a maximum Q-factor of 8 billion and $Q \times f$ product of $1.6 \cdot 10^{18}$ at liquid helium temperatures. Such high sensitivities allow analysis of intrinsic material losses in resonant phonon systems. Various mechanisms of phonon losses are discussed and estimated.

Observation of Phonon-Phonon Losses

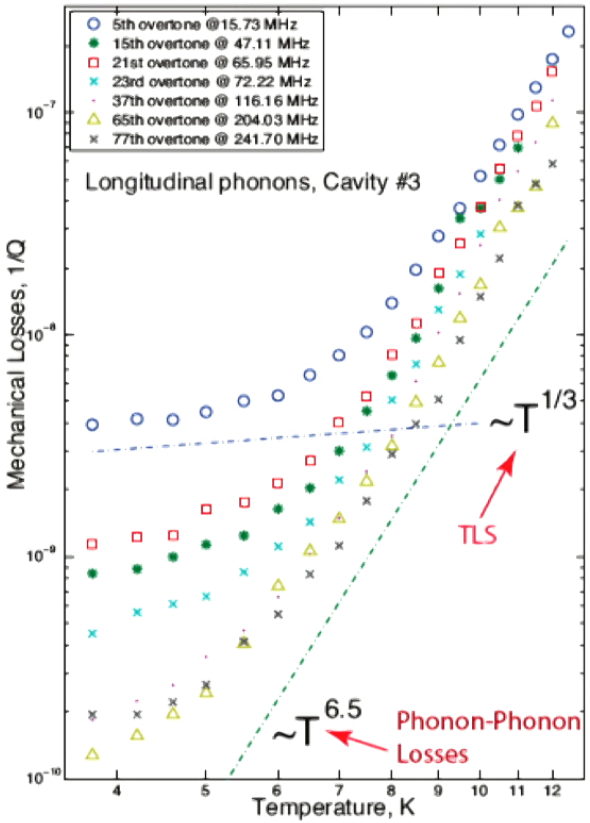

Observation of Raleigh Scattering

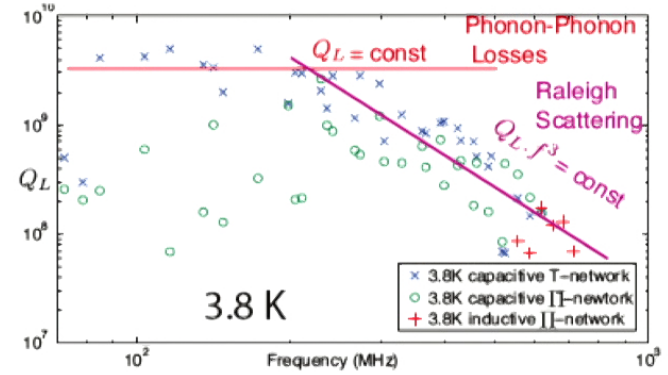

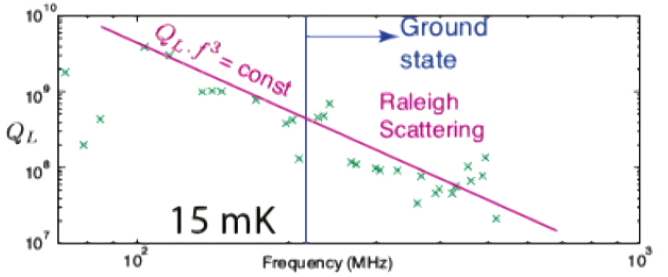

APPLIED PHYSICS LETTERS **105**, 153505 (2014)

Observation of the fundamental Nyquist noise limit in an ultra-high *Q*-factor cryogenic bulk acoustic wave cavity

Maxim Goryachev,[1,a)] Eugene N. Ivanov,[1] Frank van Kann,[2] Serge Galliou,[3] and Michael E. Tobar[1]

[1]*ARC Centre of Excellence for Engineered Quantum Systems, University of Western Australia, 35 Stirling Highway, Crawley, WA 6009, Australia*

[2]*School of Physics, University of Western Australia, 35 Stirling Highway, Crawley, WA 6009, Australia*

[3]*Department of Time and Frequency, FEMTO-ST Institute, ENSMM, 26 Chemin de l'Épitaphe, 25000 Besançon, France*

(Received 22 August 2014; accepted 9 October 2014; published online 17 October 2014)

Thermal Nyquist noise fluctuations of high-Q bulk acoustic wave cavities have been observed at cryogenic temperatures with a DC superconducting quantum interference device amplifier. High Q modes with bandwidths of few tens of milliHz produce thermal fluctuations with a signal-to-noise ratio of up to 23 dB. The estimated effective temperature from the Nyquist noise is in good agreement with the physical temperature of the device, confirming the validity of the equivalent circuit model and the non-existence of any excess resonator self-noise. The measurements also confirm that the quality factor remains extremely high ($Q > 10^8$ at low order overtones) for very weak (thermal) system motion at low temperatures, when compared to values measured with relatively strong external excitation. This result represents an enabling step towards operating such a high-Q acoustic device at the standard quantum limit.

[http://dx.doi.org/10.1063/1.4898813]

Resonator with Squid Output

Resonator with Squid Output

DC SQUID in a copper holder to be attached to the “cold finger” of the pulse-tube cryocooler

Resonator with Squid Output

DC SQUID in a copper holder to be attached to the “cold finger” of the pulse-tube cryocooler

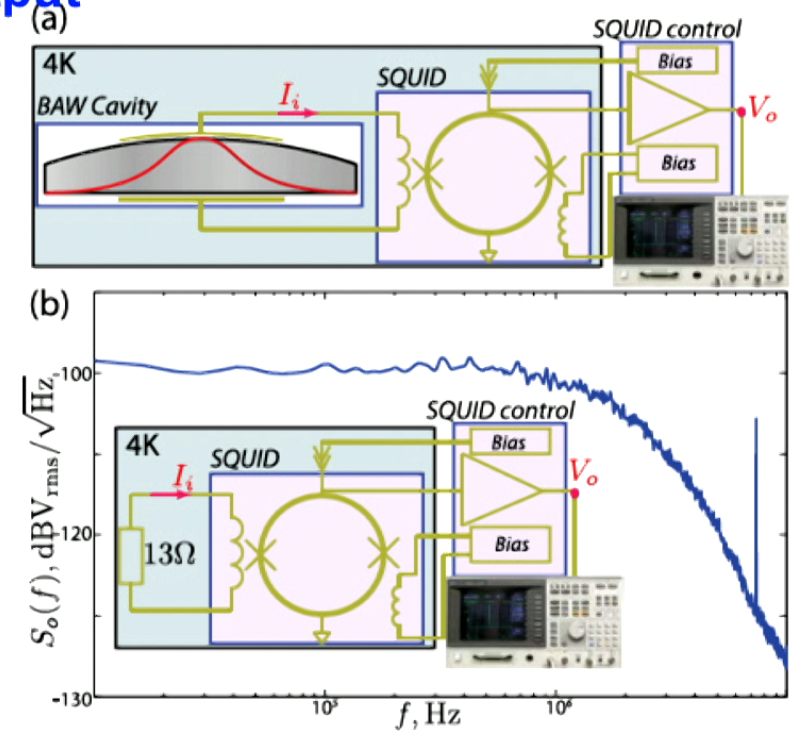

FIG. 1. (a) BAW thermal noise measurement setup for frequencies below 10 MHz. The curvature of one of the plate faces is employed to achieve the phonon trapping with the acoustic energy distribution along the plate denoted by the red curve. (b) Resistive load measurements for system calibration.

Calculate Mode Temperature

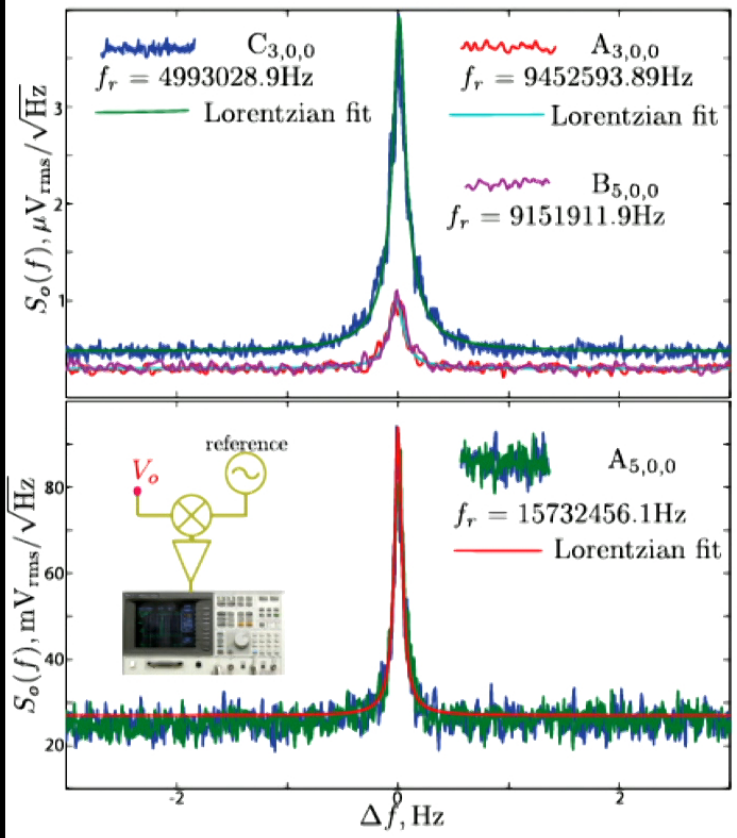

FIG. 2. Results of noise measurements for $C_{3,0,0}$, $A_{3,0,0}$, $B_{5,0,0}$, and $A_{5,0,0}$. The latter is measured using the downconversion as shown in the inset.

(i) Measurements of the SQUID voltage noise
(ii) Estimation of the RMS current through resonator (known SQUID impedance from calibration)
(iii) Calculation of power dissipated in resonator for evaluation of mode temperature.

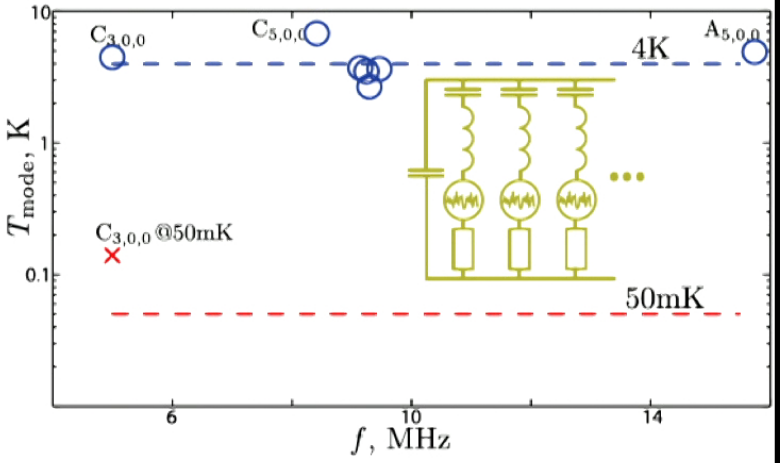

FIG. 3. Estimations of the mode temperatures compared to the ambient values. The inset shows the equivalent circuit model.

Tunable Microstrip SQUID Amplifier (MSA)

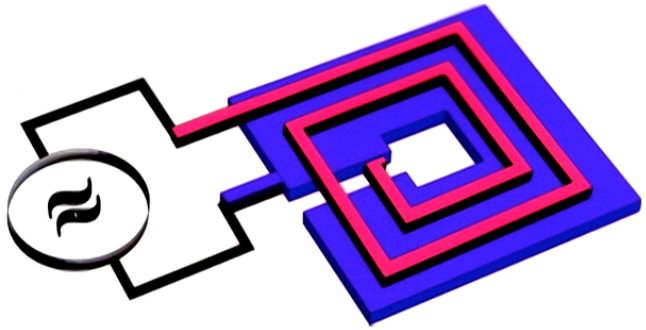

Tunable Microstrip SQUID Amplifier (MSA)

Maxim Goryachev -> John Clarke Lab Berkeley (Sean O'Kelley)

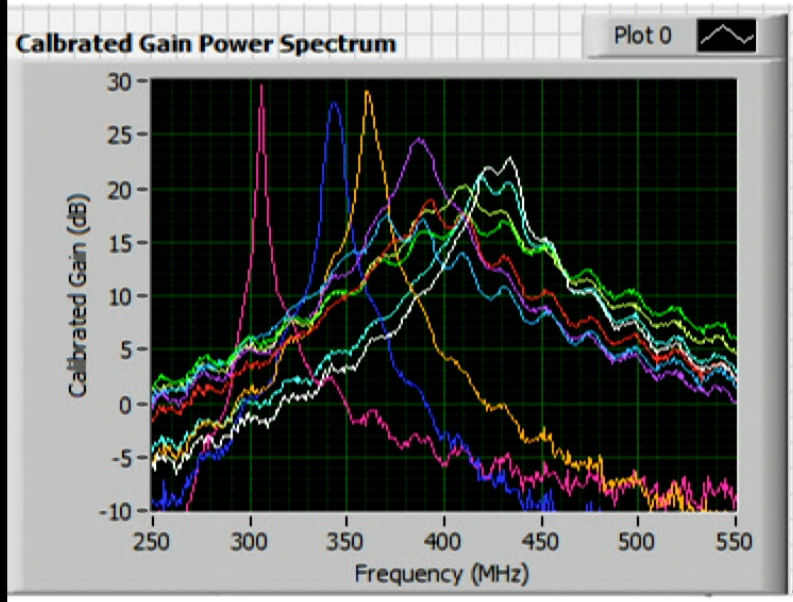

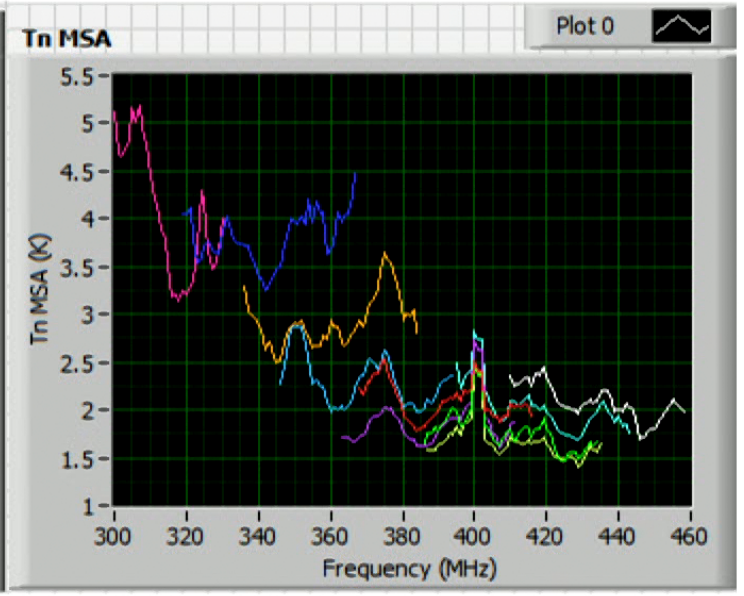

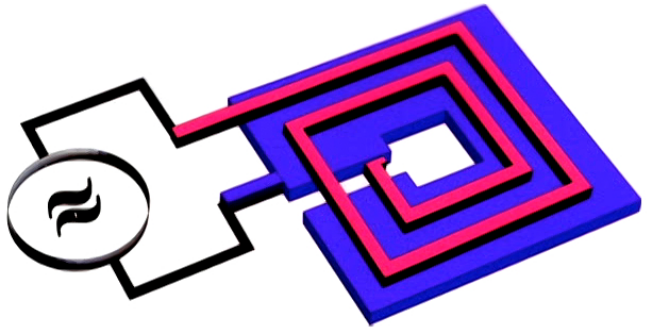

Tunable Microstrip SQUID Amplifier (MSA)

Maxim Goryachev -> John Clarke Lab Berkeley (Sean O'Kelley)

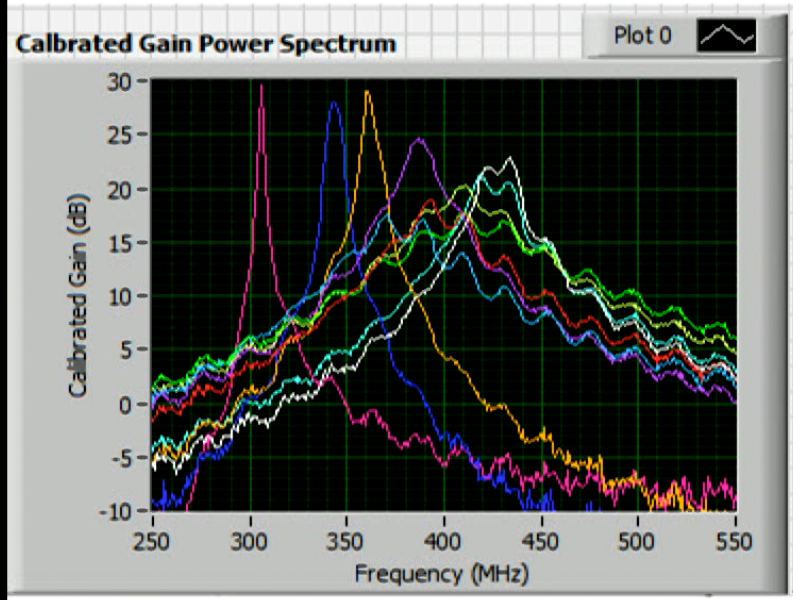

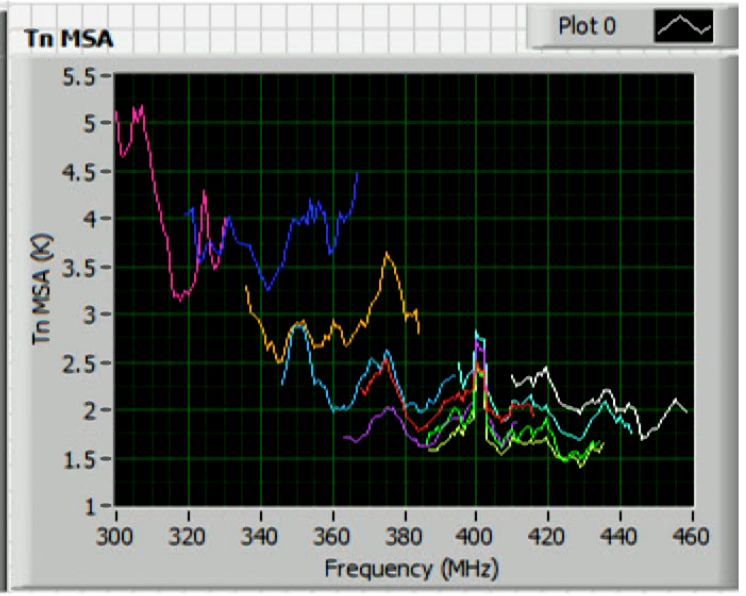

ADMX Amplifiers -> Near Quantum limited

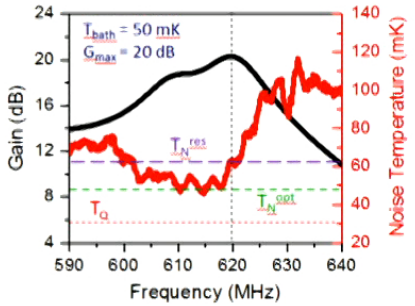

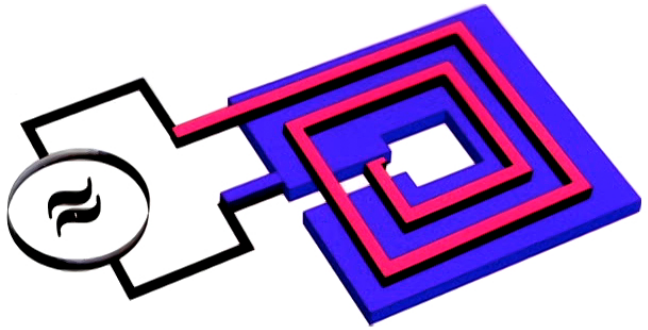

MSA Noise Temperature in Prior Device

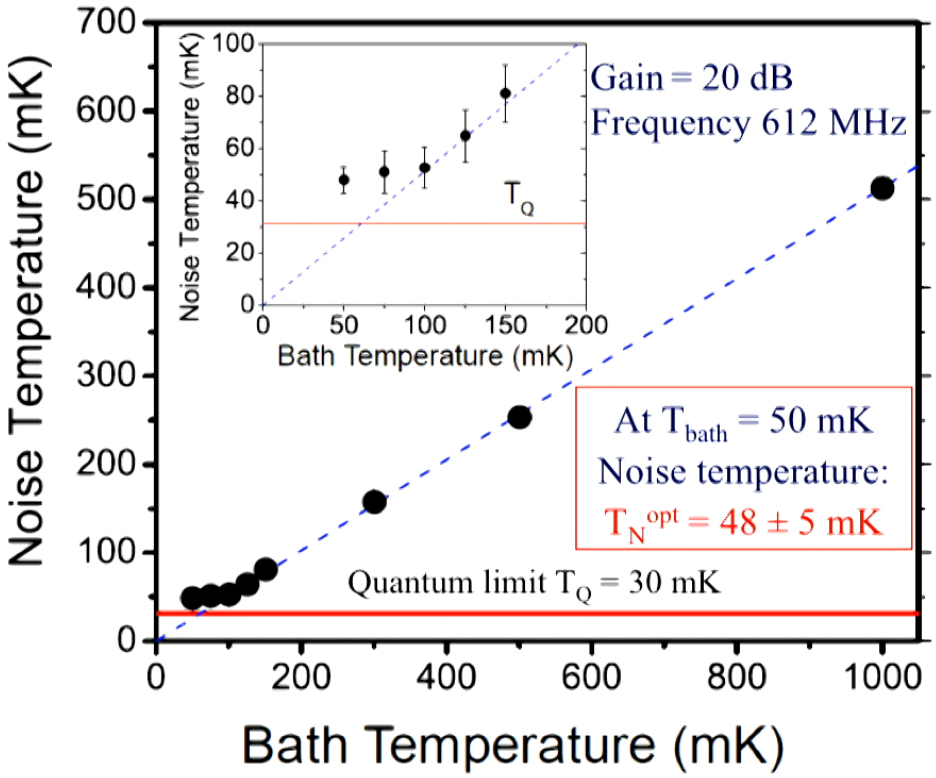

Noise temperatures of 48 ± 5 mK have been demonstrated at 612 MHz, within 1.7 times the quantum limit

$T_Q = hf/k_B$
(about 48mK per GHz)

Measured at UWA at 20 mK

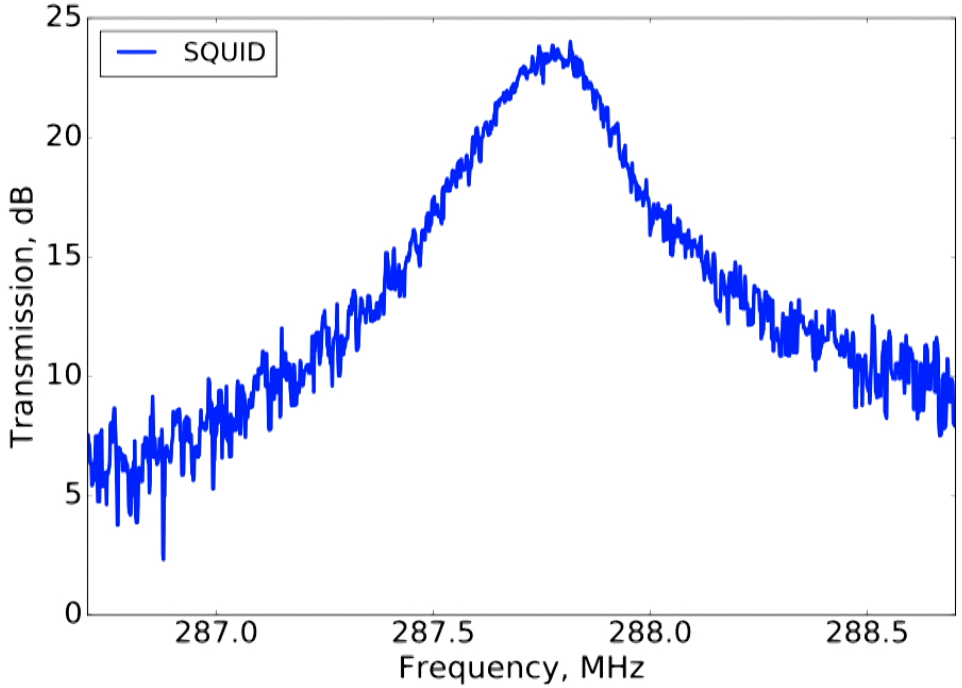

- Most of our resonators are identical 5MHz SC cut. -> do not have good modes around 300MHz where the mode density is sparse.
- 5MHz AT cut crystal (we have only one) has a good mode around this frequency, to be measured soon (varactor?), close to Ground State.

Application of high-Q devices in Physics

Applications of High-Q systems:

- quantum measurement and computation,
- single-spin detection,
- ultra-sensitive force and mass detection,
- gravity wave detection,
- and other fundsmental phenomena.

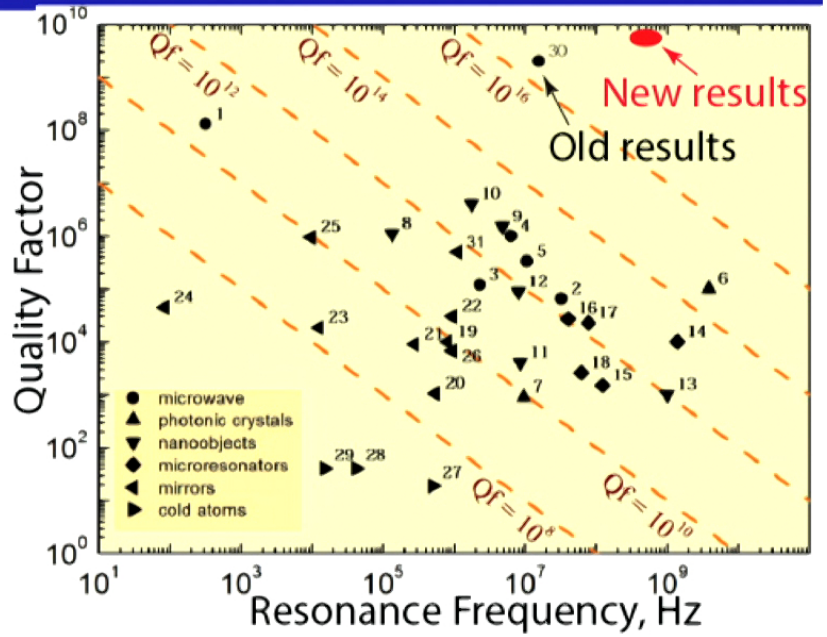

Cavity Optomechanics

Markus Aspelmeyer*
Vienna Center for Quantum Science and Technology (VCQ), Faculty of Physics, University of Vienna, 1090 Vienna Austria
Tobias J. Kippenberg†
Ecole Polytechnique Fédérale de Lausanne (EPFL), 1015 Lausanne, Switzerland
Florian Marquardt‡
University of Erlangen-Nürnberg, Institute for Theoretical Physics, Staudtstr. 7, 91058 Erlangen, Germany;

arXiv:1303.0733

BAW with Microwaves

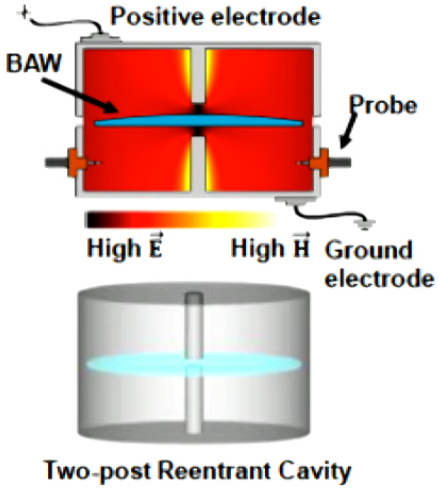

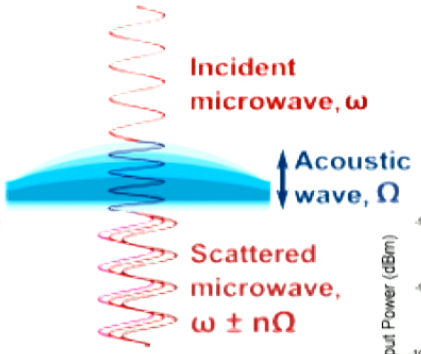

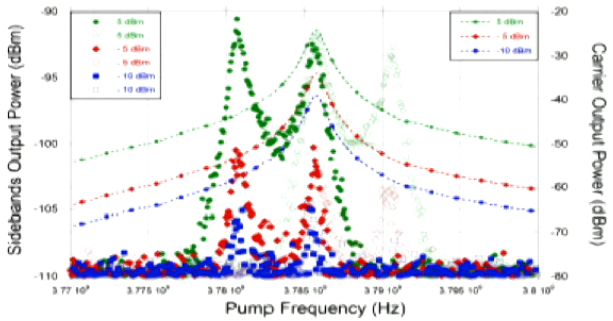

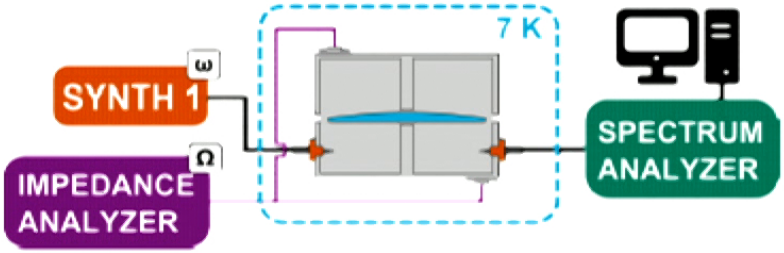

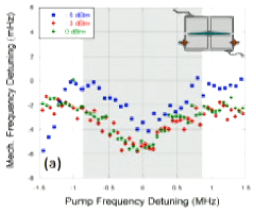

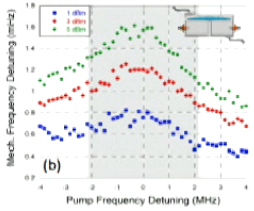

System is a sensitive GW Detector

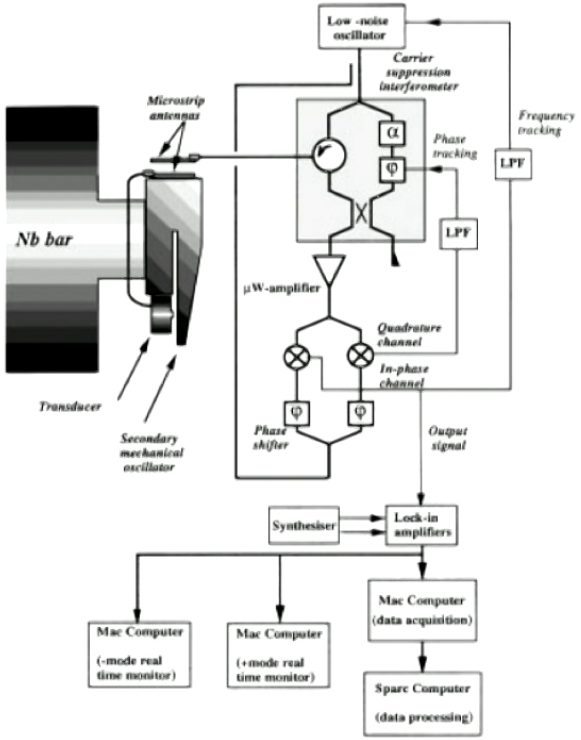

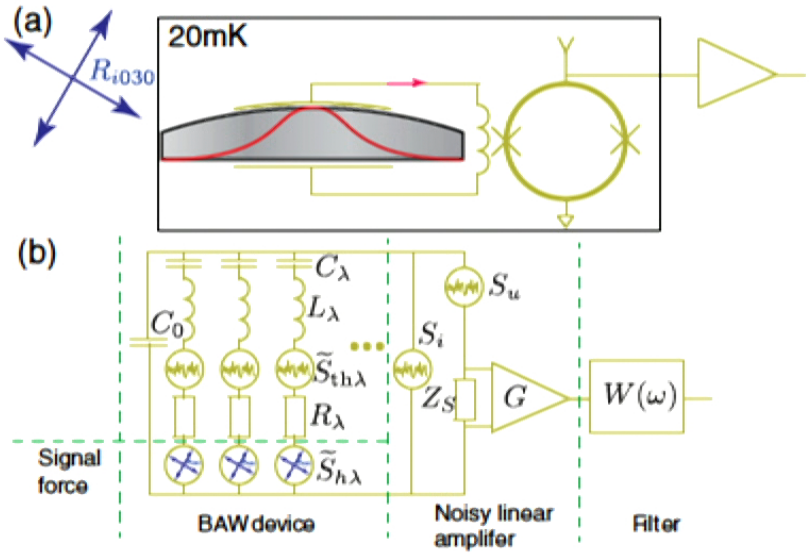

System is a sensitive GW Detector (PRD)

PHYSICAL REVIEW D **90,** 102005 (2014)

Gravitational wave detection with high frequency phonon trapping acoustic cavities

Maxim Goryachev and Michael E. Tobar*

ARC Centre of Excellence for Engineered Quantum Systems, School of Physics, University of Western Australia, 35 Stirling Highway, Crawley, Western Australia 6009, Australia

(Received 25 September 2014; published 24 November 2014)

There are a number of theoretical predictions for astrophysical and cosmological objects, which emit high frequency ($10^6 - 10^9$ Hz) gravitation waves (GW) or contribute somehow to the stochastic high frequency GW background. Here we propose a new sensitive detector in this frequency band, which is based on existing cryogenic ultrahigh quality factor quartz bulk acoustic wave cavity technology, coupled to near-quantum-limited SQUID amplifiers at 20 mK. We show that spectral strain sensitivities reaching 10^{-22} per $\sqrt{\text{Hz}}$ per mode is possible, which in principle can cover the frequency range with multiple (>100) modes with quality factors varying between 10^6 and 10^{10} allowing wide bandwidth detection. Due to its compactness and well-established manufacturing process, the system is easily scalable into arrays and distributed networks that can also impact the overall sensitivity and introduce coincidence analysis to ensure no false detections.

DOI: 10.1103/PhysRevD.90.102005 PACS numbers: 04.80.Nn, 95.55.Ym

System is a sensitive GW Detector (PRD)

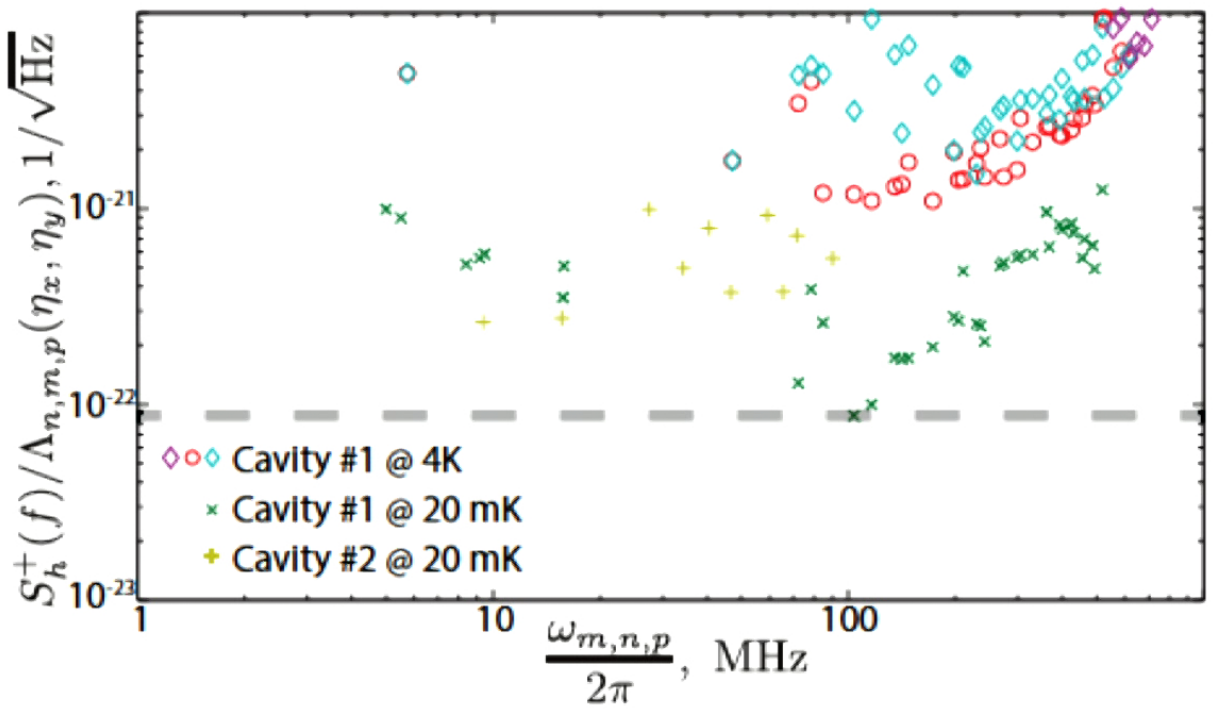

FIG. 5: Normalised the single sided power spectral density of the strain sensitivity for various OTs of the longitudinal mode of two acoustical cavities at 4K and 20mK.

- High frequency region has physically understood processes of generation of GWs
  - thermal gravitational radiation from stars
  - Radiation from low mass primordial black holes

- High frequency region has physically understood processes of generation of GWs
  - thermal gravitational radiation from stars
  - Radiation from low mass primordial black holes
  - gravitational modes of plasma flows
- Tests for many emerging theories predicting GW radiation at such frequencies.
  - stochastic sources in the early Universe
  - GW background from quintessential inflation
  - cosmic strings
  - Dilation
  - pre–big bang scenarios
  - Superinflation in loop quantum gravity
  - Postinflationary phase transitions

- High frequency region has physically understood processes of generation of GWs
  - thermal gravitational radiation from stars
  - Radiation from low mass primordial black holes
  - gravitational modes of plasma flows
- Tests for many emerging theories predicting GW radiation at such frequencies.
  - stochastic sources in the early Universe
  - GW background from quintessential inflation
  - cosmic strings
  - Dilation
  - pre–big bang scenarios
  - Superinflation in loop quantum gravity
  - Postinflationary phase transitions
  - parametric resonance at the end of inflation or preheating
  - braneworld black holes associated with extra dimensions

- High frequency region has physically understood processes of generation of GWs
  - thermal gravitational radiation from stars
  - Radiation from low mass primordial black holes
  - gravitational modes of plasma flows
- Tests for many emerging theories predicting GW radiation at such frequencies.
  - stochastic sources in the early Universe
  - GW background from quintessential inflation
  - cosmic strings
  - Dilation
  - pre–big bang scenarios
  - Superinflation in loop quantum gravity
  - Postinflationary phase transitions
  - parametric resonance at the end of inflation or preheating
  - braneworld black holes associated with extra dimensions
  - clouds of axions (super radiance)

- High frequency region has physically understood processes of generation of GWs
  - thermal gravitational radiation from stars
  - Radiation from low mass primordial black holes
  - gravitational modes of plasma flows
- Tests for many emerging theories predicting GW radiation at such frequencies.
  - stochastic sources in the early Universe
  - GW background from quintessential inflation
  - cosmic strings
  - Dilation
  - pre–big bang scenarios
  - Superinflation in loop quantum gravity
  - Postinflationary phase transitions
  - parametric resonance at the end of inflation or preheating
  - braneworld black holes associated with extra dimensions
  - clouds of axions (super radiance)
  - quark nuggets

- High frequency region has physically understood processes of generation of GWs
  - thermal gravitational radiation from stars
  - Radiation from low mass primordial black holes
  - gravitational modes of plasma flows
- Tests for many emerging theories predicting GW radiation at such frequencies.
  - stochastic sources in the early Universe
  - GW background from quintessential inflation
  - cosmic strings
  - Dilation
  - pre–big bang scenarios
  - Superinflation in loop quantum gravity
  - Postinflationary phase transitions
  - parametric resonance at the end of inflation or preheating
  - braneworld black holes associated with extra dimensions
  - clouds of axions (super radiance)
  - quark nuggets
  - One hypothetical sources (due to the Galactic center shadow brane) comes within the sensitivity of the proposed single detector

The Sound of Dark Matter: Searching for Light Scalars with Resonant-Mass Detectors

Asimina Arvanitaki,[1,*] Savas Dimopoulos,[2,†] and Ken Van Tilburg[2,‡]

[1] *Perimeter Institute for Theoretical Physics, Waterloo, Ontario, N2L 2Y5, Canada*
[2] *Stanford Institute for Theoretical Physics, Stanford University, Stanford, CA 94305, USA*

(Dated: August 11, 2015)

The fine structure constant and the electron mass in string theory are determined by the values of scalar fields called moduli. If the dark matter takes on the form of such a light modulus, it oscillates with a frequency equal to its mass and an amplitude determined by the local dark matter density. This translates into an oscillation of the size of a solid that can be observed by resonant-mass antennae. Existing and proposed resonant-mass detectors can probe dark matter moduli with frequencies between 1 kHz and 1 GHz, with much better sensitivity than force measurements.

The Sound of Dark Matter: Searching for Light Scalars with Resonant-Mass Detectors

Asimina Arvanitaki,[1,*] Savas Dimopoulos,[2,†] and Ken Van Tilburg[2,‡]

[1] *Perimeter Institute for Theoretical Physics, Waterloo, Ontario, N2L 2Y5, Canada*
[2] *Stanford Institute for Theoretical Physics, Stanford University, Stanford, CA 94305, USA*

(Dated: August 11, 2015)

The fine structure constant and the electron mass in string theory are determined by the values of scalar fields called moduli. If the dark matter takes on the form of such a light modulus, it oscillates with a frequency equal to its mass and an amplitude determined by the local dark matter density. This translates into an oscillation of the size of a solid that can be observed by resonant-mass antennae. Existing and proposed resonant-mass detectors can probe dark matter moduli with frequencies between 1 kHz and 1 GHz, with much better sensitivity than force measurements.

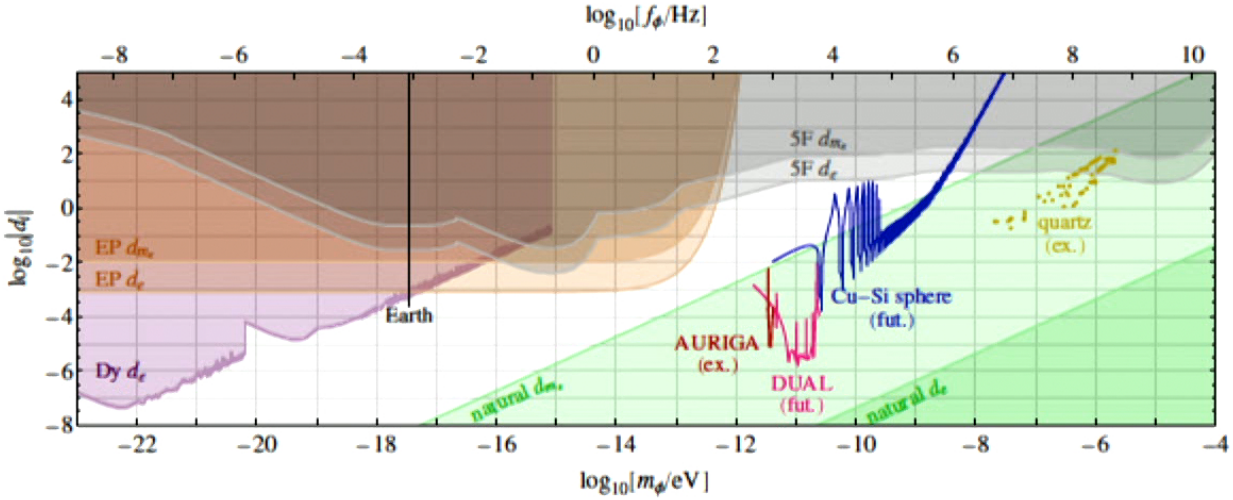

FIG. 1. Scalar field parameter space, with mass m_ϕ and corresponding DM oscillation frequency $f_\phi = m_\phi/2\pi$ on the bottom and top horizontal axes, and couplings of both an electron mass modulus ($d_i = d_{m_e}$) and electromagnetic gauge modulus ($d_i = d_e$) on the vertical axis. Natural parameter space for a 10 TeV cutoff is depicted by the green regions, while the other regions represent 95% CL limits from fifth-force tests ("5F", gray), equivalence-principle tests ("EP", orange), atomic spectroscopy in dysprosium ("Dy", purple), and low-frequency terrestrial seismology ("Earth", black). The blue curve shows the projected SNR = 1 reach of a proposed resonant-mass detector—a copper-silicon (Cu-Si) sphere 30 cm in radius—after 1.6 y of integration time, while the red curve shows the reach for the current AURIGA detector with 8 y of recasted data. Rough estimates of the 1-year reach of a proposed DUAL detector (pink) and several harmonics of two piezoelectric quartz resonators (gold points) are also shown.

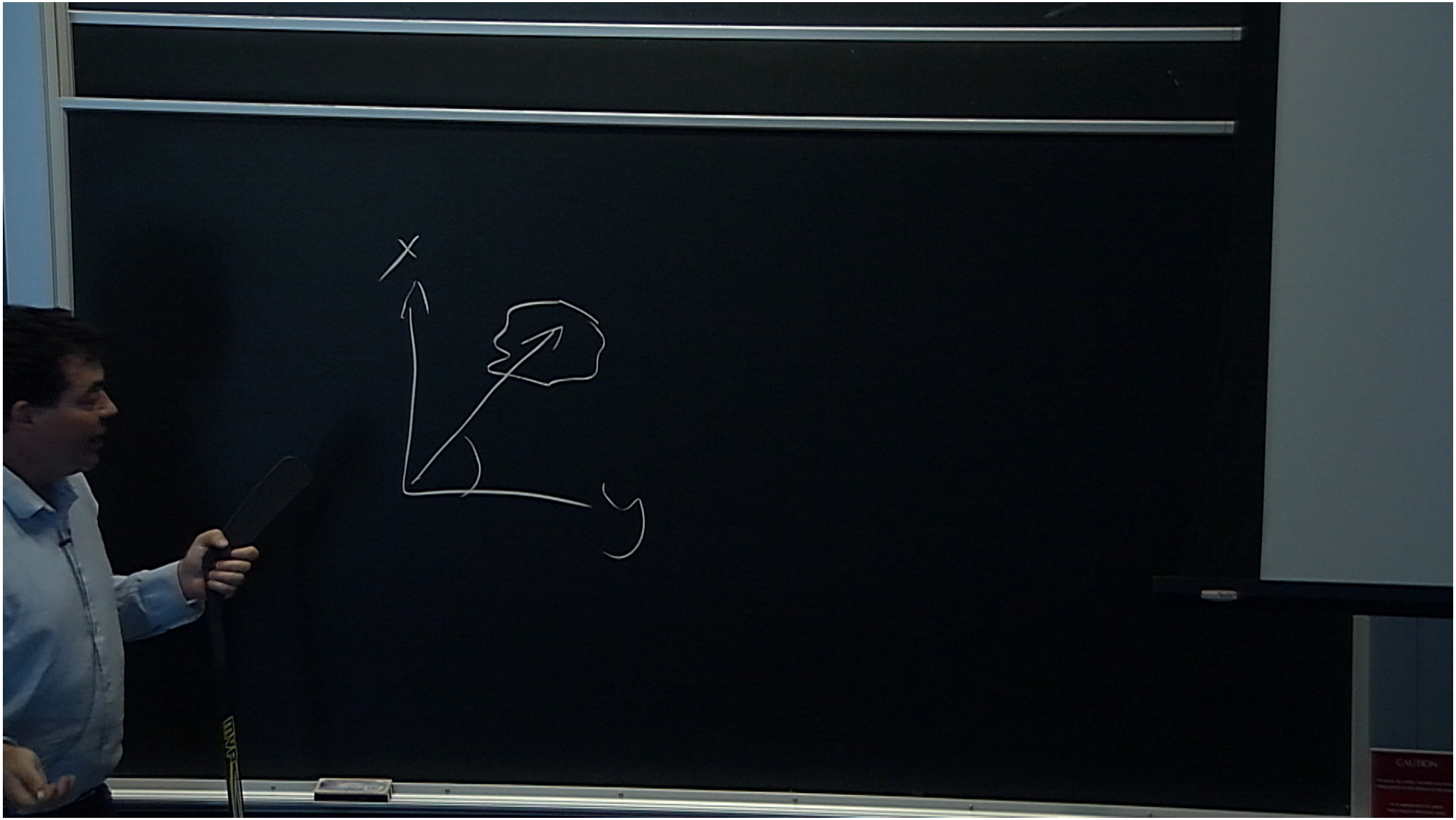
x
y

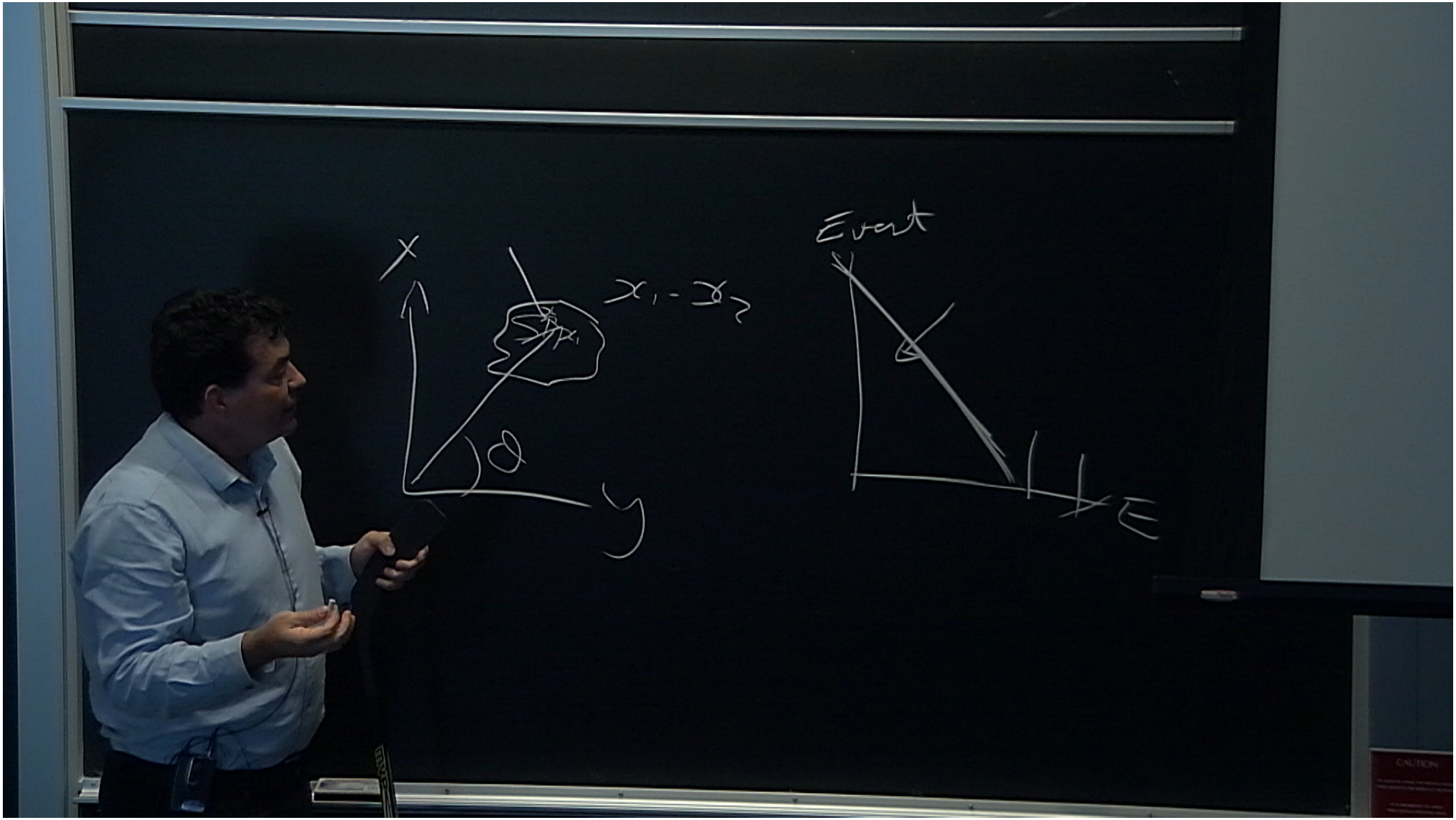
x
$x_1 - x_2$
0
y
Event
Like

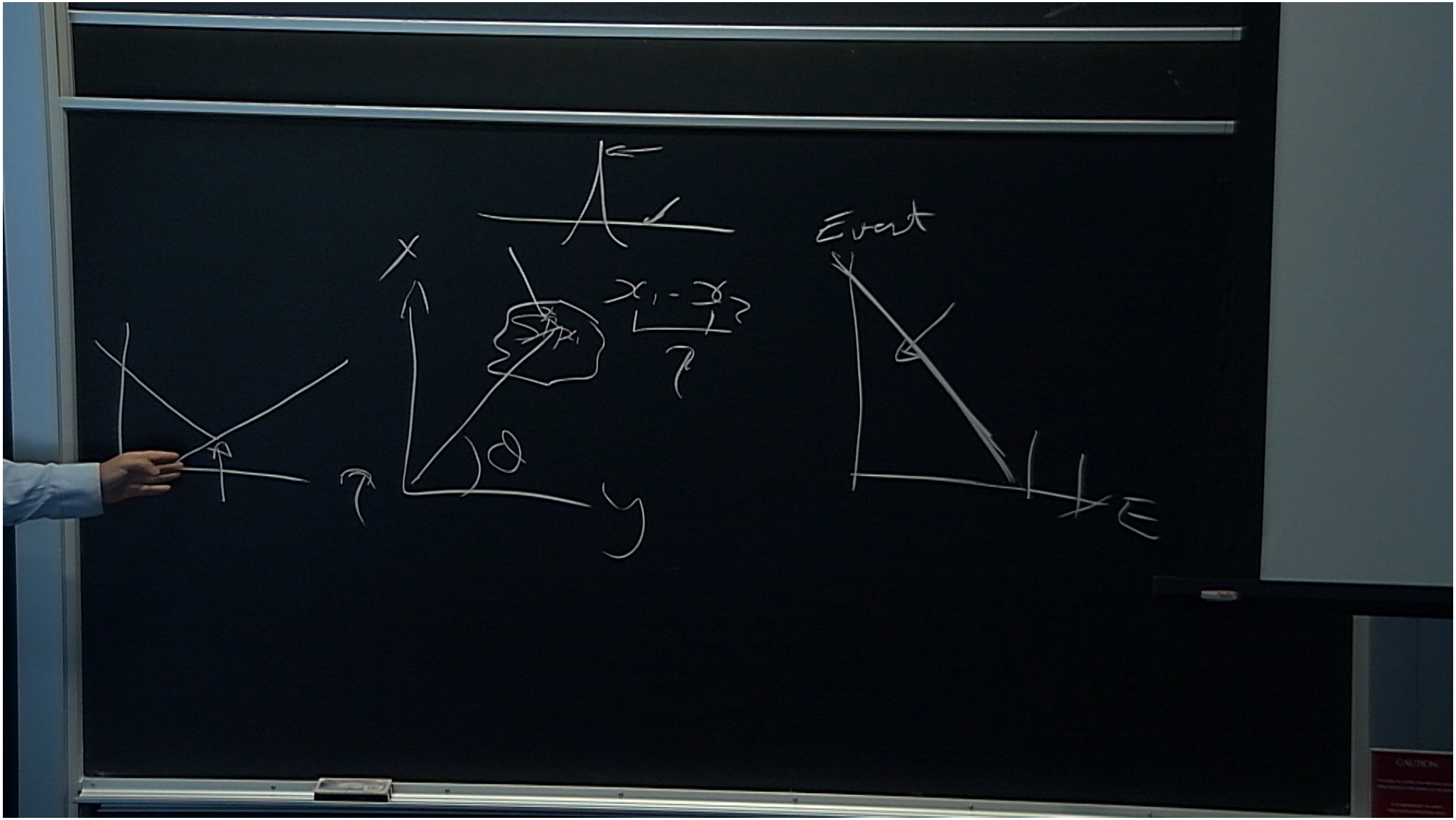
Event
x
y
0

Quantum Gravity

nature physics
ARTICLES
PUBLISHED ONLINE: 18 MARCH 2012 | DOI: 10.1038/NPHYS2262

Probing Planck-scale physics with quantum optics

Igor Pikovski[1,2]*, Michael R. Vanner[1,2], Markus Aspelmeyer[1,2], M. S. Kim[3]* and Časlav Brukner[2,4]

Theoretically proposed modification:

$$[x,p] = i\hbar\sqrt{1 + 2\eta_0 \frac{(p/c)^2 + m^2}{M_p^2}}$$

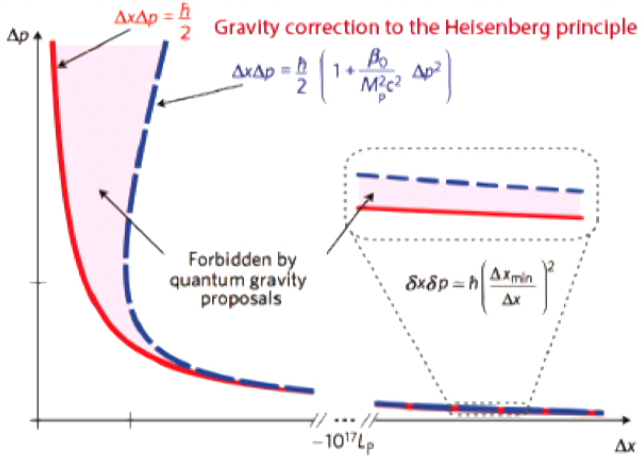

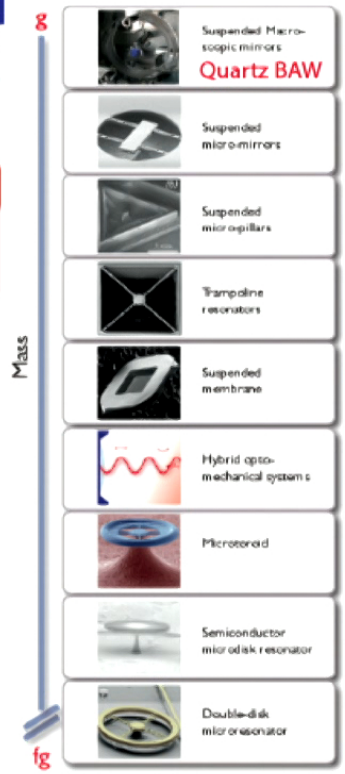

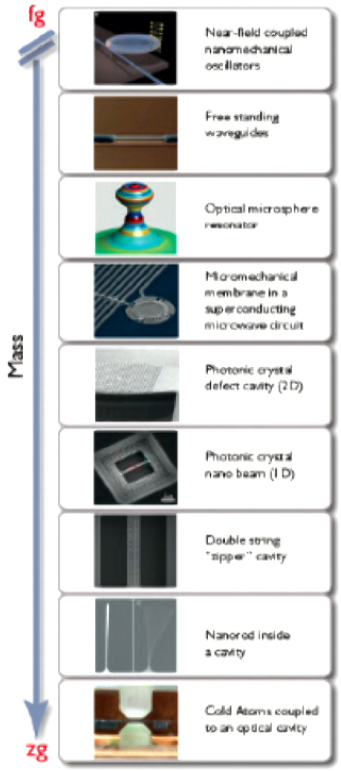

DUMBBELL (DB) RESONATOR

m = 0.5 kg | ω_0 = 115 kHz

Transductance via strain induced change in permittivity + change in radius when oscillating in the radial breathing mode:

$$\frac{\partial f}{\partial z} = \frac{f}{z}\left(\frac{\nu}{2}p_{\varepsilon_r}K_{\varepsilon_r} - \frac{1}{2}p_{\varepsilon_z}K_{\varepsilon_z} + \nu p_r - p_z\right),$$

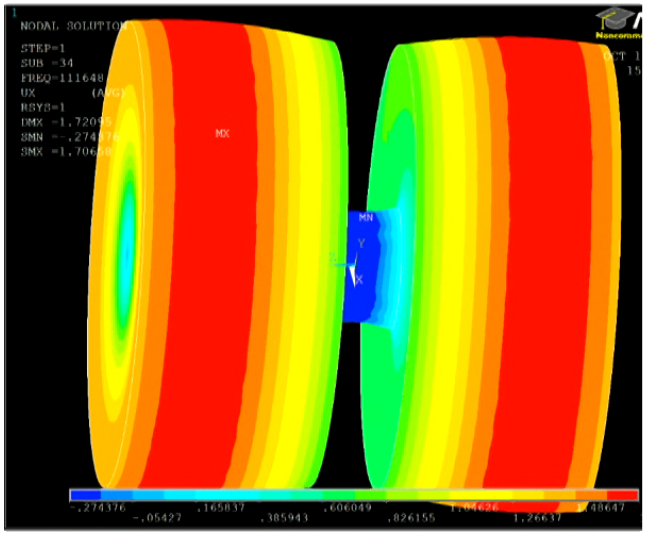

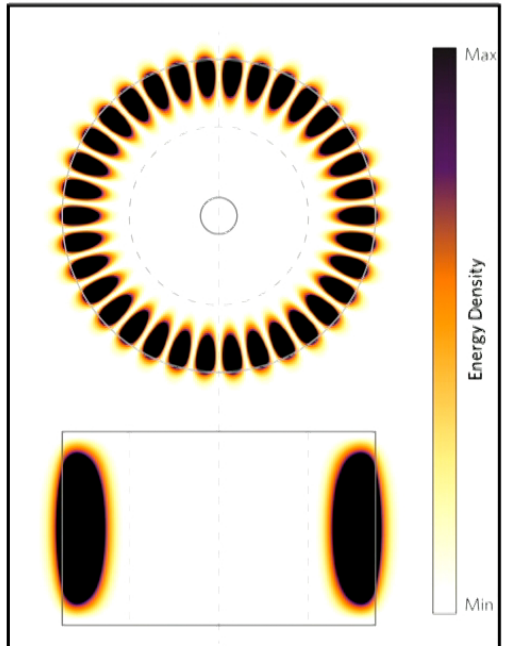

PHYSICAL REVIEW A 92, 023817 (2015)

Precision measurement of a low-loss cylindrical dumbbell-shaped sapphire mechanical oscillator using radiation pressure

J. Bourhill,* E. Ivanov, and M. E. Tobar
ARC Centre of Excellence for Engineered Quantum Systems, University of Western Australia, 35 Stirling Highway, Crawley, Western Australia 6009, Australia
(Received 27 February 2015; published 11 August 2015)

We present first results from a number of experiments conducted on a 0.53-kg cylindrical dumbbell-shaped sapphire crystal. Here we report on an optomechanical experiment utilizing a modification to the typical cylindrical architecture. Mechanical motion of the crystal structure alters the dimensions of the crystal, and the induced strain changes the permittivity. These two effects result in parametric frequency modulation of resonant microwave whispering gallery modes that are simultaneously excited within the crystal. A microwave readout system is implemented, allowing extremely low noise measurements of this frequency modulation near our modes of interest, having a phase noise floor of -165 dBc/Hz at 100 kHz. Fine tuning of the crystal's suspension has allowed for the optimization of mechanical quality factors in preparation for cryogenic experiments, with a value of $Q = 8 \times 10^7$ achieved at 127 kHz. This results in a $Q \times f$ product of 10^{13}, equivalent to the best measured values in a macroscopic sapphire mechanical system. Results are presented that demonstrate the excitation of mechanical modes via radiation pressure force, allowing an experimental method of determining the transducer's displacement sensitivity df/dx and calibrating the system. Finally, we demonstrate parametric backaction phenomenon within the system. These are all important steps towards the goal of achieving quantum limited measurements of a kilogram-scale macroscopic device for the purpose of detecting deviations from standard quantum theory resulting from quantum gravitational effects.

DOI: 10.1103/PhysRevA.92.023817 PACS number(s): 42.79.Jq, 42.50.Wk, 43.38.Zp

New Journal of Physics
The open access journal at the forefront of physics

Deutsche Physikalische Gesellschaft DPG
IOP Institute of Physics

Published in partnership with: Deutsche Physikalische Gesellschaft and the Institute of Physics

PAPER

Detecting continuous gravitational waves with superfluid ^{4}He

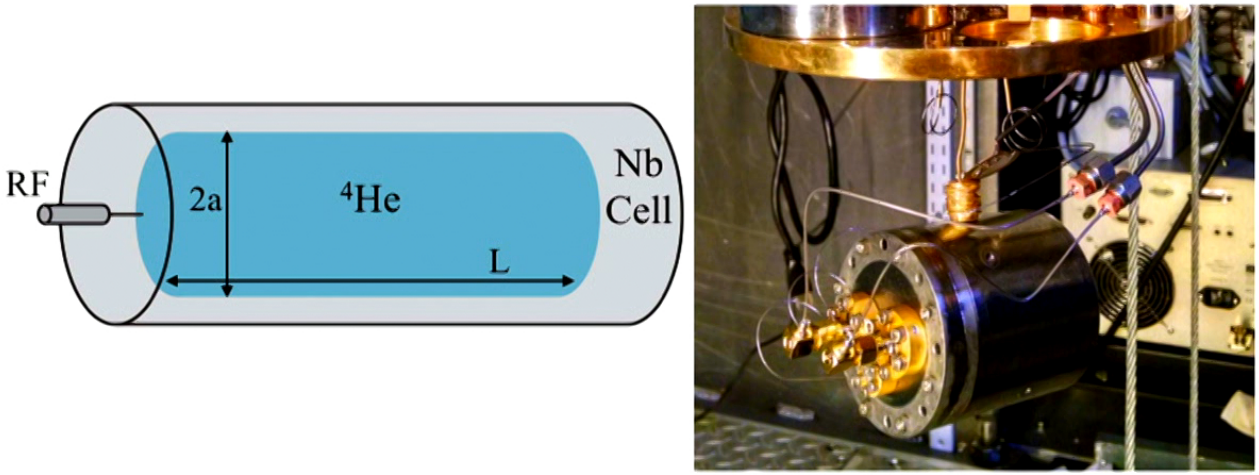

Figure 1. *Left*: schematic of the proposed GW sensor based on acoustic modes of superfluid helium. Two cylindrical geometries considered here are Gen1 (radius $a = 11$ cm, length $L = 50$ cm, mass $M = 2.7$ kg) and Gen2 ($a = 11$ cm, $L = 3$ m, $M = 16$ kg). *Right*: prototype of the detector with $a = 1.8$ cm, $L = 4$ cm, $M = 6$ g and resonant frequency 10 kHz.

of $h \sim 10^{-23}/\sqrt{\text{Hz}}$ are detectable. Measuring such strains is possible by implementing state of the art microwave transducer technology. We show that the proposed system can compete with interferometric detectors and potentially surpass the gravitational strain limits set by them for certain pulsar sources within a few months of integration time.

New Journal of Physics
The open access journal at the forefront of physics

Deutsche Physikalische Gesellschaft DPG
IOP Institute of Physics

Published in partnership with: Deutsche Physikalische Gesellschaft and the Institute of Physics

PAPER

Detecting continuous gravitational waves with superfluid ^{4}He

Cryogenic Optomechanics and the Resurgence of the Resonant-Mass Gravitational Wave Detector

Michael E. Tobar
ARC Centre of Excellence for Engineered Quantum Systems, School of Physics,
The University of Western Australia, Crawley 6009, Australia

Figure 1. *Left*: schematic of the proposed GW sensor based on acoustic modes of superfluid helium. Two cylindrical geometries considered here are Gen1 (radius $a = 11$ cm, length $L = 50$ cm, mass $M = 2.7$ kg) and Gen2 ($a = 11$ cm, $L = 3$ m, $M = 16$ kg). *Right*: prototype of the detector with $a = 1.8$ cm, $L = 4$ cm, $M = 6$ g and resonant frequency 10 kHz.

of $h \sim 10^{-23}/\sqrt{\text{Hz}}$ are detectable. Measuring such strains is possible by implementing state of the art microwave transducer technology. We show that the proposed system can compete with interferometric detectors and potentially surpass the gravitational strain limits set by them for certain pulsar sources within a few months of integration time.

Finite Element Modelling

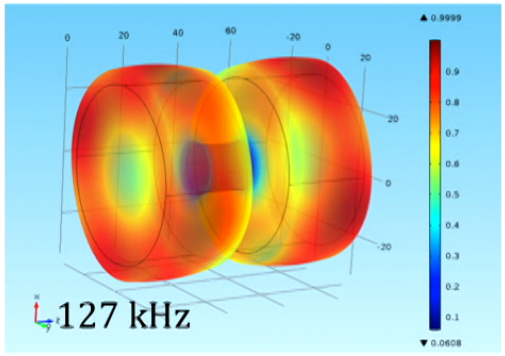

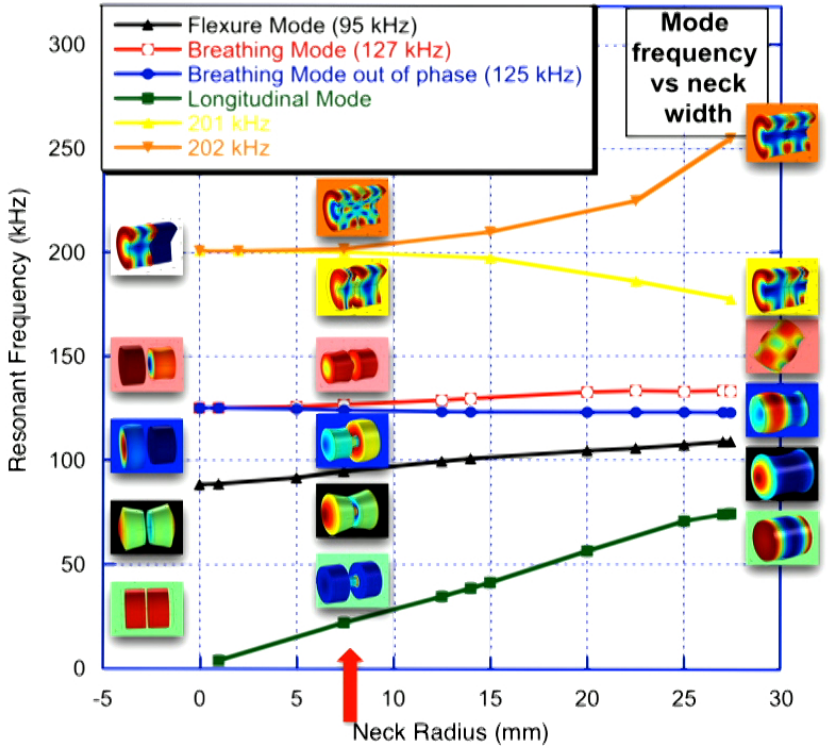

Exciting Mechanical Modes

Piezoelectric Shaker

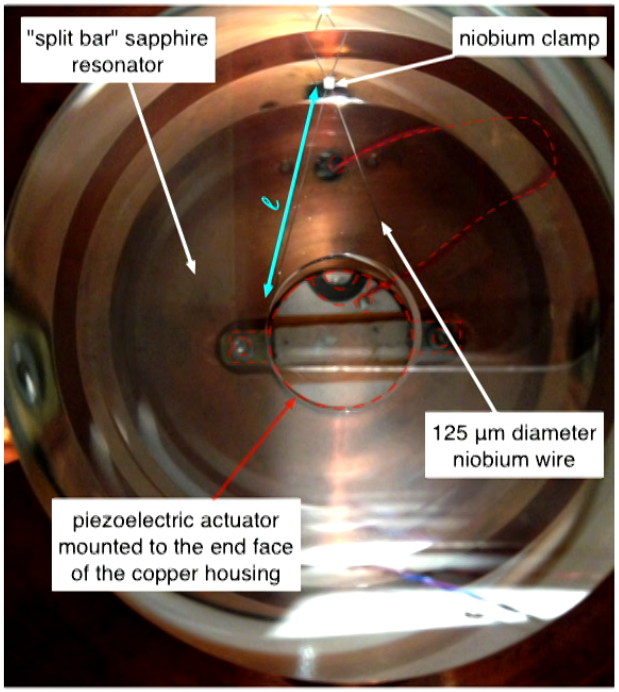

Radiation Pressure Force

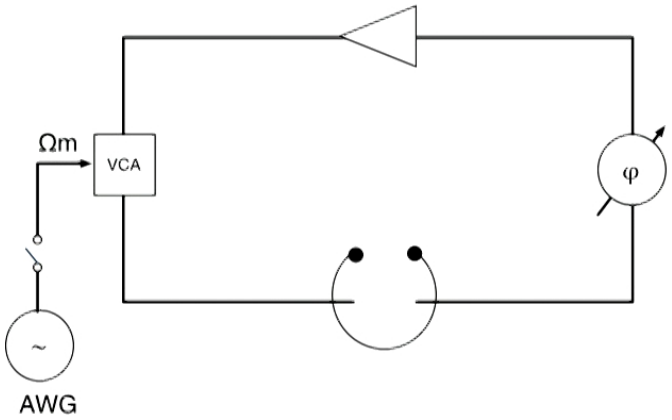

$$F_{ext}[t]|_{\omega=\omega_e} = \frac{d\omega}{dx}\frac{P_{inc}[t]Q_e}{\omega_e^2}\frac{4\beta_1}{(1+\beta_1+\beta_2)^2}$$

Piez

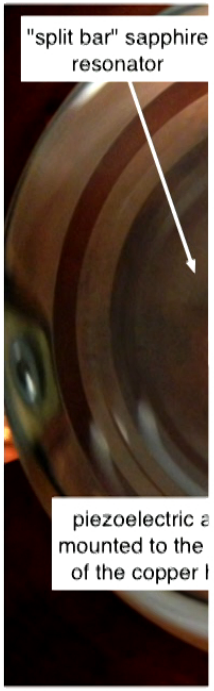

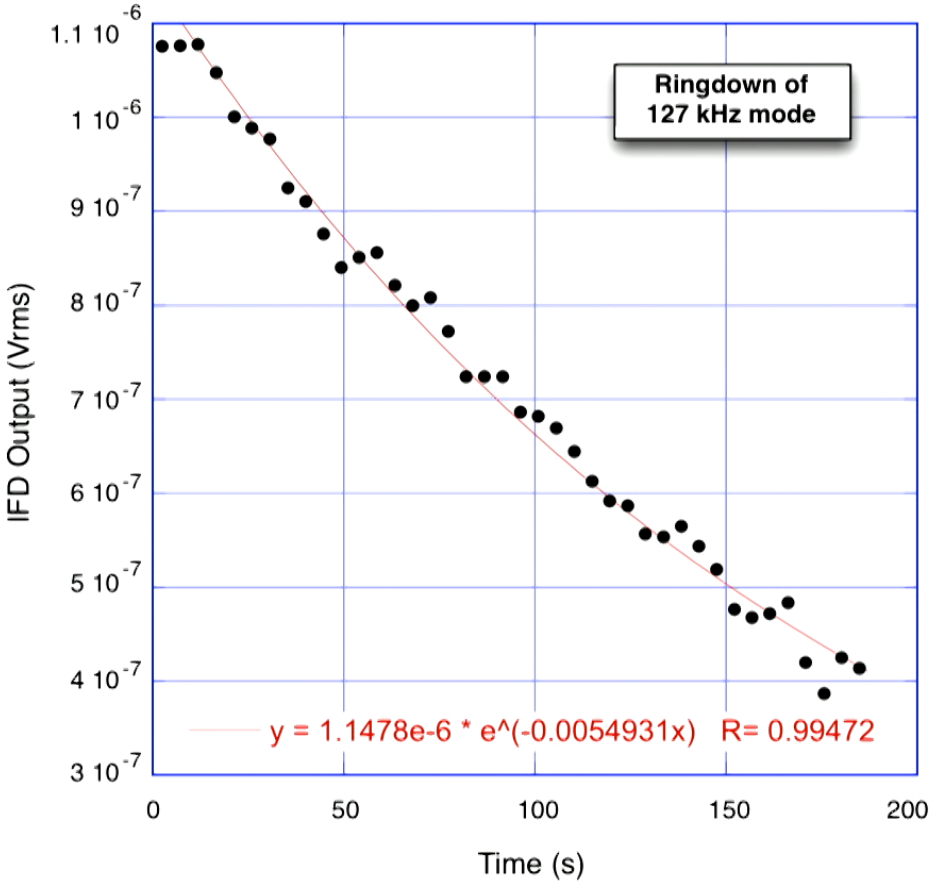

e Force

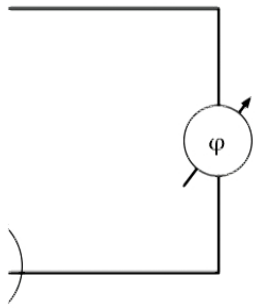

$$\frac{4\beta_1}{(1+\beta_1+\beta_2)^2}$$

Microwave Readout System Improvement

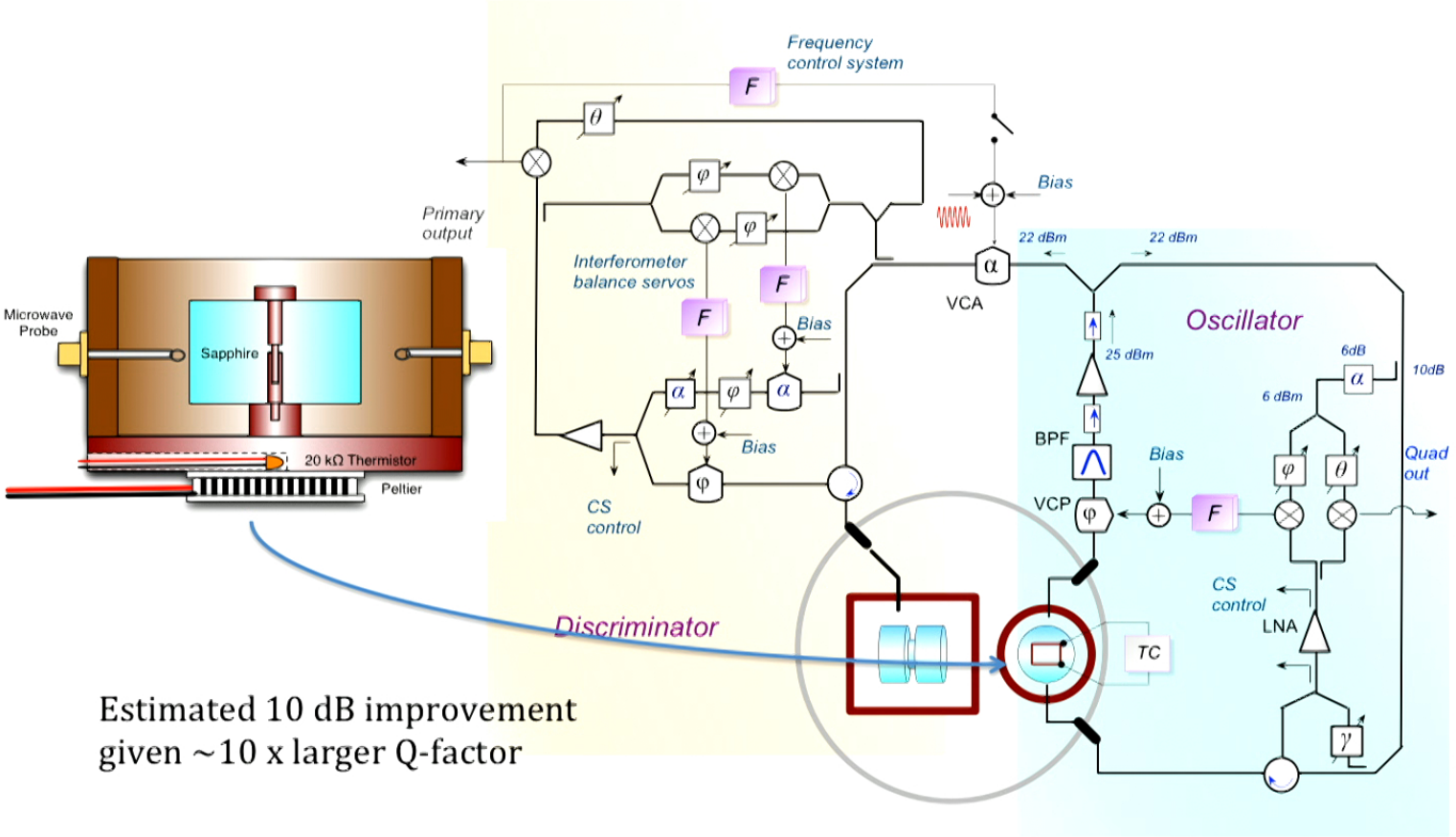

Estimated 10 dB improvement
given ~10 x larger Q-factor

Comparison With Other Results

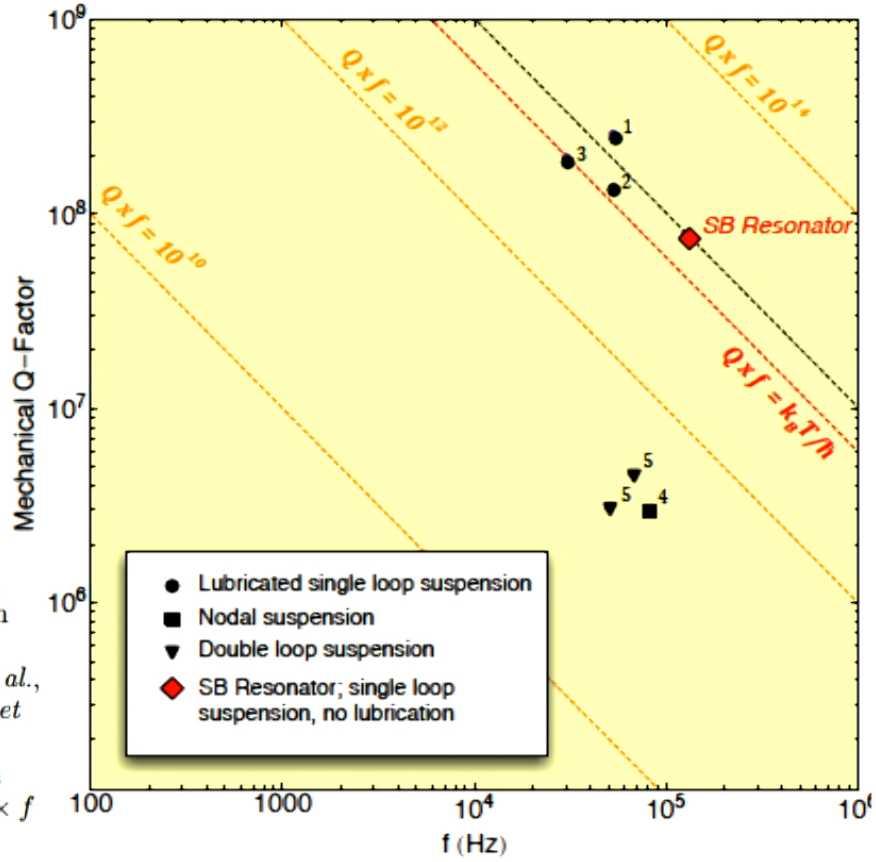

FIG. 9: Reported mechanical quality factors and resonant frequencies of published experiments with sapphire bar optomechanical systems at room temperature: 1. (Rowan *et al.*, 2000)[26], 2. (Locke *et al.*, 2001)[13], 3. (Braginsky *et al.*, 1985)[24], 4. (Numata *et al.*, 2000)[27], 5. (Uchiyama *et al.*, 1999)[28]. The experiments are differentiated by their suspension techniques. The black dashed line represents the $Q \times f$ product of the SB.

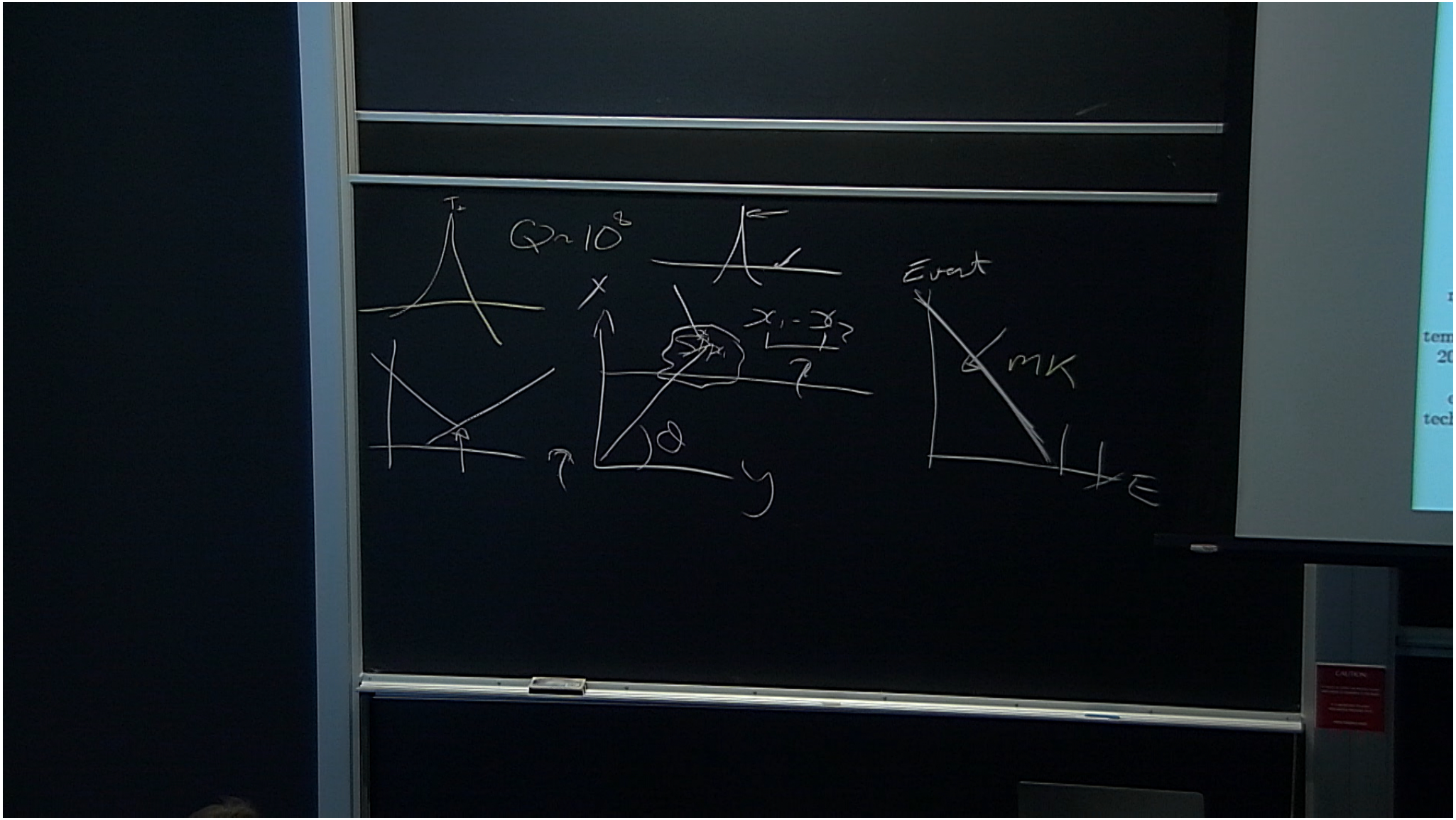
Event
MK

Comparison With Other Results

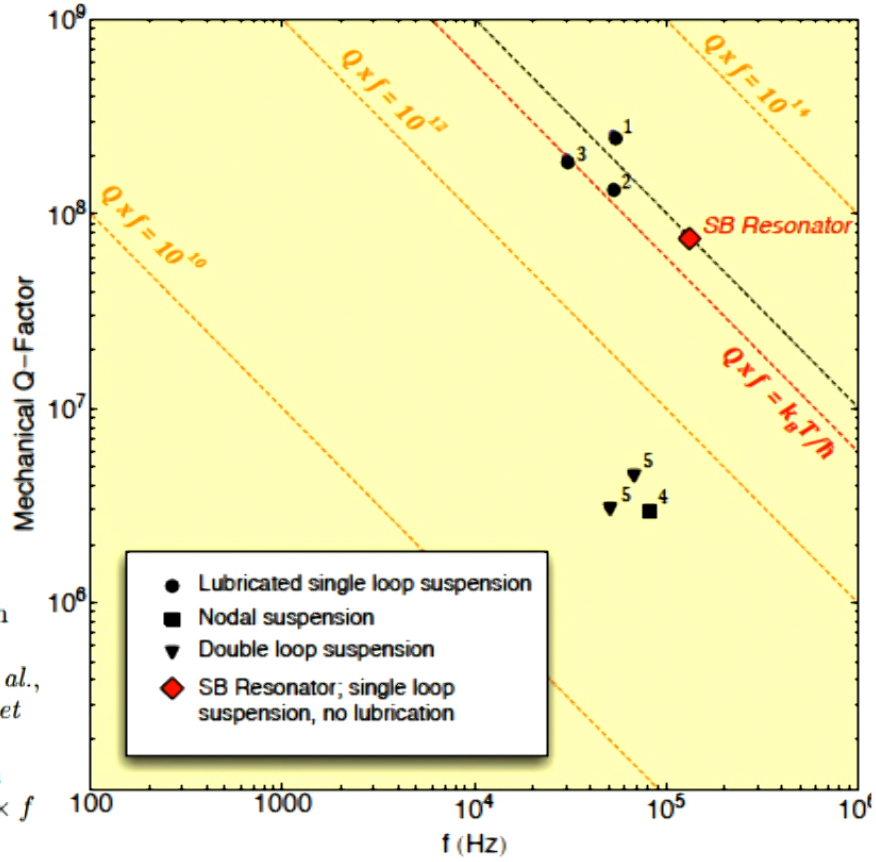

FIG. 9: Reported mechanical quality factors and resonant frequencies of published experiments with sapphire bar optomechanical systems at room temperature: 1. (Rowan *et al.*, 2000)[26], 2. (Locke *et al.*, 2001)[13], 3. (Braginsky *et al.*, 1985)[24], 4. (Numata *et al.*, 2000)[27], 5. (Uchiyama *et al.*, 1999)[28]. The experiments are differentiated by their suspension techniques. The black dashed line represents the $Q \times f$ product of the SB.

PHYSICAL REVIEW X 6, 011018 (2016)

Acoustic Tests of Lorentz Symmetry Using Quartz Oscillators

Anthony Lo, Philipp Haslinger, Eli Mizrachi, Loïc Anderegg, and Holger Müller*
Department of Physics, University of California, Berkeley, California 94720, USA

Michael Hohensee†
Lawrence Livermore National Laboratory, Livermore, California 94550, USA

Maxim Goryachev and Michael E. Tobar
ARC Centre of Excellence for Engineered Quantum Systems, School of Physics, University of Western Australia, 35 Stirling Highway, Crawley, Western Australia 6009, Australia
(Received 8 December 2014; revised manuscript received 6 July 2015; published 24 February 2016)

We propose and demonstrate a test of Lorentz symmetry based on new, compact, and reliable quartz oscillator technology. Violations of Lorentz invariance in the matter and photon sector of the standard model extension generate anisotropies in particles' inertial masses and the elastic constants of solids, giving rise to measurable anisotropies in the resonance frequencies of acoustic modes in solids. A first realization of such a "phonon-sector" test of Lorentz symmetry using room-temperature stress-compensated-cut crystals yields 120 h of data at a frequency resolution of 2.4×10^{-15} and a limit of $\tilde{c}_Q^n = (-1.8 \pm 2.2) \times 10^{-14}$ GeV on the most weakly constrained neutron-sector c coefficient of the standard model extension. Future experiments with cryogenic oscillators promise significant improvements in accuracy, opening up the potential for improved limits on Lorentz violation in the neutron, proton, electron, and photon sector.

DOI: 10.1103/PhysRevX.6.011018

Subject Areas: Acoustics, Atomic and Molecular Physics, Electronics

Local Lorentz Invariance

- Local Lorentz symmetry
  - Two kinds of transformations: **Rotations** and **Boosts**

Rotations (3)

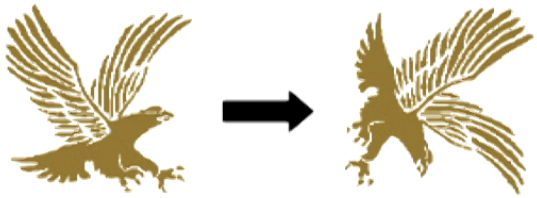

Boosts (3)

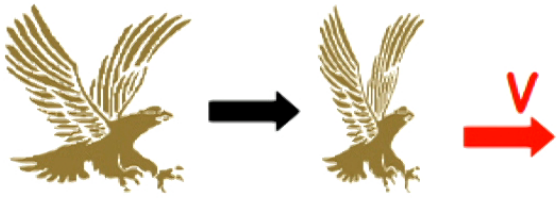

- Experimental outcomes are the same when the **apparatus** undergoes (local) Lorentz transformations

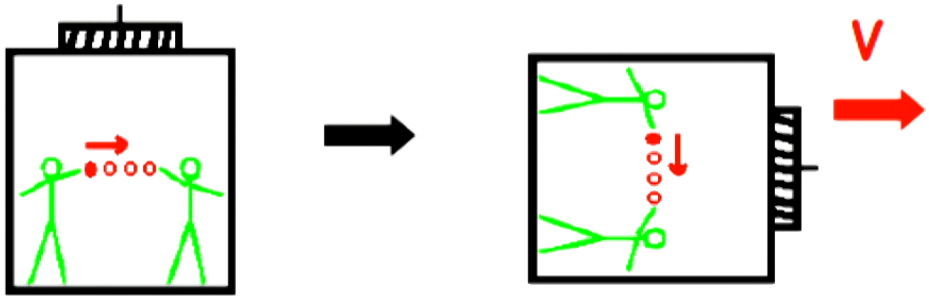

- General framework for studying Lorentz violation

Standard-Model Extension (SME)

(Developed by Kostelecký and collaborators in the 90s)

- Basic Idea:

General Relativity

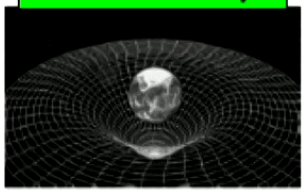

+

Standard Model

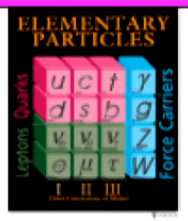

+

All possible forms of Lorentz violation

Background fields interacting with known matter

SME - effective field theory with lagrangian:

$$\mathcal{L}_{SME} = \mathcal{L}_{GR} + \mathcal{L}_{SM} + \mathcal{L}_{LV} + \ldots$$

Usual GR lagrangian

Usual SM fields

All possible Lorentz-violating terms constructed from SM & GR fields and background coefficients

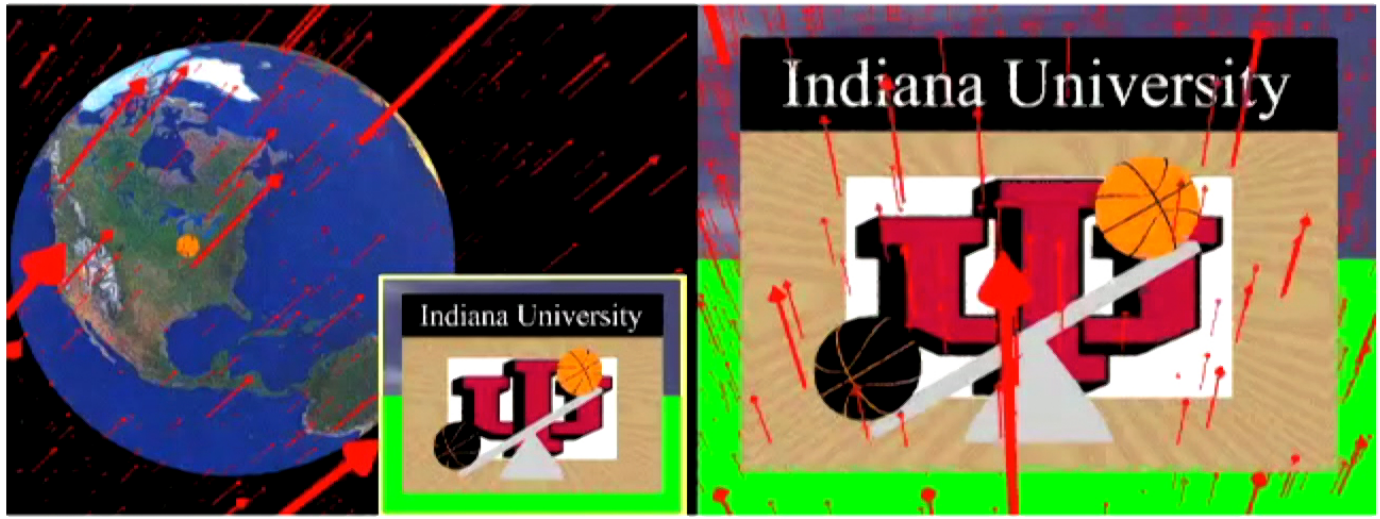

Tested Across Many Different Particle Sectors

-> Photon

-> Matter (neutron, proton, electron, neutrino..)

http://www.physics.indiana.edu/~kostelec/

Tested Across Many Different Particle Sectors

-> Photon

-> Matter (neutron, proton, electron, neutrino..)

-> Gravity (Wuhan and Josh Long)

http://www.physics.indiana.edu/~kostelec/

Tested Across Many Different Particle Sectors

-> Photon

-> Matter (neutron, proton, electron, neutrino..)

-> Gravity (Wuhan and Josh Long)

http://www.physics.indiana.edu/~kostelec/

Collaboration with Humboldt University of Berlin (HUB): Achim Peters

- Combined precision test of Lorentz Invariance between optical and microwave frequencies

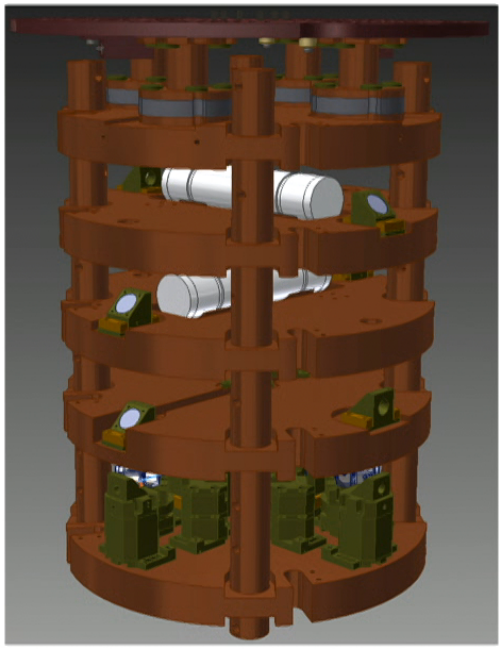

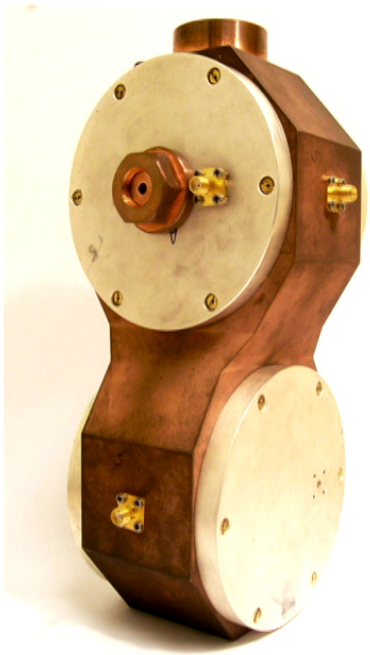

nature COMMUNICATIONS

ARTICLE

Received 17 Jan 2015 | Accepted 25 Jul 2015 | Published 1 Sep 2015

DOI: 10.1038/ncomms9174 OPEN

Direct terrestrial test of Lorentz symmetry in electrodynamics to 10^{-18}

Moritz Nagel[1,*], Stephen R. Parker[2,*], Evgeny V. Kovalchuk[1], Paul L. Stanwix[2], John G. Hartnett[2,3], Eugene N. Ivanov[2], Achim Peters[1] & Michael E. Tobar[2]

Lorentz symmetry is a foundational property of modern physics, underlying the standard model of particles and general relativity. It is anticipated that these two theories are low-energy approximations of a single theory that is unified and consistent at the Planck scale. Many unifying proposals allow Lorentz symmetry to be broken, with observable effects appearing at Planck-suppressed levels; thus, precision tests of Lorentz invariance are needed to assess and guide theoretical efforts. Here we use ultrastable oscillator frequency sources to perform a modern Michelson–Morley experiment and make the most precise direct terrestrial test to date of Lorentz symmetry for the photon, constraining Lorentz violating orientation-dependent relative frequency changes $\Delta\nu/\nu$ to $9.2 \pm 10.7 \times 10^{-19}$ (95% confidence interval). This order of magnitude improvement over previous Michelson–Morley experiments allows us to set comprehensive simultaneous bounds on nine boost and rotation

Standard Model Extension for Photon Fields

$$\mathcal{L} = -\frac{1}{4}F_{\mu\nu}F^{\mu,\nu} + \frac{1}{2}\left(k_{AF}\right)^{\kappa}\epsilon_{\kappa\lambda\mu\nu}A^{\lambda}F^{\mu\nu} - \frac{1}{4}\left(k_{F}\right)_{\kappa\lambda\mu\nu}F^{\kappa\lambda}F^{\mu\nu}$$

The Photon Sector of the SME

Electromagnetic Tests ⇒ Photon Sector ⇒ Modified Maxwell Equations

$$\begin{pmatrix} D \\ H \end{pmatrix} = \begin{pmatrix} \varepsilon_0(\varepsilon_r + \kappa_{DE}) & \sqrt{\frac{\varepsilon_0}{\mu_0}}\kappa_{DB} \\ \sqrt{\frac{\varepsilon_0}{\mu_0}}\kappa_{HE} & \mu_0^{-1}(\mu_r^{-1} + \kappa_{HB}) \end{pmatrix} \begin{pmatrix} E \\ B \end{pmatrix}$$

Linear combinations:

$\kappa_{e+}{}^{jk}$, $\kappa_{e-}{}^{jk}$,

$\kappa_{o+}{}^{jk}$, $\kappa_{o-}{}^{jk}$,

$\kappa_{trace} = 1/3\,\mathrm{Tr}(\kappa_{DE})$

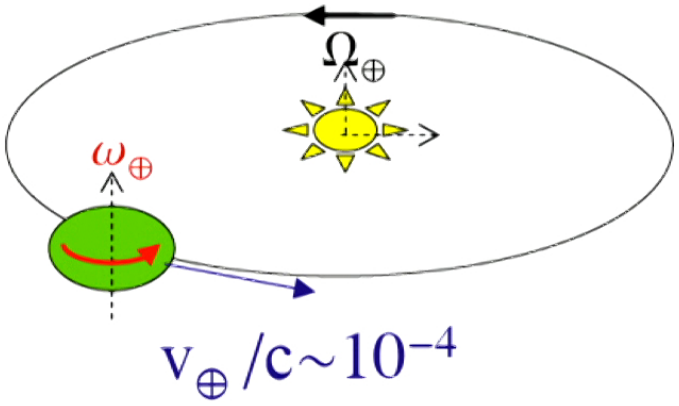

Existing Limits in sun-centred frame:

$\kappa_{e+}{}^{jk}$, $\kappa_{o-}{}^{jk} < 2\times10^{-37}$

$\kappa_{e-}{}^{jk} < 10^{-15}$, $\kappa_{o+}{}^{jk} < 10^{-11}$

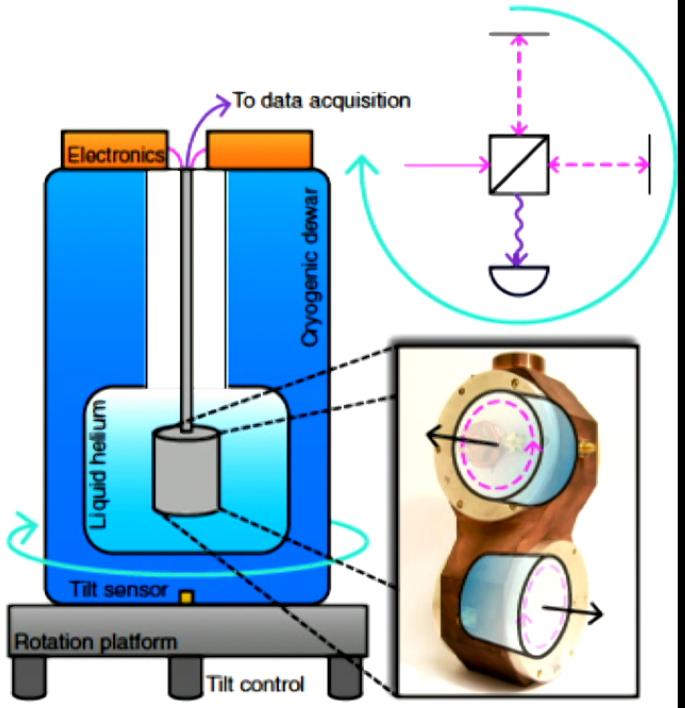
To data acquisition
Electronics
Cryogenic dewar
Liquid helium
Tilt sensor
Rotation platform
Tilt control

The Photon Sector of the SME

Electromagnetic Tests ⇒ Photon Sector ⇒ Modified Maxwell Equations

$$\begin{pmatrix} D \\ H \end{pmatrix} = \begin{pmatrix} \varepsilon_0(\varepsilon_r + \kappa_{DE}) & \sqrt{\frac{\varepsilon_0}{\mu_0}}\kappa_{DB} \\ \sqrt{\frac{\varepsilon_0}{\mu_0}}\kappa_{HE} & \mu_0^{-1}(\mu_r^{-1} + \kappa_{HB}) \end{pmatrix} \begin{pmatrix} E \\ B \end{pmatrix}$$

Linear combinations:

$\kappa_{e+}{}^{jk}$, $\kappa_{e-}{}^{jk}$,

$\kappa_{o+}{}^{jk}$, $\kappa_{o-}{}^{jk}$,

$\kappa_{trace} = 1/3\,\mathrm{Tr}(\kappa_{DE})$

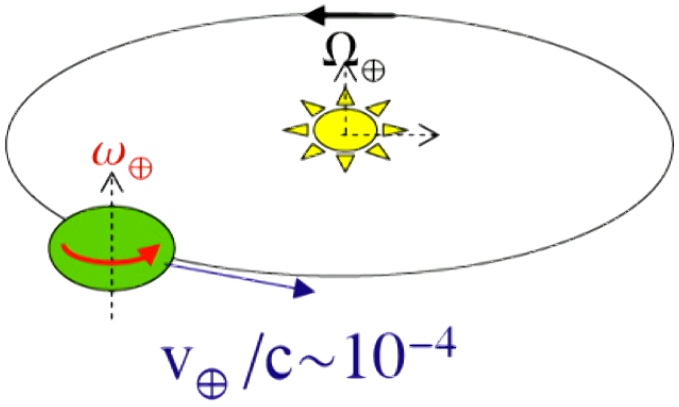

Existing Limits in sun-centred frame:

$\kappa_{e+}{}^{jk}$, $\kappa_{o-}{}^{jk} < 2\times10^{-37}$

$\kappa_{e-}{}^{jk} < 10^{-15}$, $\kappa_{o+}{}^{jk} < 10^{-11}$

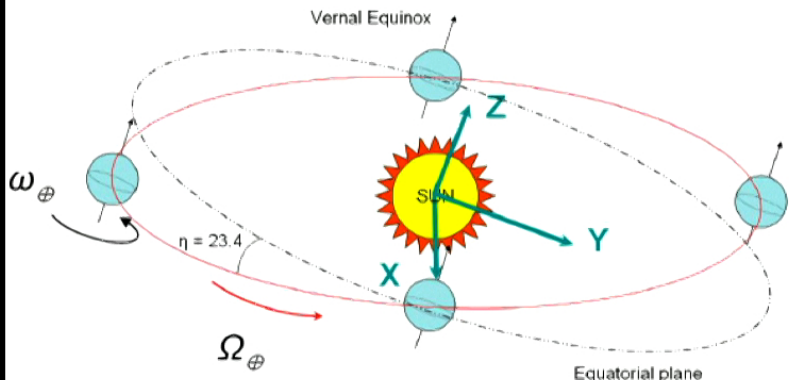
Vernal Equinox
Z
SUN
Y
X
η = 23.4
Equatorial plane

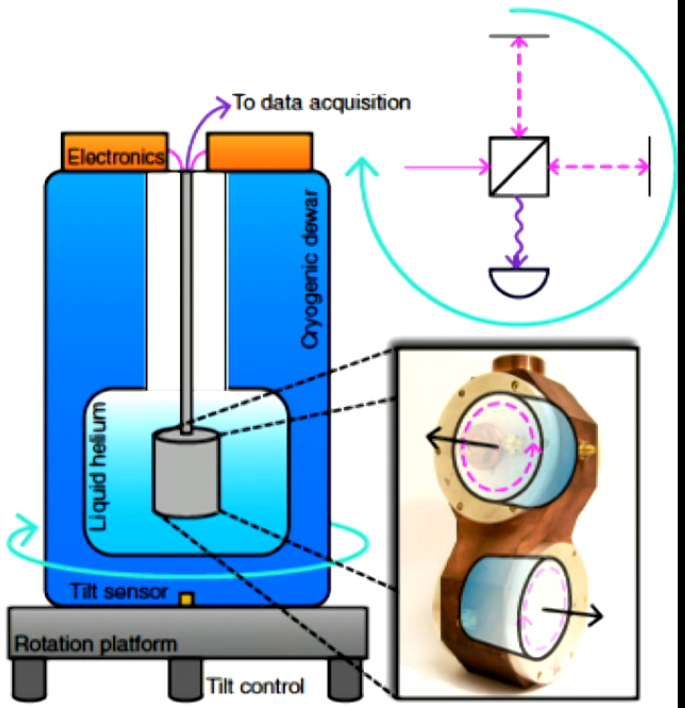
To data acquisition
Electronics
Cryogenic dewar
Liquid helium
Tilt sensor
Rotation platform
Tilt control

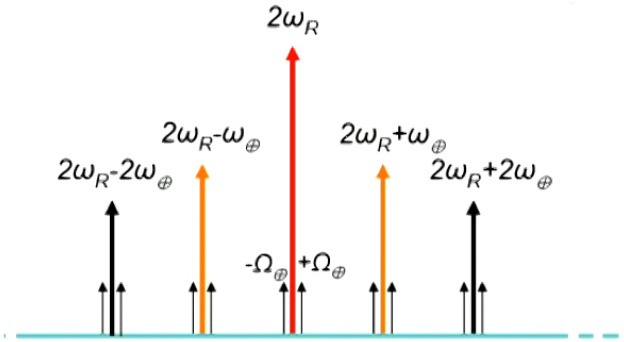

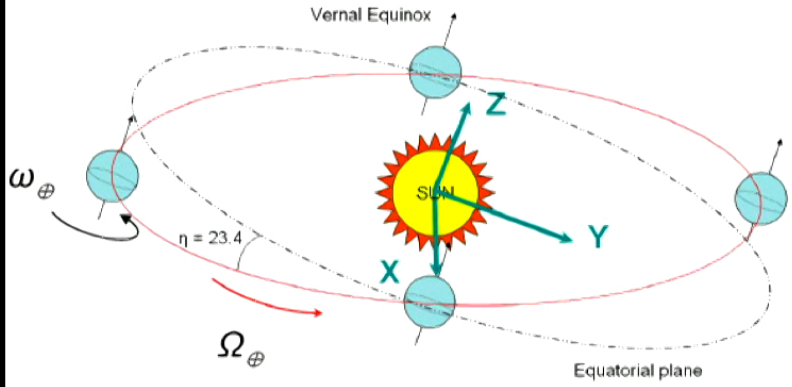

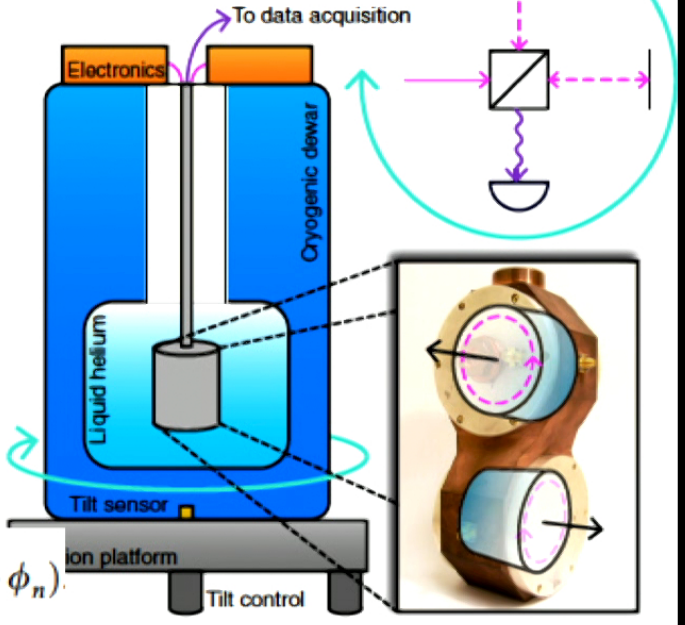

$$\frac{\Delta\nu_{\text{beat}}}{\nu_{\text{beat}}} = A + Bt + \sum_{n=1,2} C_n \cos(n\omega_R t + \phi_n) + S_n \sin(n\omega_R t + \phi_n)$$

Data Analysis

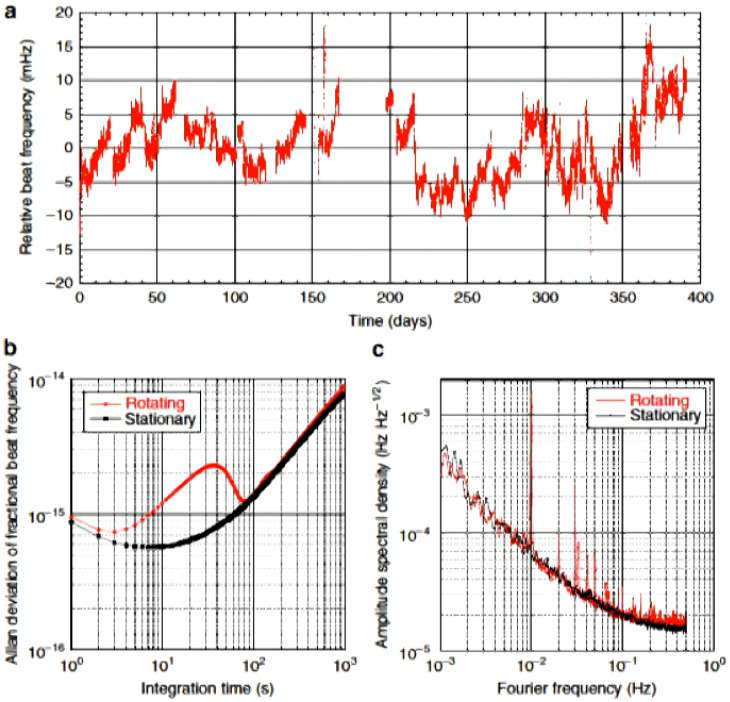

$$\frac{\Delta\nu_{\mathrm{beat}}}{\nu_{\mathrm{beat}}} = A + Bt + \sum_{n=1,2} C_n \cos(n\omega_{\mathrm{R}}t + \phi_n) + S_n \sin(n\omega_{\mathrm{R}}t + \phi_n)$$

Data Analysis

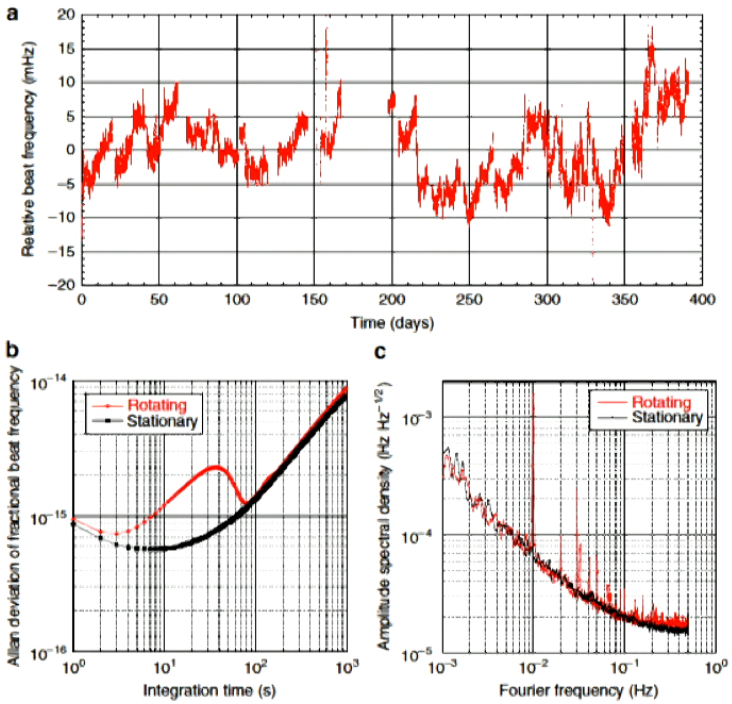

$$\frac{\Delta\nu_{\text{beat}}}{\nu_{\text{beat}}} = A + Bt + \sum_{n=1,2} C_n \cos(n\omega_R t + \phi_n) + S_n \sin(n\omega_R t + \phi_n)$$

Fit -> Demodulated data

10 rotations: 1000 seconds

-> Broken to 100 entries (1.2 days) fit the following

$$C_{2\omega_R}(t) = C_0 + CC_{\omega_\oplus}\cos(\omega_\oplus t + \phi_\oplus) + CS_{\omega_\oplus}\sin(\omega_\oplus t + \phi_\oplus) + CC_{2\omega_\oplus}\cos(2\omega_\oplus t + 2\phi_\oplus) + CS_{2\omega_\oplus}\sin(2\omega_\oplus t + 2\phi_\oplus)$$

$$S_{2\omega_R}(t) = S_0 + SC_{\omega_\oplus}\cos(\omega_\oplus t + \phi_\oplus) + SS_{\omega_\oplus}\sin(\omega_\oplus t + \phi_\oplus) + SC_{2\omega_\oplus}\cos(2\omega_\oplus t + 2\phi_\oplus) + SS_{2\omega_\oplus}\sin(2\omega_\oplus t + 2\phi_\oplus)$$

Data Analysis

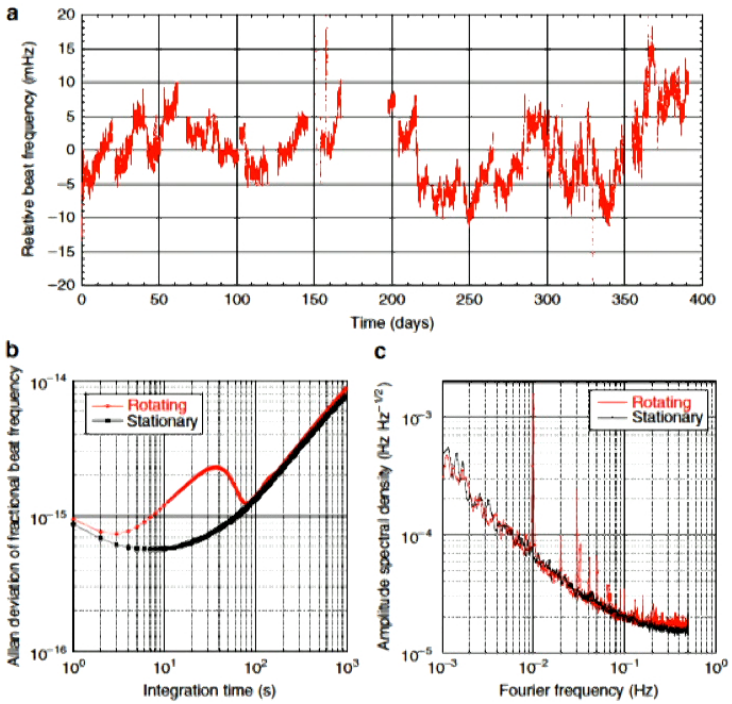

$$\frac{\Delta\nu_{\text{beat}}}{\nu_{\text{beat}}} = A + Bt + \sum_{n=1,2} C_n \cos(n\omega_R t + \phi_n) + S_n \sin(n\omega_R t + \phi_n)$$

Fit -> Demodulated data

10 rotations: 1000 seconds

-> Broken to 100 entries (1.2 days) fit the following

$$C_{2\omega_R}(t) = C_0 + CC_{\omega_\oplus}\cos(\omega_\oplus t + \phi_\oplus) + CS_{\omega_\oplus}\sin(\omega_\oplus t + \phi_\oplus) + CC_{2\omega_\oplus}\cos(2\omega_\oplus t + 2\phi_\oplus) + CS_{2\omega_\oplus}\sin(2\omega_\oplus t + 2\phi_\oplus)$$

$$S_{2\omega_R}(t) = S_0 + SC_{\omega_\oplus}\cos(\omega_\oplus t + \phi_\oplus) + SS_{\omega_\oplus}\sin(\omega_\oplus t + \phi_\oplus) + SC_{2\omega_\oplus}\cos(2\omega_\oplus t + 2\phi_\oplus) + SS_{2\omega_\oplus}\sin(2\omega_\oplus t + 2\phi_\oplus)$$

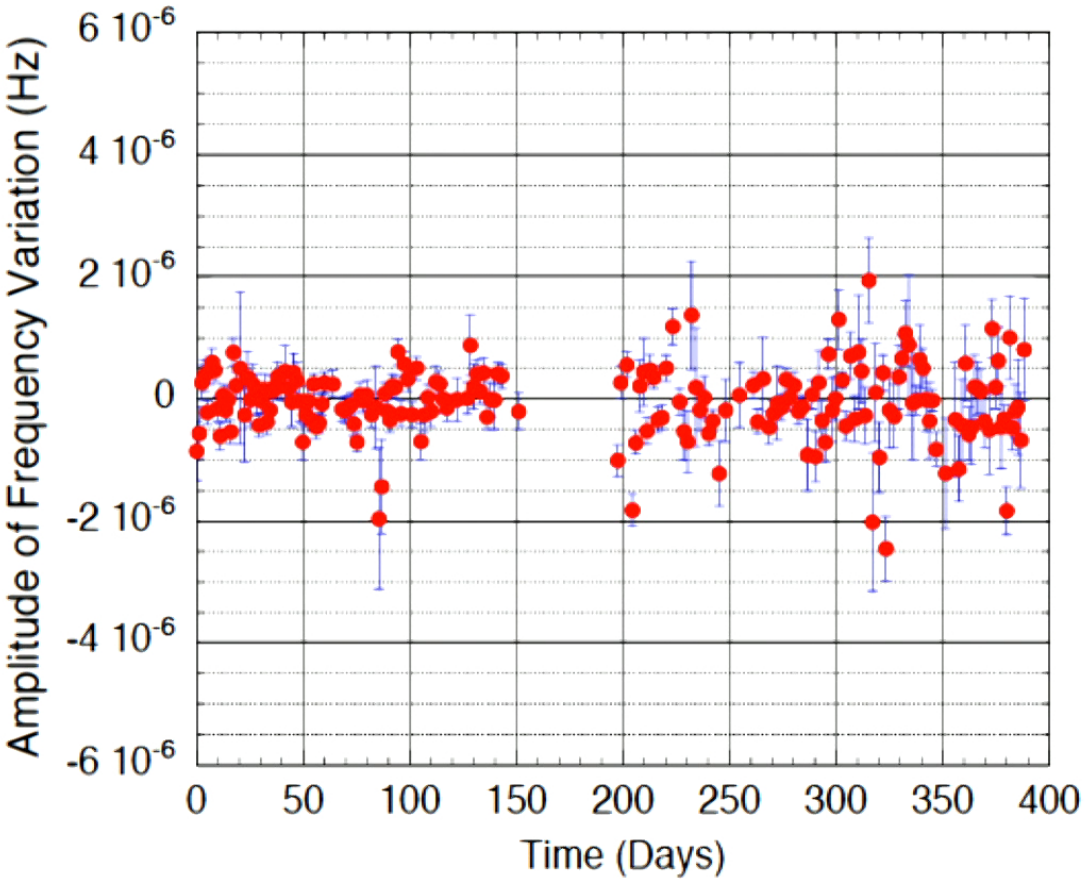

Supplementary Figure 3: **Subset fits to sidereal amplitude** $CC_{2\omega_\oplus}$ from equation (3) obtained as discussed in the main text. Statistical 1σ error bars are shown in blue.

Amplitude	Sensitivity	Numerical Weight
S_0	-	-
$SS^0_{\omega_\oplus}$	$4F_1 \sin(\chi)\tilde{\kappa}^{YZ}_{e-}$	1.1
$SS_{\omega_\oplus}C_{\Omega_\oplus}$	$-4F_2\beta_\oplus \sin(\chi)\left(\cos(\eta)\tilde{\kappa}^{XY}_{o+} - \sin(\eta)\tilde{\kappa}^{XZ}_{o+}\right)$	4.9E-5 $\tilde{\kappa}^{XZ}_{o+}$-1.1E-4 $\tilde{\kappa}^{XY}_{o+}$
$SS_{\omega_\oplus}C_{2\Omega_\oplus}$	$-F_1\beta^2_\oplus \sin(2\eta)\sin(\chi)\tilde{\kappa}_{tr}$	-2E-9
$SC^0_{\omega_\oplus}$	$-4F_1 \sin(\chi)\tilde{\kappa}^{XZ}_{e-}$	-1.1
$SC_{\omega_\oplus}S_{\Omega_\oplus}$	$4F_2\beta_\oplus \sin(\chi)\tilde{\kappa}^{XY}_{o+}$	1.2E-4
$SC_{\omega_\oplus}C_{\Omega_\oplus}$	$4F_2\beta_\oplus \sin(\eta)\sin(\chi)\tilde{\kappa}^{YZ}_{o+}$	4.8E-5
$SC_{\omega_\oplus}S_{2\Omega_\oplus}$	$2F_1\beta^2_\oplus \sin(\eta)\sin(\chi)\tilde{\kappa}_{tr}$	2.2E-9
$SS^0_{2\omega_\oplus}$	$-4F_1 \cos(\chi)\tilde{\kappa}^{XY}_{e-}$	-1.5
$SS_{2\omega_\oplus}S_{\Omega_\oplus}$	$-4F_2\beta_\oplus \cos(\chi)\tilde{\kappa}^{XZ}_{o+}$	-1.6E-4
$SS_{2\omega_\oplus}C_{\Omega_\oplus}$	$4F_2\beta_\oplus \cos(\eta)\cos(\chi)\tilde{\kappa}^{YZ}_{o+}$	1.5E-4
$SS_{2\omega_\oplus}S_{2\Omega_\oplus}$	$2F_1\beta^2_\oplus \cos(\eta)\cos(\chi)\tilde{\kappa}_{tr}$	6.6E-9
$SC^0_{2\omega_\oplus}$	$2F_1 \cos(\chi)\left(\tilde{\kappa}^{XX}_{e-} - \tilde{\kappa}^{YY}_{e-}\right)$	7.2E-1
$SC_{2\omega_\oplus}C_{\Omega_\oplus}$	$-4F_2\beta_\oplus \cos(\eta)\cos(\chi)\tilde{\kappa}^{XZ}_{o+}$	-1.5E-4
$SC_{2\omega_\oplus}S_{\Omega_\oplus}$	$-4F_2\beta_\oplus \cos(\chi)\tilde{\kappa}^{YZ}_{o+}$	-1.6E-4
$SC_{2\omega_\oplus}C_{2\Omega_\oplus}$	$0.5F_1\beta^2_\oplus (3+\cos(2\eta))\cos(\chi)\tilde{\kappa}_{tr}$	6.6E-9
C_0	$-3F_1 \sin(\chi)^2\tilde{\kappa}^{ZZ}_{e-}$	-5.1E-1
$CS^0_{\omega_\oplus}$	$4F_1 \sin(\chi)\tilde{\kappa}^{YZ}_{e-}$	8.8E-1
$CS_{\omega_\oplus}C_{\Omega_\oplus}$	$2F_2\beta_\oplus \sin(2\chi)\left(\sin(\eta)\tilde{\kappa}^{XZ}_{o+} - \cos(\eta)\tilde{\kappa}^{XY}_{o+}\right)$	3.9E-5 $\tilde{\kappa}^{XZ}_{o+}$-8.9E-5 $\tilde{\kappa}^{XY}_{o+}$
$CS_{\omega_\oplus}C_{2\Omega_\oplus}$	$2F_1\beta^2_\oplus \sin(\eta)\cos(\eta)\sin(\chi)\cos(\chi)\tilde{\kappa}_{tr}$	1.6E-9
$CC^0_{\omega_\oplus}$	$4F_1 \sin(\chi)\tilde{\kappa}^{XZ}_{e-}$	8.8E-1
$CC_{\omega_\oplus}S_{\Omega_\oplus}$	$2F_2\beta_\oplus \sin(2\chi)\tilde{\kappa}^{XY}_{o+}$	9.7E-5
$CC_{\omega_\oplus}C_{\Omega_\oplus}$	$-2F_2\beta_\oplus \sin(2\chi)\sin(\eta)\tilde{\kappa}^{YZ}_{o+}$	-3.8E-5
$CC_{\omega_\oplus}S_{2\Omega_\oplus}$	$-F_1\beta^2_\oplus \sin(\eta)\sin(2\chi)\tilde{\kappa}_{tr}$	-1.7E-9
$CS^0_{2\omega_\oplus}$	$-F_1 (3+\cos(2\chi))\tilde{\kappa}^{XY}_{e-}$	-1.5
$CS_{2\omega_\oplus}C_{\Omega_\oplus}$	$F_2\beta_\oplus (3+\cos(2\chi))\cos(\eta)\tilde{\kappa}^{YZ}_{o+}$	1.5E-4
$CC^0_{2\omega_\oplus}$	$-0.5F_1 (3+\cos(2\chi))\left(\tilde{\kappa}^{XX}_{e-} - \tilde{\kappa}^{YY}_{e-}\right)$	-7.4E-1
$CC_{2\omega_\oplus}C_{\Omega_\oplus}$	$F_2\beta_\oplus (3+\cos(2\chi))\cos(\eta)\tilde{\kappa}^{XZ}_{o+}$	1.5E-4
$CC_{2\omega_\oplus}S_{\Omega_\oplus}$	$-F_2\beta_\oplus (3+\cos(2\chi))\tilde{\kappa}^{YZ}_{o+}$	-1.6E-4
$CC_{2\omega_\oplus}C_{2\Omega_\oplus}$	$0.13F_1\beta^2_\oplus (3+\cos(2\eta))(3+\cos(2\chi))\tilde{\kappa}_{tr}$	6.8E-9

Table 1 | Bounds on non-birefringent photon-sector coefficients of the minimal SME.

Coefficient	Bound (Error)
$\tilde{\kappa}_{e-}^{XY}$	−0.7 (1.6)
$\tilde{\kappa}_{e-}^{XZ}$	−5.5 (4.0)
$\tilde{\kappa}_{e-}^{YZ}$	−1.9 (3.2)
$\tilde{\kappa}_{e-}^{XX} - \tilde{\kappa}_{e-}^{YY}$	−1.5 (3.4)
$\tilde{\kappa}_{e-}^{ZZ}$	−286 (279)
$\tilde{\kappa}_{o+}^{XY}$	−3.0 (3.4)
$\tilde{\kappa}_{o+}^{XZ}$	0.2 (1.7)
$\tilde{\kappa}_{o+}^{YZ}$	−2.0 (1.6)
$\tilde{\kappa}_{tr}$	−6.0 (4.0)

SME, standard model extension.
Errors are standard 1σ of statistical origin. Values for $\tilde{\kappa}_{e-}$ are given in 10^{-18}, $\tilde{\kappa}_{o+}$ in 10^{-14} and $\tilde{\kappa}_{tr}$ in 10^{-10}.

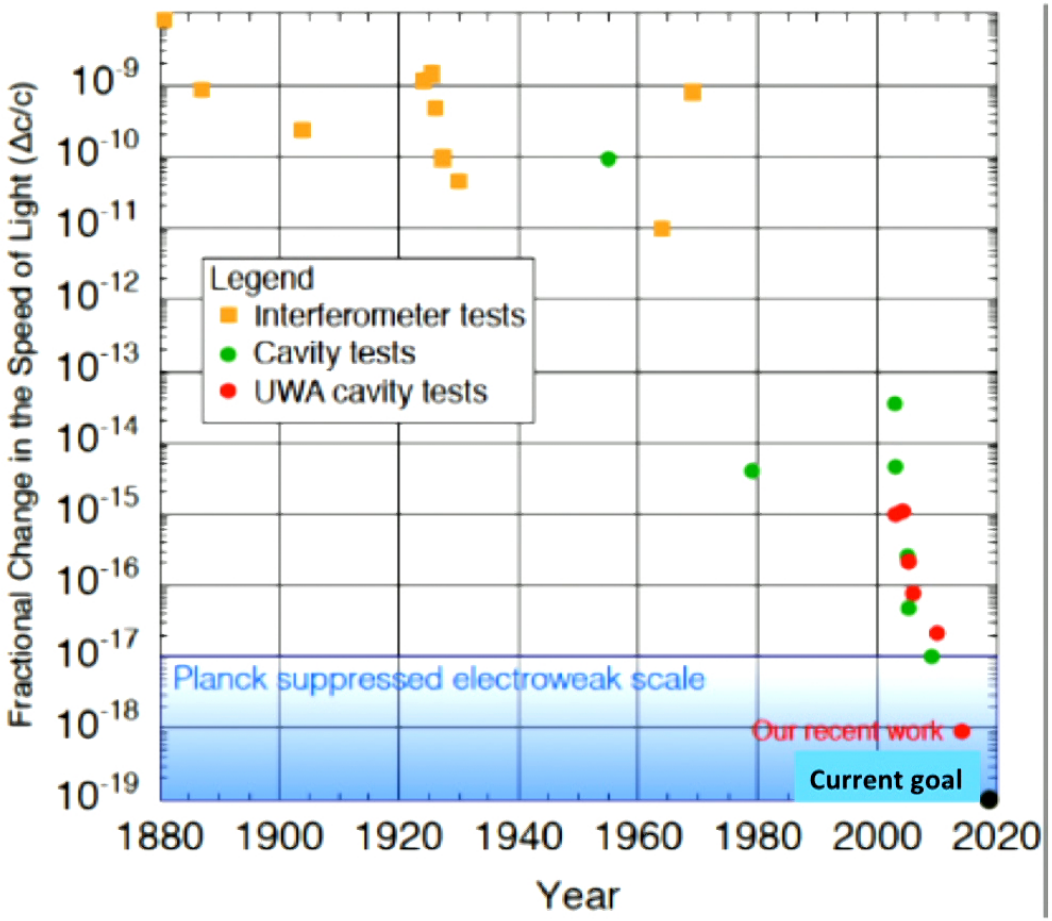
Fractional Change in the Speed of Light (Δc/c)
10-9
10-10
10-11
10-12
10-13
10-14
10-15
10-16
10-17
10-18
10-19
Legend
Interferometer tests
Cavity tests
UWA cavity tests
Planck suppressed electroweak scale
Our recent work
Current goal
1880
1900
1920
1940
1960
1980
2000
2020
Year

Back to Phonons

First Experiment (PRX) in Berkeley Labs (Müller)

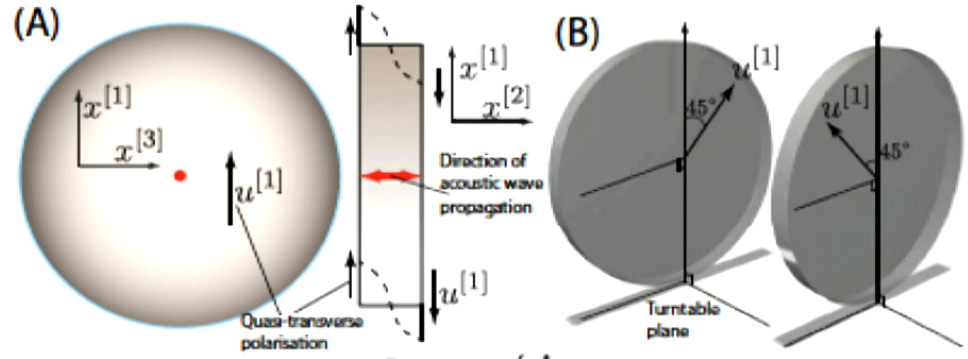

$$(\delta\nu/\nu) = -\tfrac{1}{2}\delta m/m$$

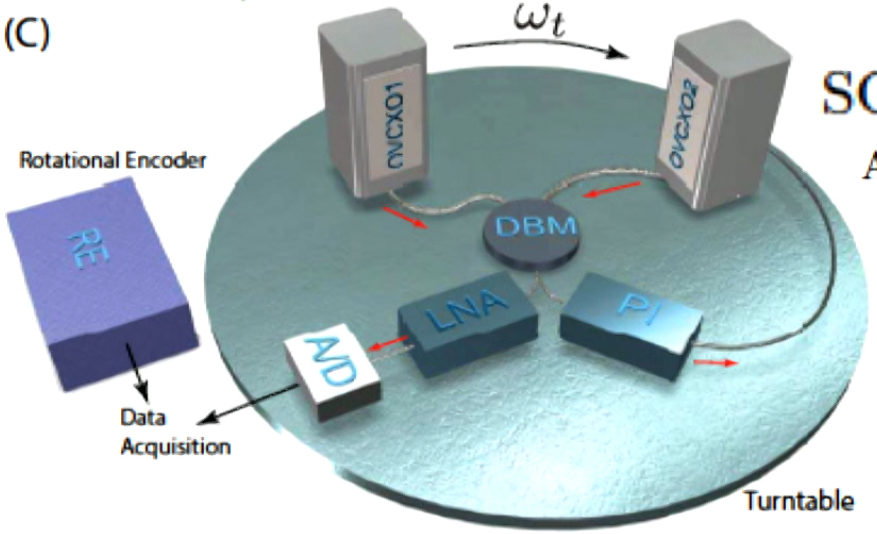

SC-10

Alan variance of 2×10^{-12} at 1 s

$$\omega_t = 2\pi \times 0.36\,\mathrm{Hz}$$

Professional Instruments, model 10R-606

The experiment is in principle sensitive to any Lorentz violation that changes the inertial masses of protons and neutrons.

TABLE III: Signal components for an experiment with two rotating crystal oscillators compared against one another. Components suppressed by $\beta_\oplus^2$ and higher powers have been omitted. These coefficients are to be inserted in Eq. (9) and are multiplied by 1/8 to give the frequency change.

l,m,n	cos	sin
DC	$-4c_Q^{\mathrm{T}}\cos(2\theta)$	
2,-2,-1	$(\cos\eta-1)(\cos\chi-1)^2c_{TY}^{\mathrm{T}}\beta_\oplus$	$(\cos\eta-1)(\cos\chi-1)^2c_{TX}^{\mathrm{T}}\beta_\oplus$
2,-2,0	$2(\cos\chi-1)^2c_M^{\mathrm{T}}$	0
2,-2,1	$(1+\cos\eta)(-1+\cos\chi)^2c_{TY}^{\mathrm{T}}\beta_\oplus$	$(1+\cos\eta)(\cos\chi-1)^2c_{TX}^{\mathrm{T}}\beta_\oplus$
2,-1,-1	$2(\cos\chi-1)c_{TX}^{\mathrm{T}}\sin\eta\sin\chi\beta_\oplus$	$2(1-\cos\chi)((\cos\eta-1)c_{TZ}^{\mathrm{T}}+c_{TY}^{\mathrm{T}}\sin\eta)\sin\chi\beta_\oplus$
2,-1,0	$4(\cos\chi-1)c_Y^{\mathrm{T}}\sin\chi$	$4(\cos\chi-1)c_X^{\mathrm{T}}\sin\chi$
2,-1,1	$2(\cos\chi-1)c_{TX}^{\mathrm{T}}\sin\eta\sin\chi\beta_\oplus$	$2(1-\cos\chi)(c_{TZ}^{\mathrm{T}}+\cos\eta c_{TZ}^{\mathrm{T}}+c_{TY}^{\mathrm{T}}\sin\eta)\sin\chi\beta_\oplus$
2,0,-1	$2\sin^2\chi(\cos\eta c_{TY}^{\mathrm{T}}-2c_{TZ}^{\mathrm{T}}\sin\eta)\beta_\oplus$	$2\sin^2\chi c_{TX}^{\mathrm{T}}\beta_\oplus$
2,0,0	$-4\sin^2\chi c_Q^{\mathrm{T}}$	0
2,0,1	$2\sin^2\chi(\cos\eta c_{TY}^{\mathrm{T}}-2c_{TZ}^{\mathrm{T}}\sin\eta)\beta_\oplus$	$-2\sin^2\chi c_{TX}^{\mathrm{T}}\beta_\oplus$
2,1,-1	$2(1+\cos\chi)c_{TX}^{\mathrm{T}}\sin\eta\sin\chi\beta_\oplus$	$2(1+\cos\chi)(c_{TZ}^{\mathrm{T}}+\cos\eta c_{TZ}^{\mathrm{T}}+c_{TY}^{\mathrm{T}}\sin\eta)\sin\chi\beta_\oplus$
2,1,0	$-4(1+\cos\chi)c_Y^{\mathrm{T}}\sin\chi$	$-4(1+\cos\chi)c_X^{\mathrm{T}}\sin\chi$
2,1,1	$2(1+\cos\chi)c_{TX}^{\mathrm{T}}\sin\eta\sin\chi\beta_\oplus$	$2(1+\cos\chi)((-1+\cos\eta)c_{TZ}^{\mathrm{T}}+c_{TY}^{\mathrm{T}}\sin\eta)\sin\chi\beta_\oplus$
2,2,-1	$(1+\cos\eta)(1+\cos\chi)^2c_{TY}^{\mathrm{T}}\beta_\oplus$	$-(1+\cos\eta)(1+\cos\chi)^2c_{TX}^{\mathrm{T}}\beta_\oplus$
2,2,0	$2c_-^{\mathrm{T}}(1+\cos\chi)^2$	$2(1+\cos\chi)^2c_Z^{\mathrm{T}}$
2,2,1	$(\cos\eta-1)(1+\cos\chi)^2c_{TY}^{\mathrm{T}}\beta_\oplus$	$(1-\cos\eta)(1+\cos\chi)^2c_{TX}^{\mathrm{T}}\beta_\oplus$

$$\frac{\delta\nu}{\nu}=\frac{1}{8}\sum_{l,m,n}\left(C_{lmn}\cos\omega_{lmn}T+S_{lmn}\sin\omega_{lnm}T\right), \quad (9)$$

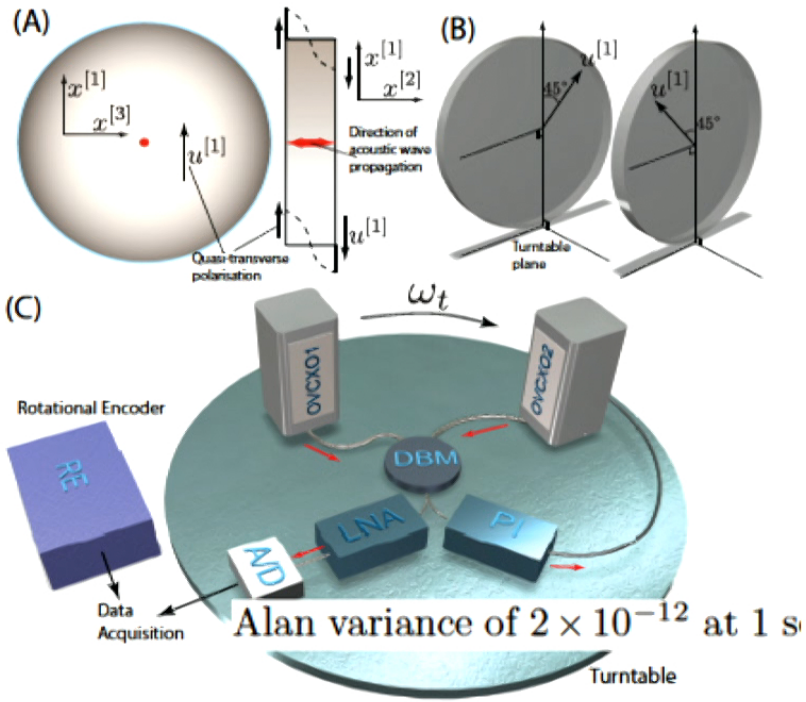
(A)
$x^{[1]}$
$x^{[3]}$
$u^{[1]}$
Quasi-transverse polarisation
$x^{[1]}$
$x^{[2]}$
Direction of acoustic wave propagation
$u^{[1]}$
(B)
$u^{[1]}$
45°
$u^{[1]}$
45°
Turntable plane
(C)
ω_t
OVCXO1
OVCXO2
Rotational Encoder
RE
DBM
LNA
PI
AD
Data Acquisition
Alan variance of 2×10^{-12} at 1 s
Turntable

120 h = 5 days

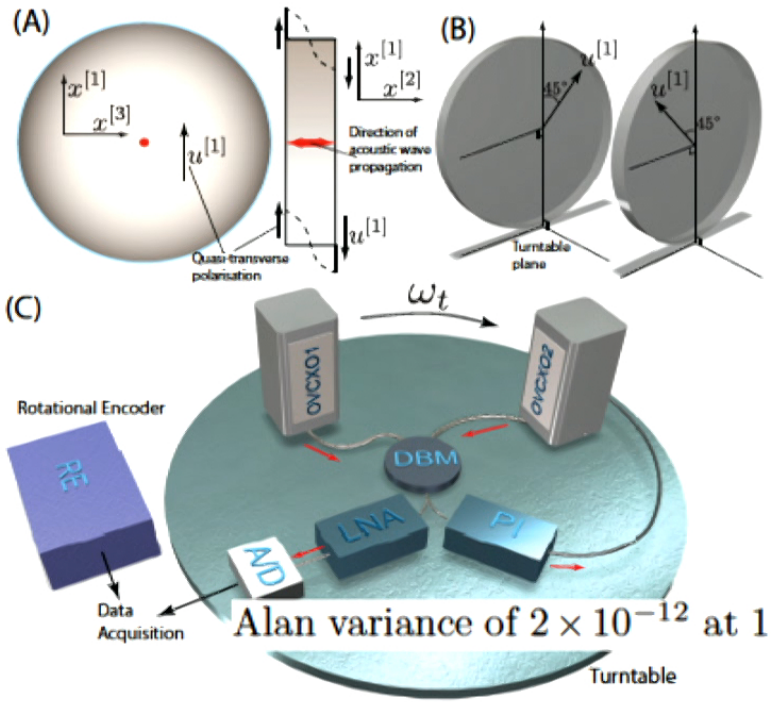

Alan variance of 2×10^{-12} at 1 s

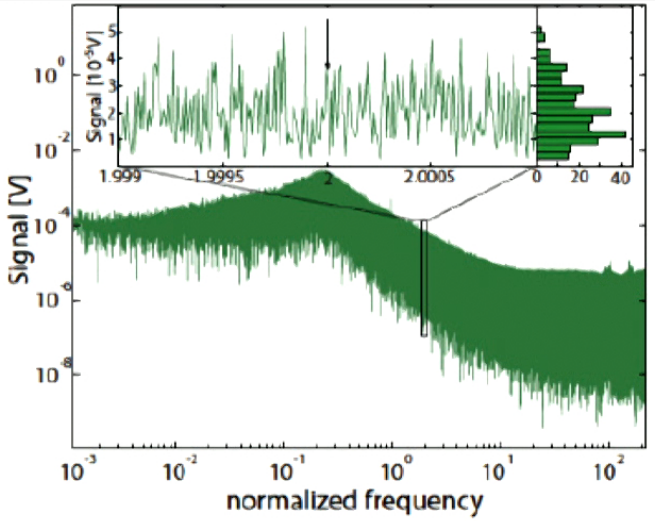

FIG. 3: Fourier transform of 120 hours of data.

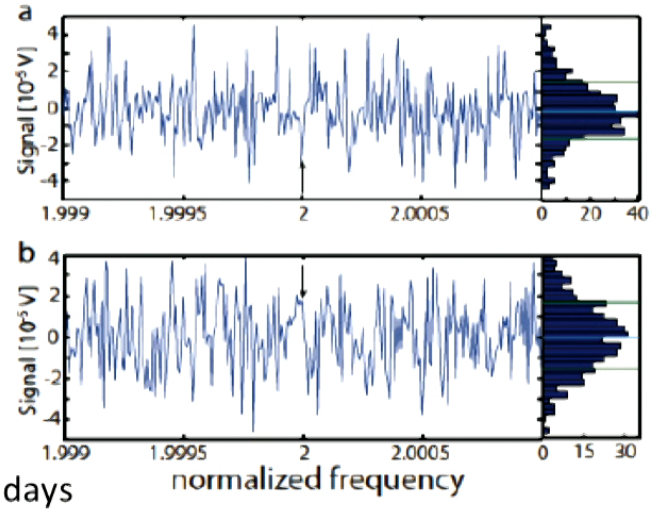

120 h = 5 days

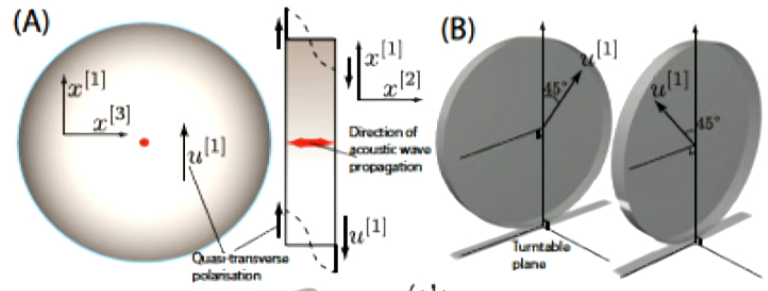

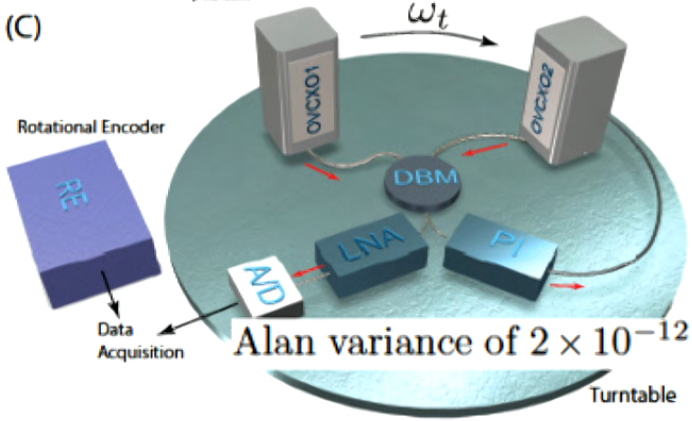

Alan variance of 2×10^{-12} at 1 s

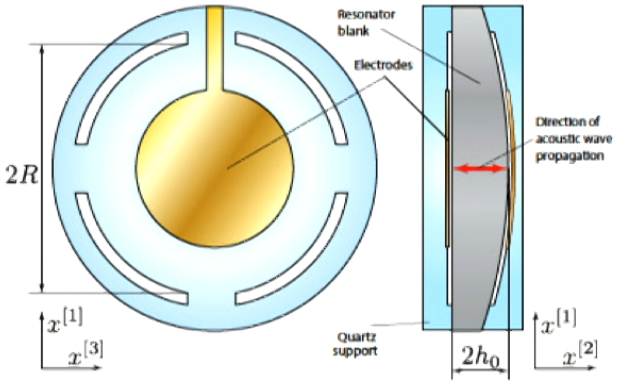

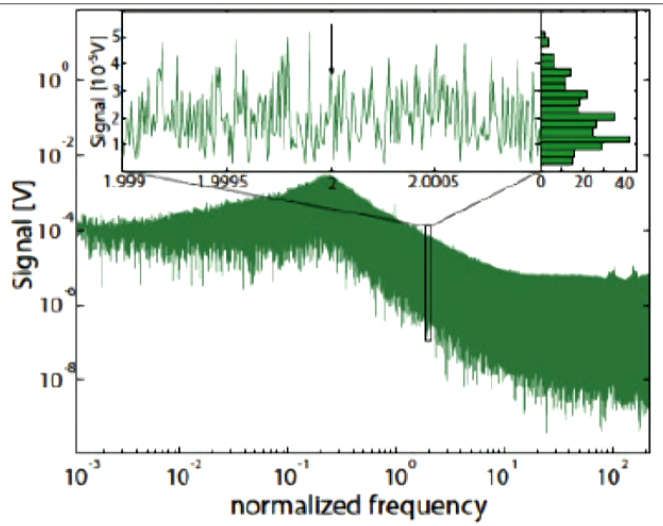

FIG. 3: Fourier transform of 120 hours of data.

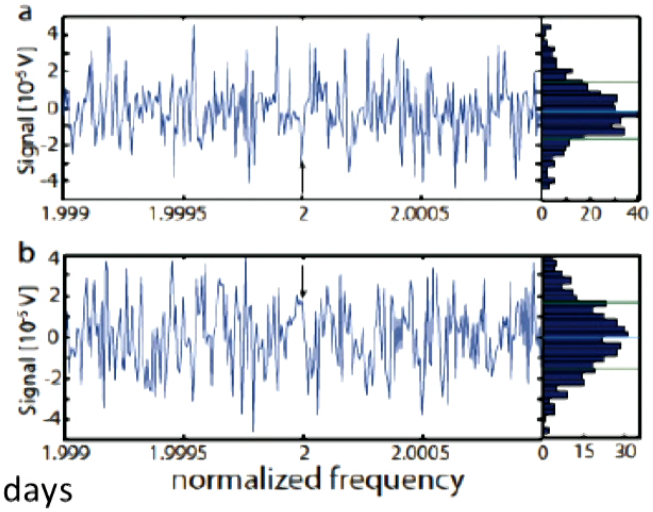

120 h = 5 days

Limit the most weakly constrained mode of neutron-sector violations (as described by the Standard Model Extension, SME)

$$\tilde{c}_Q = (-1.8 \pm 2.2) \times 10^{-14}\,\mathrm{GeV}$$

$$c^{\mathrm{T}}_{\mu\nu} = \frac{1}{m^{\mathrm{T}}} \sum_{\mathrm{w}} n^{\mathrm{w}} m^{\mathrm{w}} c^{\mathrm{w}}_{\mu\nu}, \quad m^{\mathrm{T}} = \sum_{\mathrm{w}} n^{\mathrm{w}} m^{\mathrm{w}}$$

$$\begin{aligned}
\tilde{c}^{w}_{Q} &= m^{w}(c^{w}_{XX} + c^{w}_{YY} - 2c^{w}_{ZZ}),\\
\tilde{c}^{w}_{-} &= m^{w}(c_{XX} - c_{YY}),\\
\tilde{c}^{w}_{J} &= m^{w}|\varepsilon_{JKL}|c_{KL},\\
\tilde{c}^{w}_{TJ} &= m^{w}(c_{TJ} + c_{JT}),\\
\tilde{c}^{w}_{TT} &= m^{w} c_{TT}.
\end{aligned}$$

Voltage Noise Measurements with Interferometric Readout System

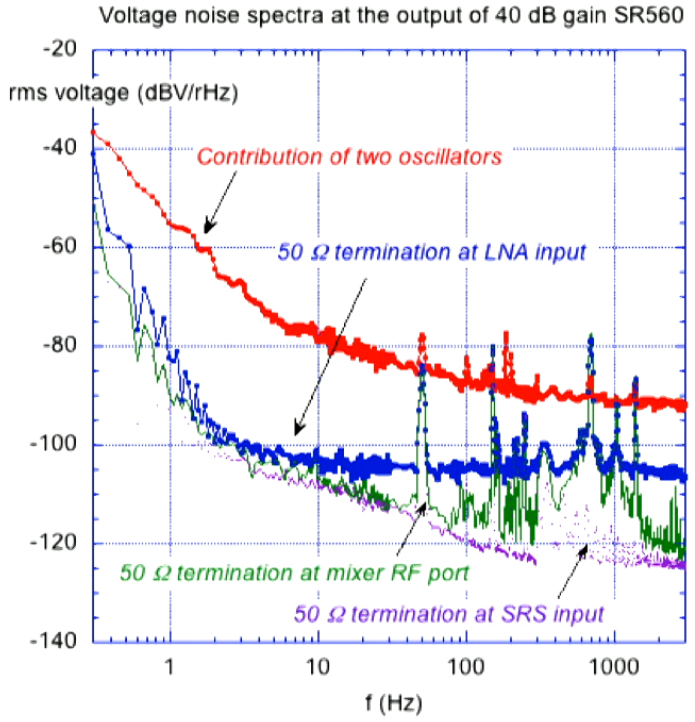

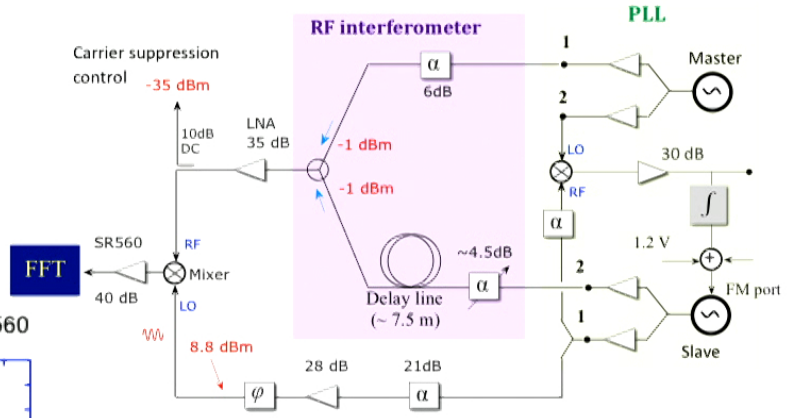

Two Oscillator Measurement Rotating Quartz

Interferometric Phase Detector IPD [Vrms/rad]
(~ 40 dB higher than a conventional mixer based phase detector)

In[4]:= **IPD = 18**

Out[4]= 18

Gain on output to data collection, measurement

In[5]:= **Gain = N[10^(30/20)]**

Out[5]= 31.6228

Volts/Rad Sensitivity

In[6]:= **dudϕ = IPD * Gain**

Out[6]= 569.21

Phase Noise Spectrum of 5 MHz Oscilloquartz oscillator

Phase noise (BW = 1 Hz) Options

Frequencies	5 MHz		10 MHz	
Standard / Option L	Standard	Option L	Standard	Option L
Phase noise 1 Hz	- 125 dBc	- 130 dBc	-118 dBc	- 122 dBc
10 Hz	- 145 dBc	- 145 dBc	-137 dBc	- 137 dBc
100 Hz	- 153 dBc	- 153 dBc	-143 dBc	- 143 dBc
1'000 Hz	- 156 dBc	- 156 dBc	-145 dBc	- 145 dBc
10'000 Hz	- 156 dBc	- 156 dBc	- 145 dBc	- 145 dBc

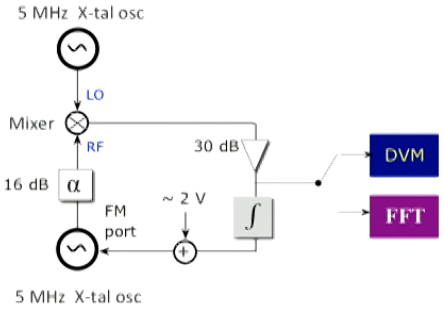

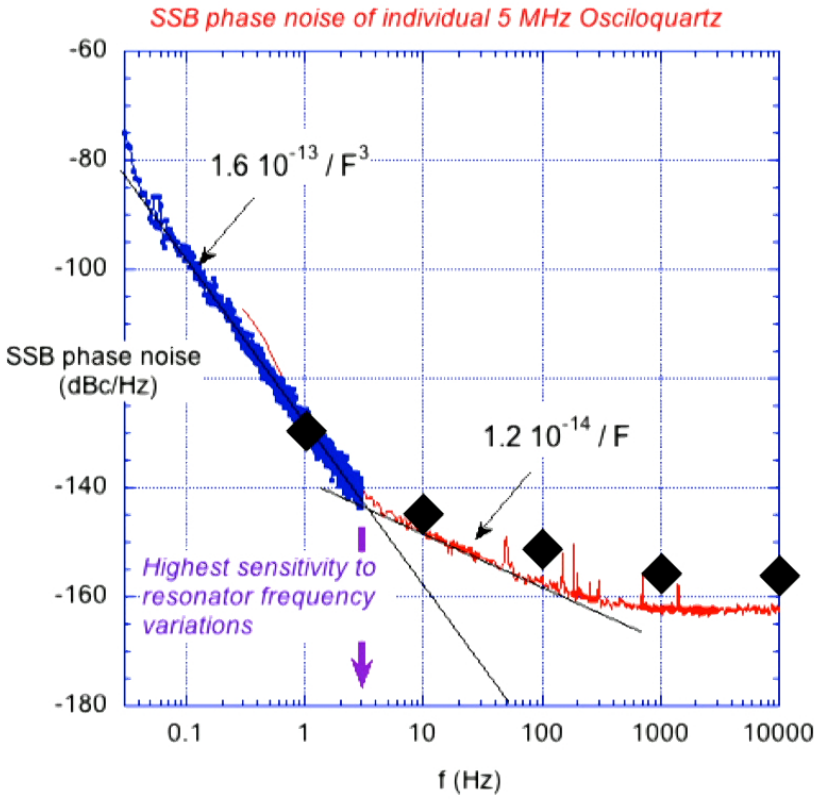

Effect of Rotation on Oscillator Frequency: 1

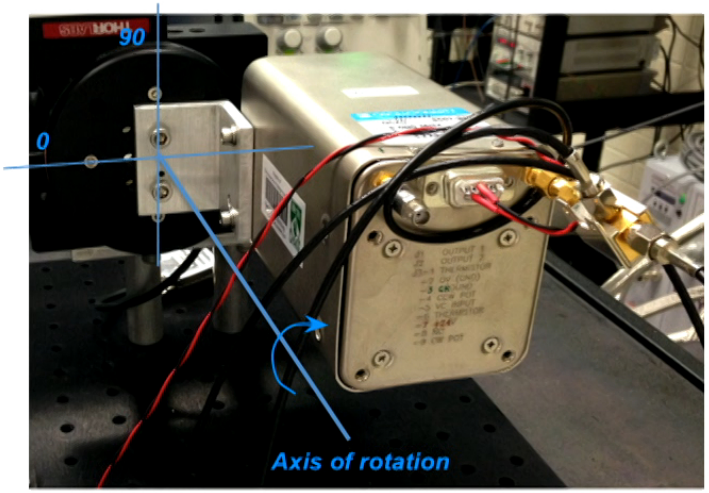

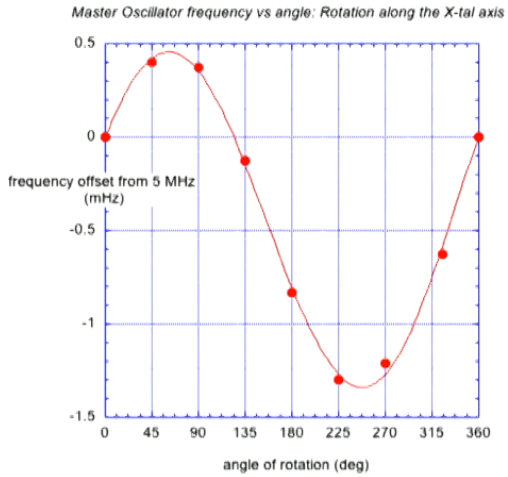

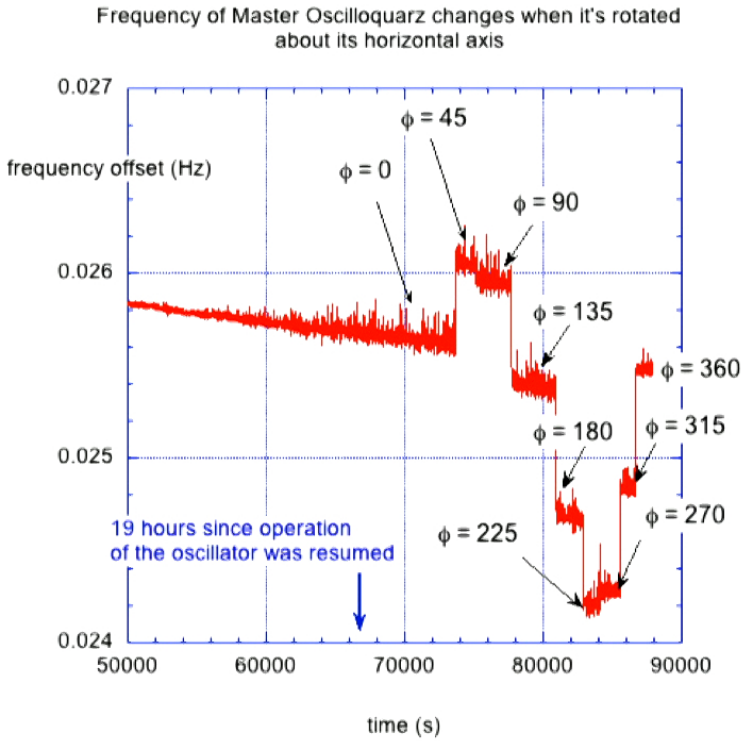

Effect of Rotation on Oscillator Frequency: 2

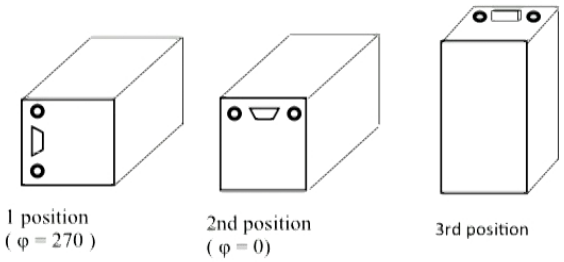

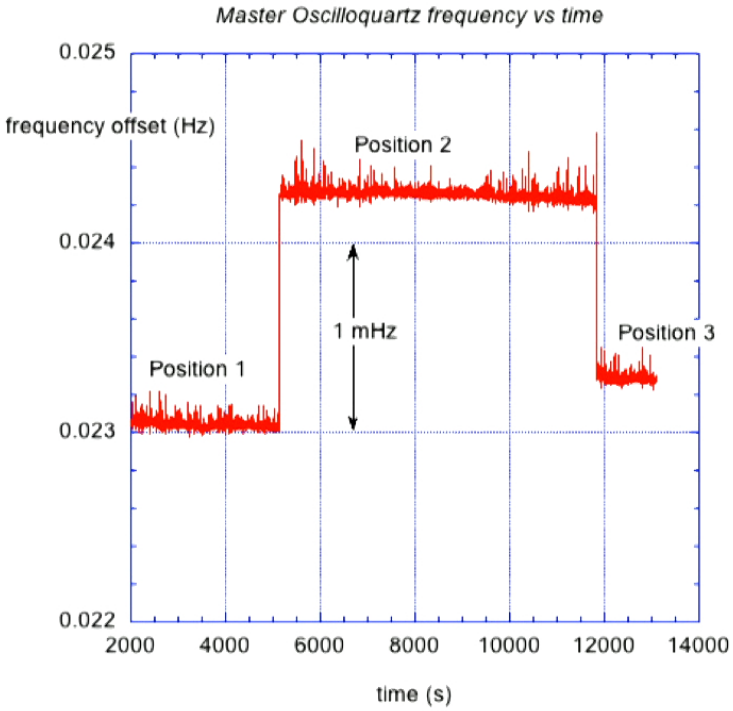

Rotating Quartz Oscillators

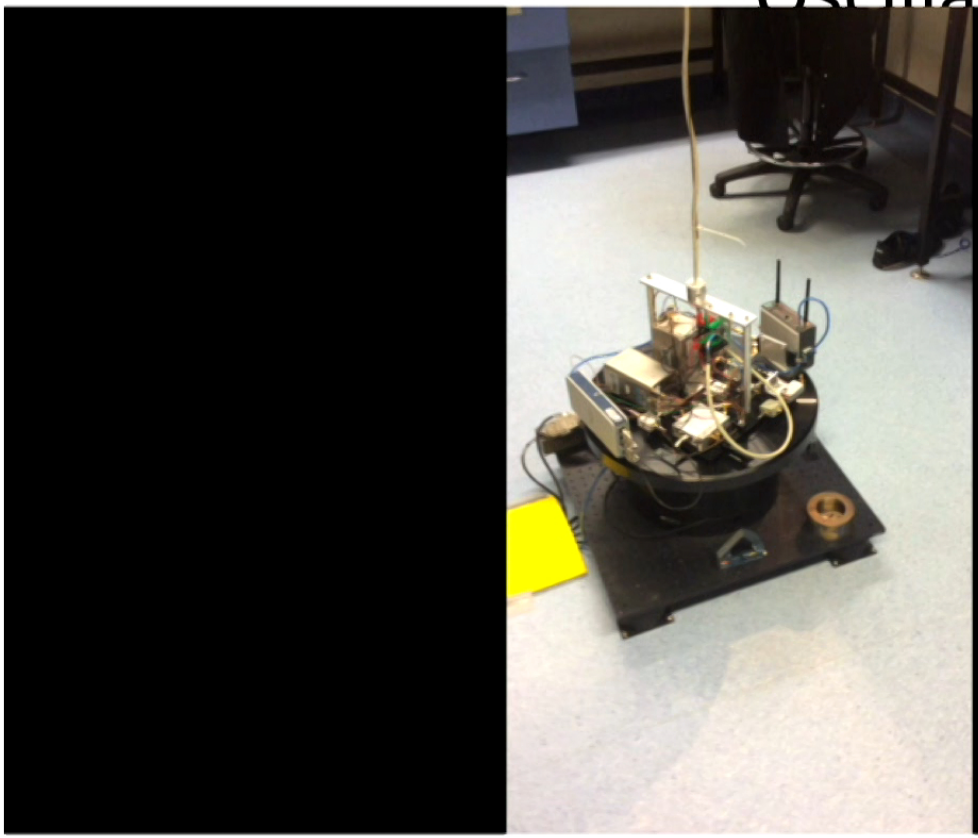

Rotating Quartz Oscillators

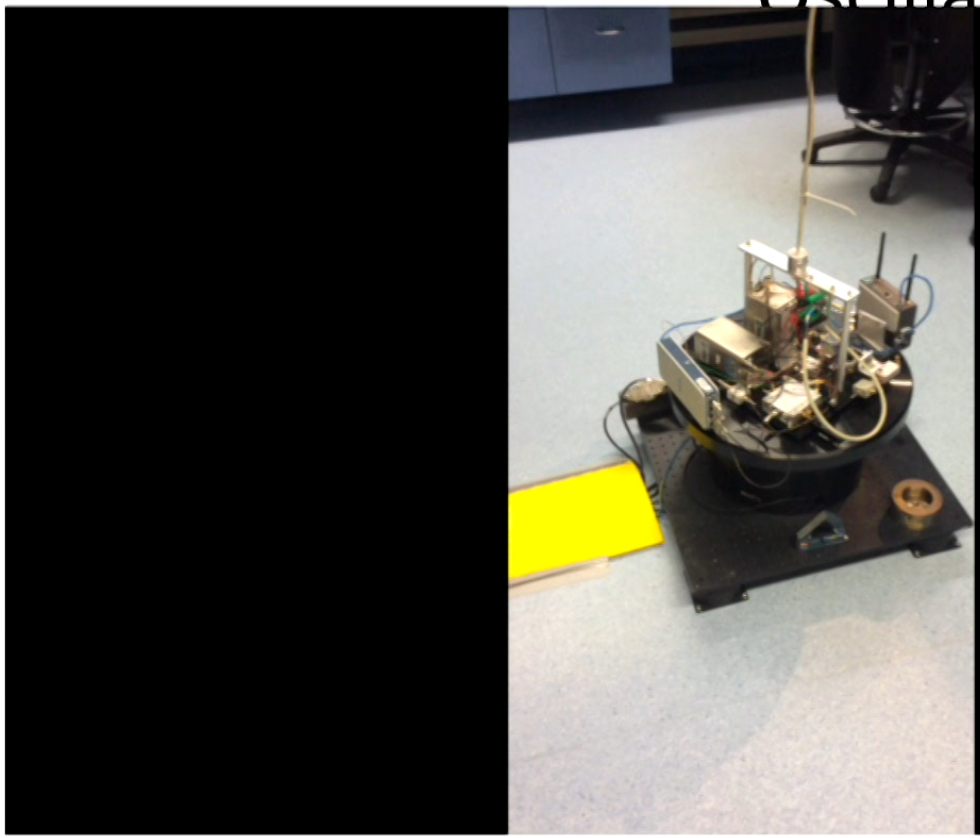

Rotating Quartz Oscillators

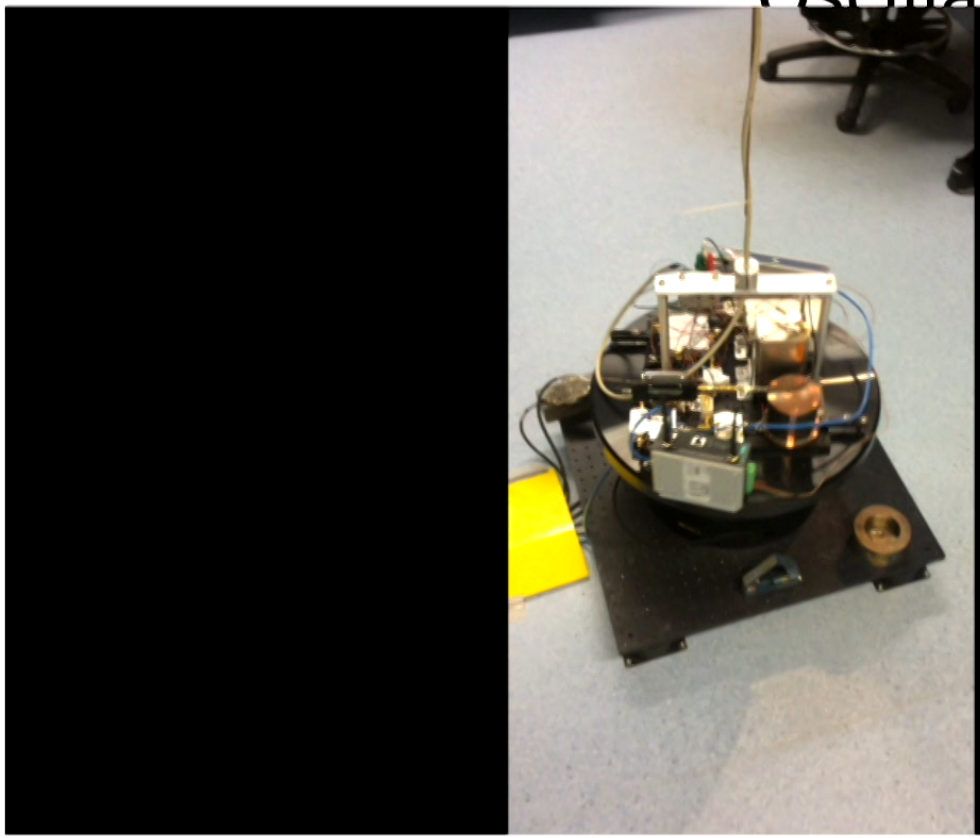

Rotating Quartz Oscillators

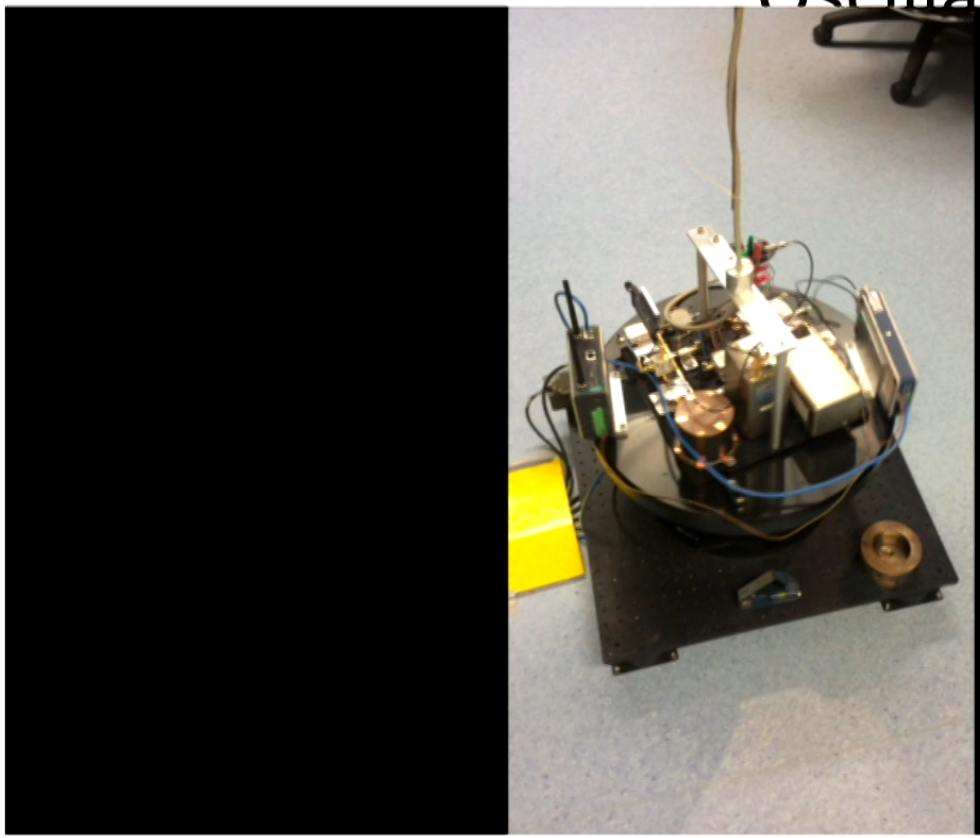

Rotating Quartz Oscillators

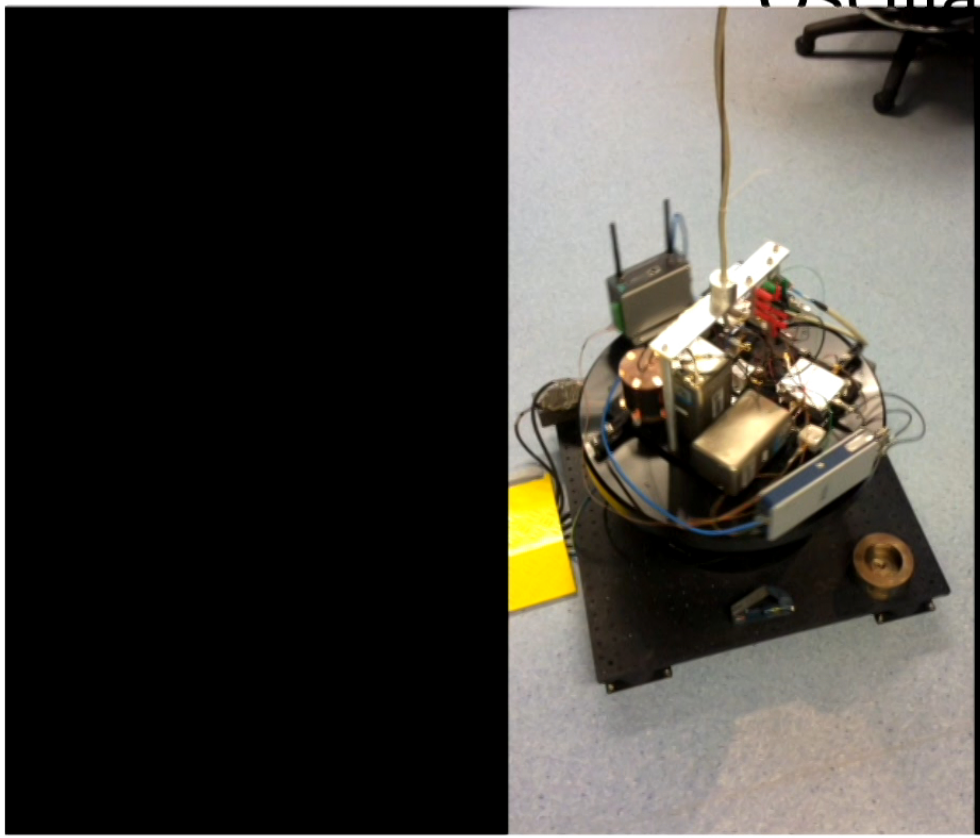

Rotating Quartz Oscillators

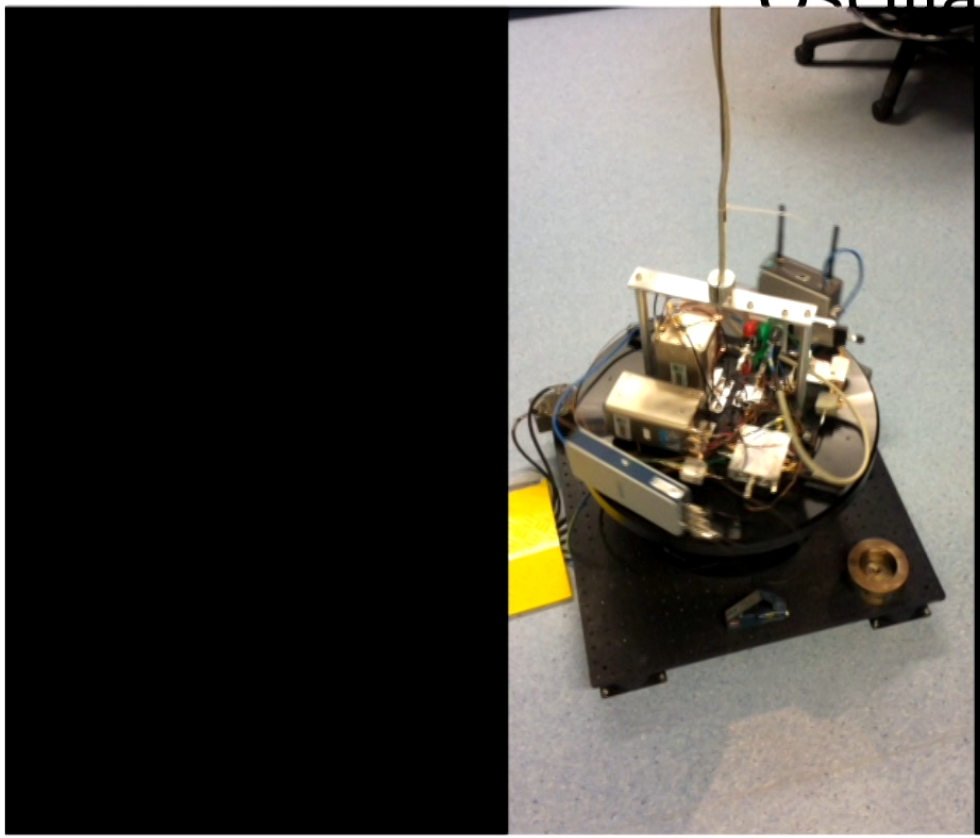

Demodulated Least Square Method

$$\frac{\Delta f}{f} = A + S(t_s)\sin(2\omega_R t_s + \phi) + C(t_s)\cos(2\omega_R t_s + \phi)$$

$$S(t_s) = S_0 + \sum_i S_{s,i}\sin(\omega_i t_s + \phi_i) + S_{c,i}\cos(\omega_i t_s + \phi_i)$$

$$C(t_s) = C_0 + \sum C_{s,i}\sin(\omega_i t_s + \phi_i) + C_{c,i}\cos(\omega_i t_s + \phi_i).$$

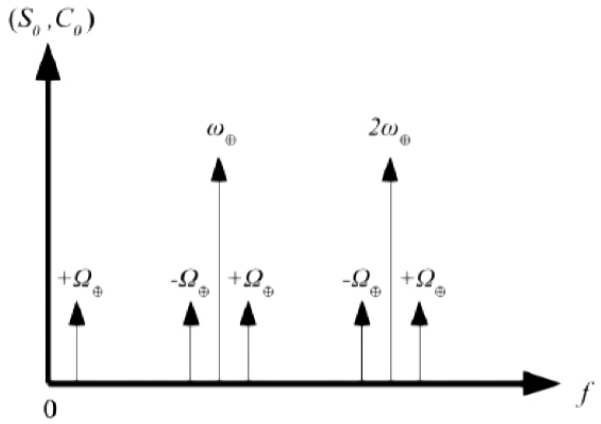

ω_i	C_{C,ω_i}	C_{S,ω_i}
0	$-4\sin^2\chi c_Q^T$	0
$\Omega_\oplus$	$4\sin^2\chi(\cos\eta c_{TY}^T - 2c_{TZ}^T\sin\eta)\beta_\oplus$	$-4\sin^2\chi c_{TX}^T\beta\oplus$
$\omega_\oplus - \Omega_\oplus$	$4\cos\chi c_{TX}^T\sin\eta\sin\chi\beta_\oplus$	$4\cos\chi(c_{TZ}^T + \cos\eta c_{TZ}^T + c_{TY}^T\sin\eta)\times$ $\sin\chi\beta_\oplus$
$\omega_\oplus$	$-8c_Y^T\sin\chi$	$-8\cos\chi c_X^T\sin\chi$
$\omega_\oplus + \Omega_\oplus$	$4\cos\chi c_{TX}^T\sin\eta\sin\chi\beta_\oplus$	$4[(-1+\cos\eta)c_{TZ}^T + \cos\chi c_{TY}^T\sin\eta]\times$ $\sin\chi\beta_\oplus$
$2\omega_\oplus - \Omega_\oplus$	$2(1+\cos\eta)(1+\cos^2\chi)c_{TY}^T\beta_\oplus$	$-2(1+\cos^2\chi)(1+\cos\eta)c_{TX}^T\beta_\oplus$
$2\omega_\oplus$	$2c_-^T(1+\cos\chi)^2 + 2(\cos\chi-1)^2c_M^T$	$2(1+\cos\chi)^2c_Z^T$
$2\omega_\oplus + \Omega_\oplus$	$2(1+\cos^2\chi)(\cos\eta-1)c_{TY}^T\beta_\oplus$	$2(1-\cos\eta)(1+\cos^2\chi)c_{TX}^T\beta_\oplus$

ω_i	S_{C,ω_i}	S_{S,ω_i}
0	0	0
$\Omega_\oplus$	0	0
$\omega_\oplus - \Omega_\oplus$	$4(c_{TZ}^T + \cos\eta c_{TZ}^T + c_{TY}^T\sin\eta)\sin\chi\beta_\oplus$	$-4c_{TX}^T\sin\eta\sin\chi\beta_\oplus$
$\omega_\oplus$	$-8c_X^T\sin\chi$	$8\cos\chi c_Y^T\sin\chi$
$\omega_\oplus + \Omega_\oplus$	$4[\cos\chi(-1+\cos\eta)c_{TZ}^T + c_{TY}^T\sin\eta]\sin\chi\beta_\oplus$	$-4c_{TX}^T\sin\eta\sin\chi\beta_\oplus$
$2\omega_\oplus - \Omega_\oplus$	$-4(1+\cos\eta)\cos\chi c_{TX}^T\beta_\oplus$	$-4(1+\cos\eta)\cos\chi c_{TY}^T\beta_\oplus$
$2\omega_\oplus$	$2(1+\cos\chi)^2c_Z^T$	$-2c_-^T(1+\cos\chi)^2 + 2(\cos\chi-1)^2c_M^T$
$2\omega_\oplus + \Omega_\oplus$	$4(1-\cos\eta)\cos\chi c_{TX}^T\beta_\oplus$	$-4\cos\chi(\cos\eta-1)c_{TY}^T\beta_\oplus$

	run 8	run 9	run 10	run 11
Date	16th March 2017	29th March 2017	23rd May 2017	16th June 2017
Time	5:41:09 am	8:06:14 am	1:30:23 pm	10:57:57 am
ω_R	$360°/s$	$360°/s$	$420°/s$	$320°/s$
Days	13	54	23	63

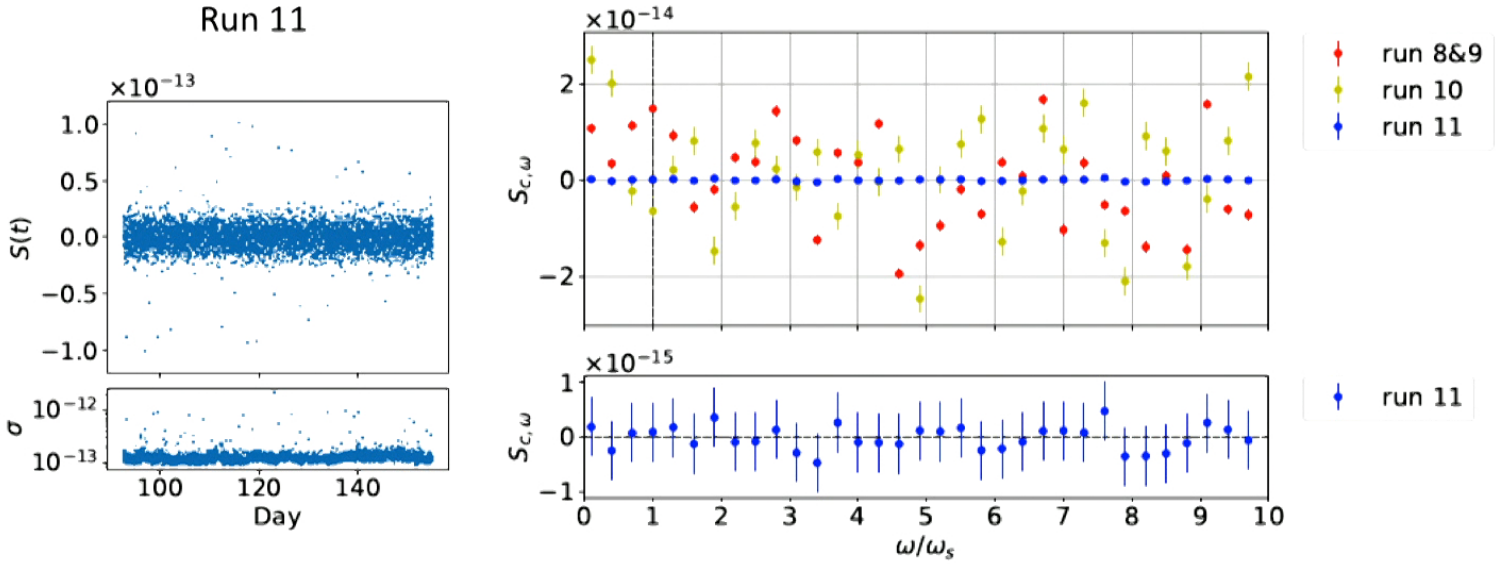

Figure 8: Components for different frequencies in different runs, $N_r = 10$

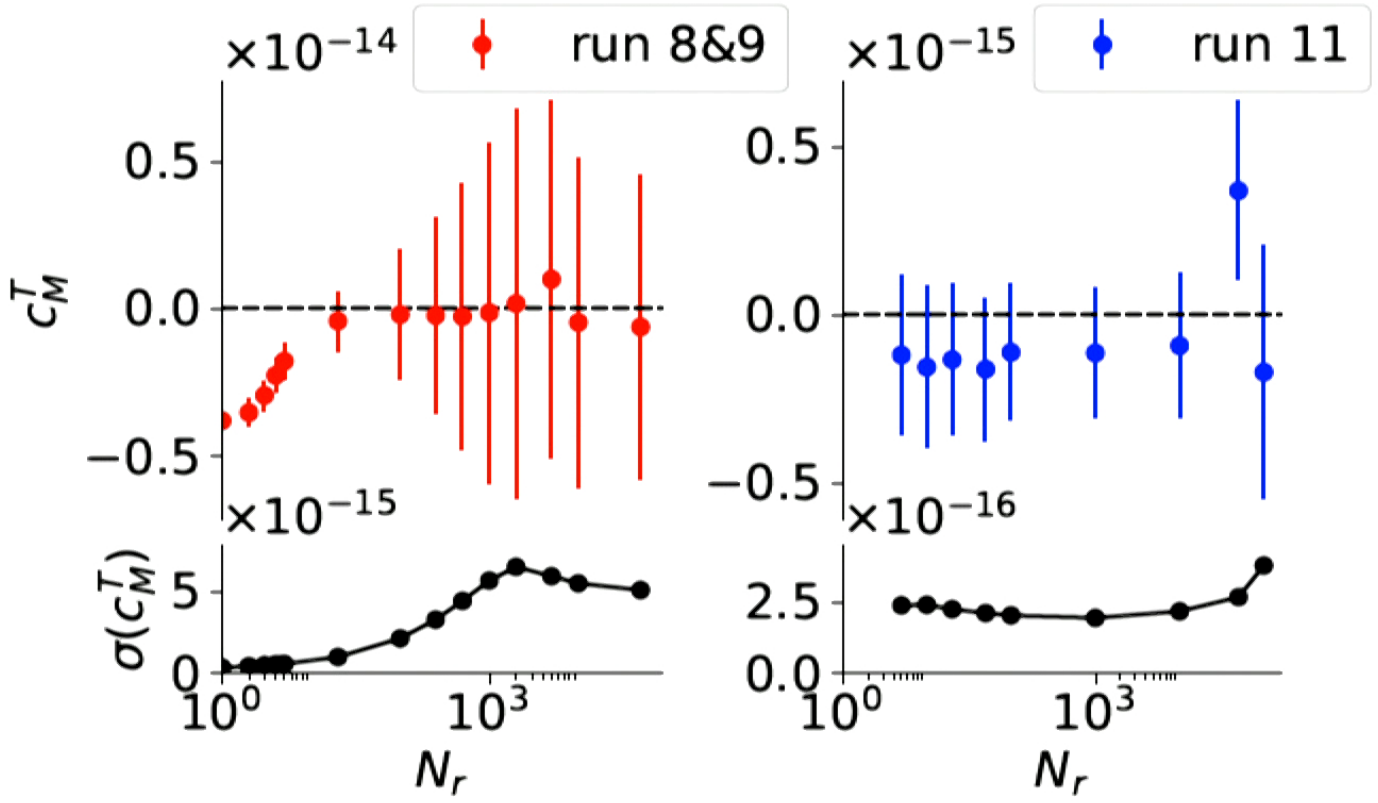

Figure 9: Optimization over the demodulated subset for run 8&9 and run 11.

SME coefficients	result
c_Q^T	$(8 \pm 6) \times 10^{-17}$
c_Y^T	$(-5 \pm 3) \times 10^{-17}$
c_X^T	$(-2 \pm 3) \times 10^{-17}$
c_Z^T	$(-4 \pm 4) \times 10^{-17}$
c_M^T	$(-1 \pm 2) \times 10^{-16}$
c_-^T	$(1 \pm 2) \times 10^{-17}$

Table 6: Demodulated Least Square Fitting result of SME coefficients. Parameter: $N_r = 1000$, run 11.

63 days of data rotation f_R=0.89 Hz (Berkeley 5 days f_R=0.33 Hz) -> factor 5.8 improvement

Stability improvement = 44 -> Expect at least factor of 255 better than in PRX
Get: 300, optimized data anaysis squeezes a bit more.

The ORGAN Experiment

THE UNIVERSITY OF WESTERN AUSTRALIA

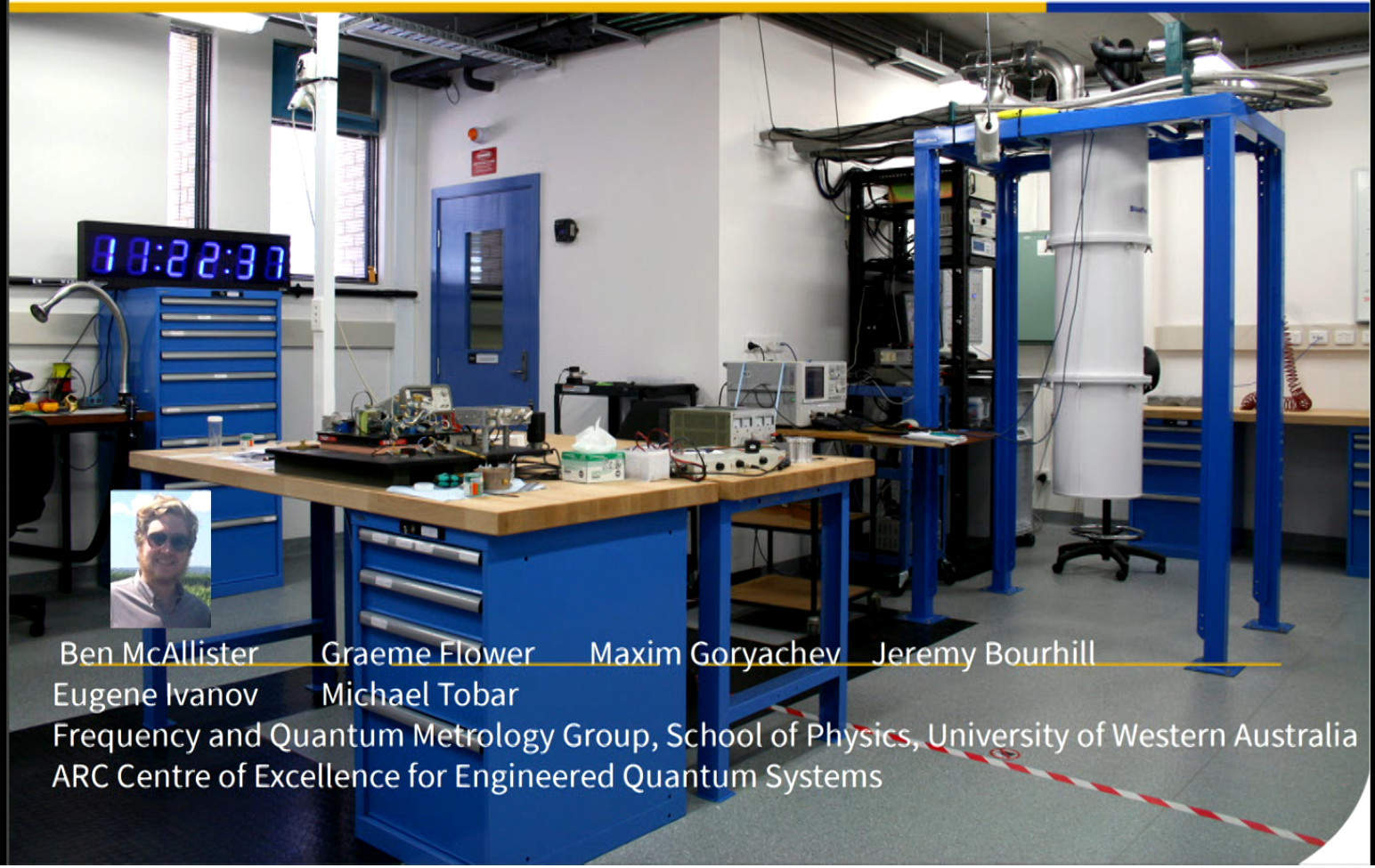

Ben McAllister Graeme Flower Maxim Goryachev Jeremy Bourhill
Eugene Ivanov Michael Tobar
Frequency and Quantum Metrology Group, School of Physics, University of Western Australia
ARC Centre of Excellence for Engineered Quantum Systems

[1] arXiv:1706.00209 [pdf, other]

The ORGAN Experiment: An axion haloscope above 15 GHz

Ben T. McAllister, Graeme Flower, Justin Kruger, Eugene N. Ivanov, Maxim Goryachev, Jeremy Bourhill, Michael E. Tobar

Comments: 6 pages, 5 figures

Subjects: **Instrumentation and Detectors (physics.ins-det)**; High Energy Physics - Experiment (hep-ex)

[2] arXiv:1705.06028 [pdf, other]

Tunable Super-Mode Dielectric Resonators for Axion Haloscopes

Ben T. McAllister, Graeme Flower, Lucas E. Tobar, Michael E. Tobar

Comments: 10 pages, 11 figures. V2: minor updates

Subjects: **Instrumentation and Detectors (physics.ins-det)**; High Energy Physics - Experiment (hep-ex)

[4] arXiv:1703.07207 [pdf, other]

Axion Detection with Cavity Arrays

Maxim Goryachev, Ben T. McAllister, Michael E. Tobar

Subjects: **Instrumentation and Detectors (physics.ins-det)**; General Relativity and Quantum Cosmology (gr-qc); High Energy Physics - Experiment (hep-ex)

The ORGAN Experiment: An axion haloscope above 15 GHz

Ben T. McAllister,[1,*] Graeme Flower,[1] Justin Kruger,[1] Eugene N. Ivanov,[2] Maxim Goryachev,[1] Jeremy Bourhill,[1] and Michael E. Tobar[1,†]

[1] *ARC Centre of Excellence for Engineered Quantum Systems, School of Physics, The University of Western Australia, Crawley 6009, Australia*

[2] *School of Physics, The University of Western Australia, Crawley 6009, Australia*

(Dated: June 2, 2017)

We present first results and future plans for the **O**scillating **R**esonant **G**roup **A**xio**N** (ORGAN) experiment, a microwave cavity axion haloscope situated in Perth, Western Australia designed to probe for high mass axions motivated by several theoretical models. The first stage focuses around 26.6 GHz in order to directly test a claimed result, which suggests axions exist at the corresponding mass of 110 μeV. Later stages will move to a wider scan range of 15-50 GHz ($60 - 210$ μeV). We present the results of the pathfinding run, which sets a limit on $g_{a\gamma\gamma}$ of $2.02 \times 10^{-12}\text{eV}^{-1}$ at 26.531 GHz, or 110 μeV, in a span of 2.5 neV (shaped by the Lorentzian resonance) with 90% confidence. Furthermore, we outline the current design and future strategies to eventually attain the sensitivity to search for well known axion models over the wider mass range.

Axions and WISPs

Weakly **I**nteracting **S**lim **P**articles **A**xion **L**ike **P**articles

Slim = sub-eV

Axions constituting our local galactic halo would have huge number density ~10^{14} cm^{-3}

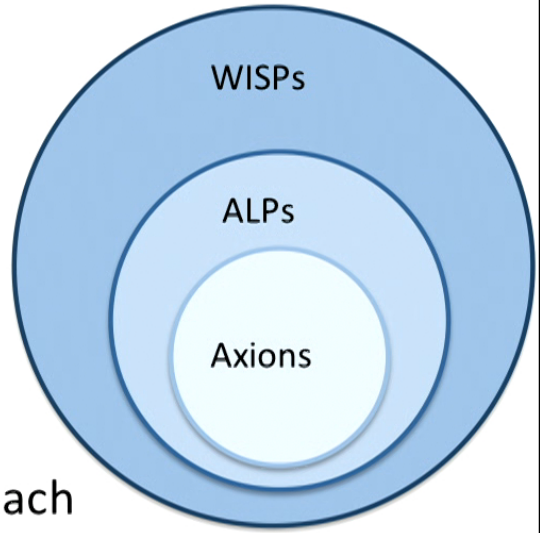

Weakly interacting, small mass,
so offers compelling solutions to:

Dark Matter (i.e. Axions, hidden photons)
Dark Energy (i.e. Chameleons)

Low energy scale dictates experimental approach
(i.e. don't need a particle collider)

WISP searches are *complementary* to WIMP searches

Pierre Sikivie's RF-cavity idea (1983): Axion and electromagnetic fields exchange energy: WISP-Photon Coupling

Pierre Sikivie's RF-cavity idea (1983): Axion and electromagnetic fields exchange energy: WISP-Photon Coupling

WISP-photon coupling provides very important experimental and observational access (with minimal model dependence).

$$\mathcal{L}_{a\gamma\gamma} = -\frac{1}{4} g_{a\gamma}\, a\, F_{\mu\nu}\tilde{F}^{\mu\nu} = g_{a\gamma}\, a\, \vec{E}\cdot\vec{B}$$

$$\frac{\partial\left(\mathbf{E}^2/2\right)}{\partial t} - \mathbf{E}\cdot\left(\nabla\times\mathbf{B}\right) = g_{a\gamma}\dot{a}\left(\mathbf{E}\cdot\mathbf{B}\right)$$

Pierre Sikivie's RF-cavity idea (1983): Axion and electromagnetic fields exchange energy: WISP-Photon Coupling

WISP-photon coupling provides very important experimental and observational access (with minimal model dependence).

$$\mathcal{L}_{a\gamma\gamma} = -\frac{1}{4} g_{a\gamma}\, a F_{\mu\nu}\tilde{F}^{\mu\nu} = g_{a\gamma}\, a\, \vec{E}\cdot\vec{B}$$

$$\frac{\partial\left(\mathbf{E}^2/2\right)}{\partial t} - \mathbf{E}\cdot\left(\nabla\times\mathbf{B}\right) = g_{a\gamma}\dot{a}\left(\mathbf{E}\cdot\mathbf{B}\right)$$

Primakoff Conversion

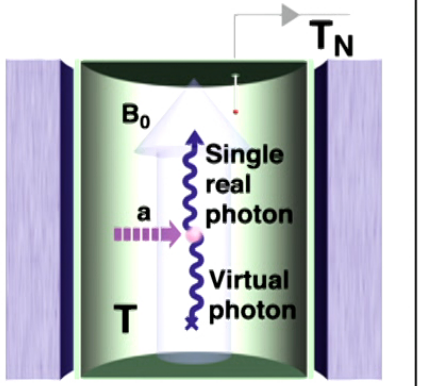

For example, the axion couples to 2 photons:

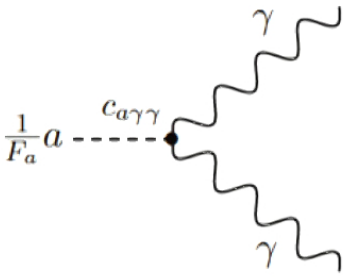

B field can act as 2nd virtual photon to induce axion-photon conversion

Axion mass dictates photon frequency

Want to test / bound $g_{a\gamma\gamma}$

What values of f_a make sense for axion dark matter?

Axion Mass / Photon Coupling

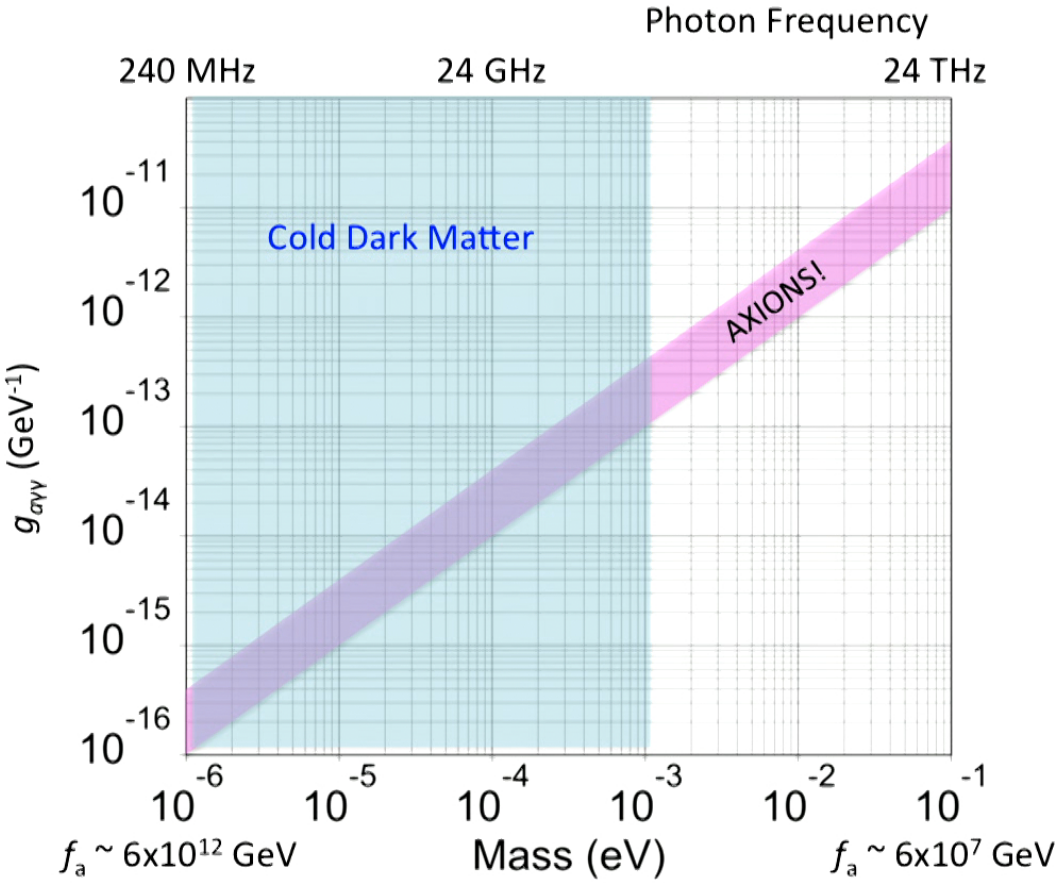

ADMX Gen 2 Science Prospects: Year 1 (0.5 – 1 GHz)

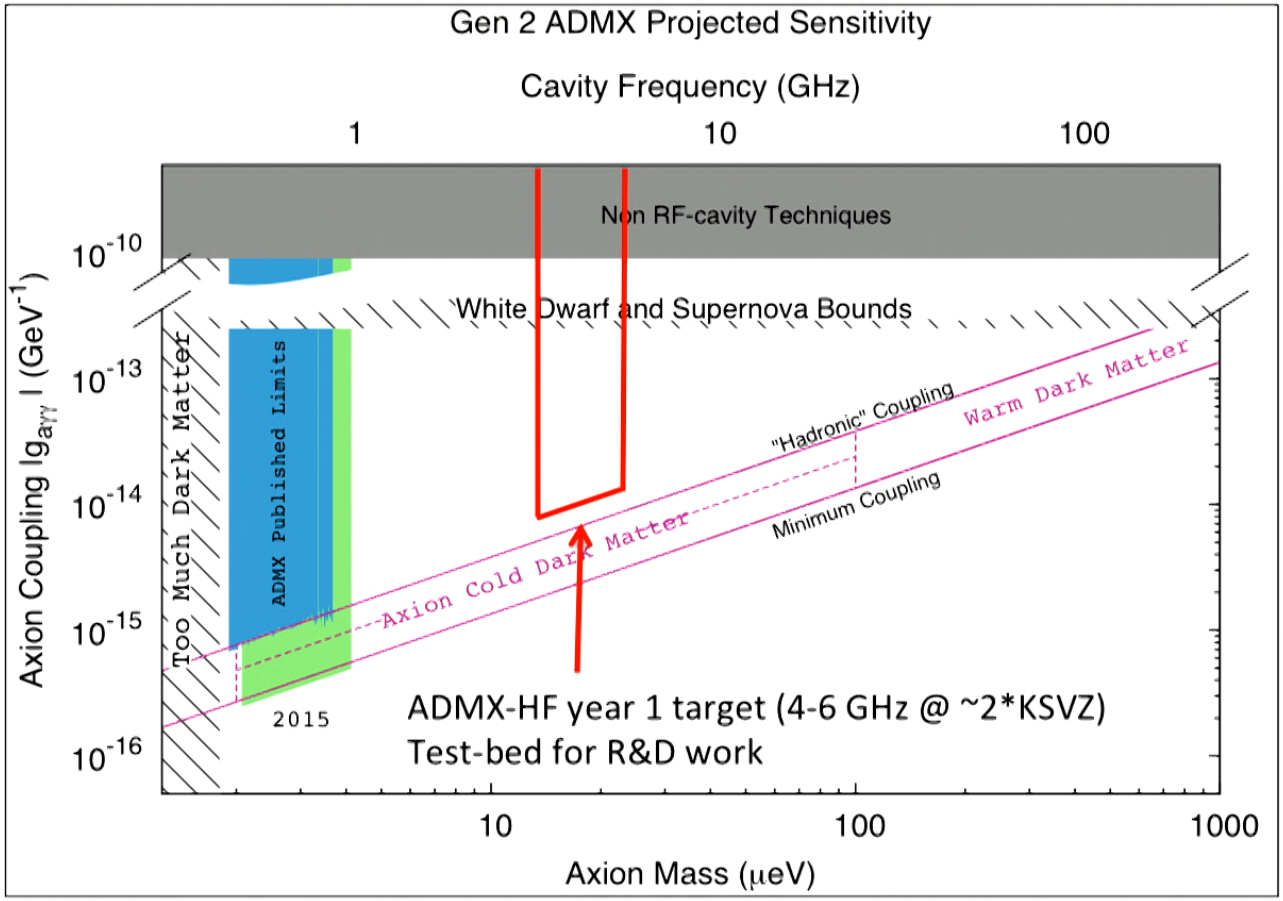

ADMX Gen 2 Science Prospects: Year 1 (0.5 – 1 GHz)

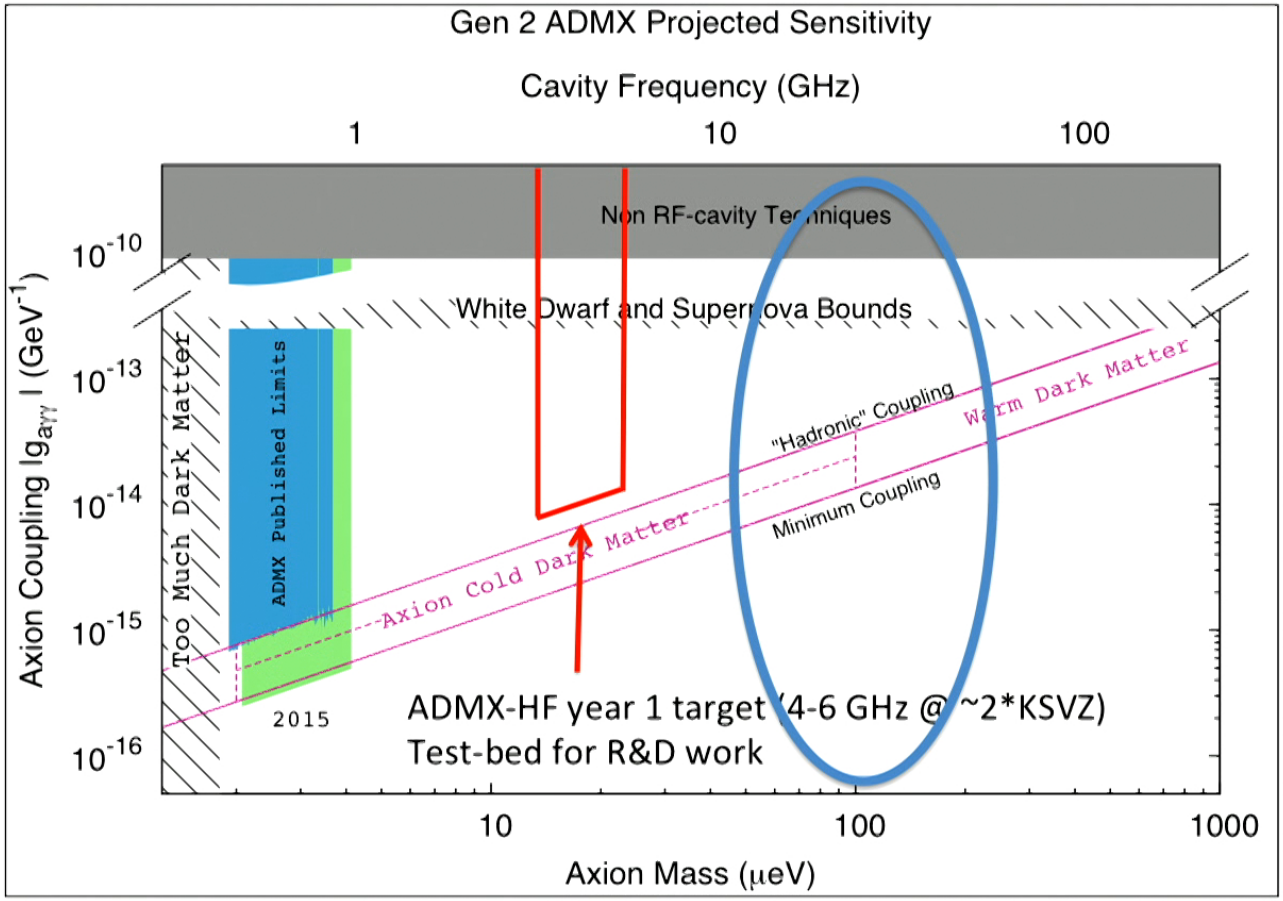

ADMX Gen 2 Science Prospects: Year 1 (0.5 – 1 GHz)

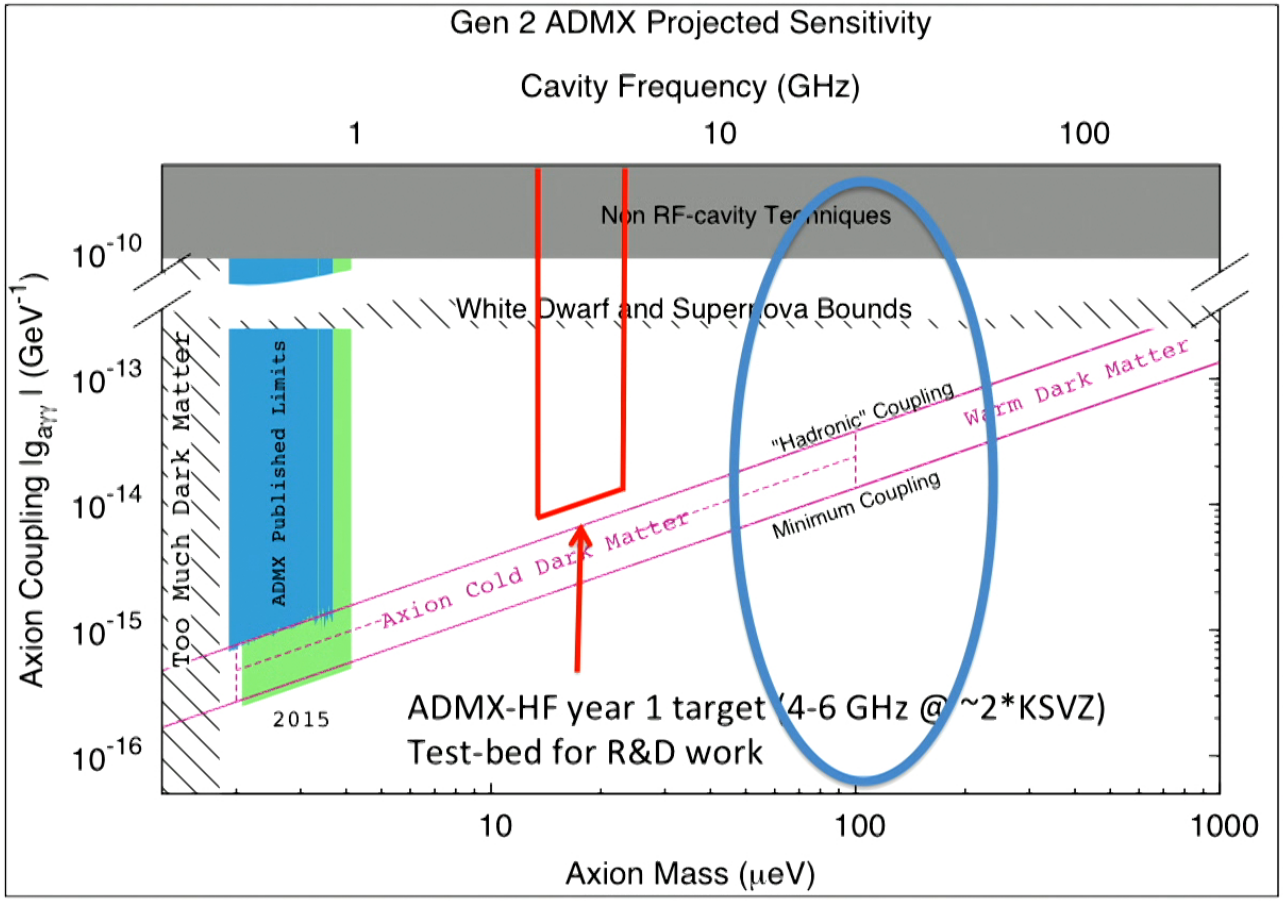

PHYSICAL REVIEW D 94, 042001 (2016)

3D lumped LC resonators as low mass axion haloscopes

Ben T. McAllister,* Stephen R. Parker, and Michael E. Tobar†

ARC Centre of Excellence for Engineered Quantum Systems, School of Physics, The University of Western Australia, 35 Stirling Highway, Crawley 6009, Western Australia, Australia

(Received 18 May 2016; published 11 August 2016)

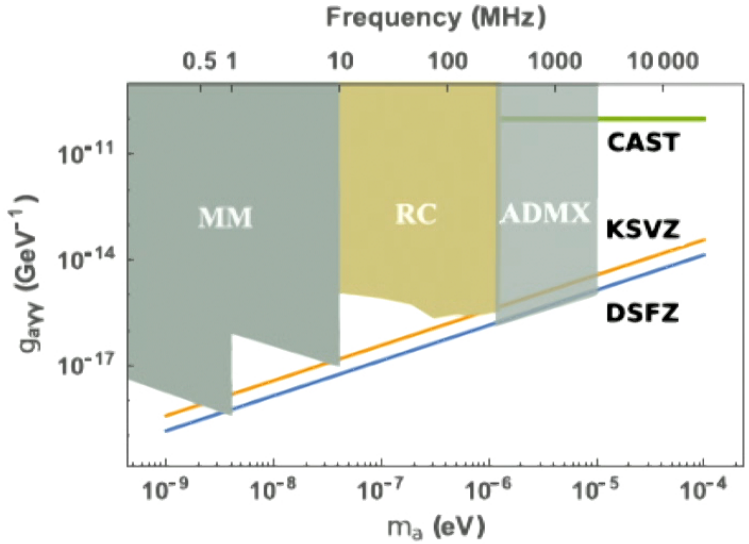

FIG. 6. Predicted axion-photon coupling exclusion limits for the reentrant cavity designs, using the assumptions outlined in the main text (RC). Current and future bounds from ADMX and CAST are shown for comparison, along with the predicted exclusion limits for magnetometer experiments (MM) presented in Ref. [21].

ORGAN

- High frequency haloscope at UWA (>15 GHz), known as the **ORGAN Experiment**
  Oscillating **R**esonant **G**roup **A**xio**N Experiment**
- Multi-stage project:
  →Narrow Search around 26-27 GHz (short term plan)
  → Wider scan at high frequency (15-50 GHz – long term goal)
- Lots of motivation for high frequency searches:
  →SMASH model
  →Claimed results in Josephson Junctions
  →**No one is looking there with a haloscope**

Group introduces six new particles to standard model to solve five enduring problems

February 20, 2017 by Bob Yirka report

Feb 2017

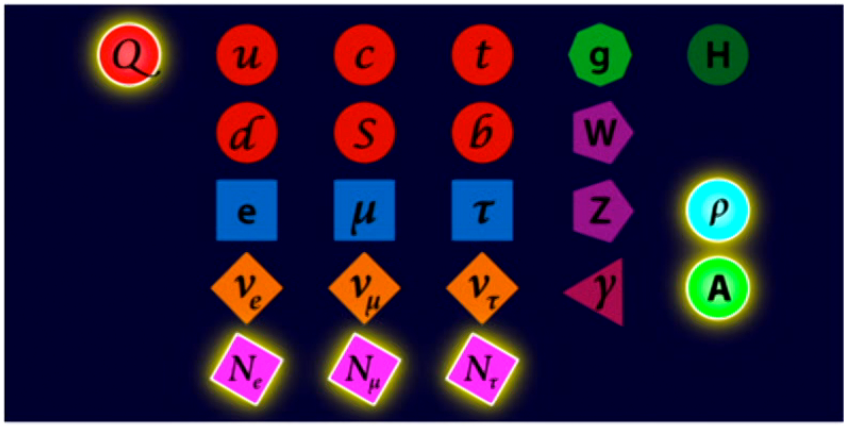

Standard Model-Axion-Seesaw-Higgs Portal Inflation. Five problems of particle physics and cosmology solved in one stroke

Guillermo Ballesteros [1] , Javier Redondo [2, 3] , Andreas Ringwald [4] , Tamarit Carlos Details

1 IPHT - Institut de Physique Théorique - UMR CNRS 3681
2 Universidad Zaragosa [Zaragoza]
3 MPI-P - Max-Planck-Institut für Physik
4 DESY - Deutsches Elektronen-Synchrotron [Hamburg]

Abstract : We present a minimal extension of the Standard Model (SM) providing a consistent picture of particle physics from the electroweak scale to the Planck scale and of cosmology from inflation until today. Three right-handed neutrinos Ni, a new color triplet Q and a complex SM-singlet scalar σ, whose vacuum expectation value vσ~10^11 GeV breaks lepton number and a Peccei-Quinn symmetry simultaneously, are added to the SM. At low energies, the model reduces to the SM, augmented by seesaw generated neutrino masses and mixing, plus the axion. The latter solves the strong CP problem and accounts for the cold dark matter in the Universe. The inflaton is comprised by a mixture of σ and the SM Higgs and reheating of the Universe after inflation proceeds via the Higgs portal. Baryogenesis occurs via thermal leptogenesis. Thus, five fundamental problems of particle physics and cosmology are solved at one stroke in this unified Standard Model - Axion - Seesaw - Higgs portal inflation (SMASH) model. It can be probed decisively by upcoming cosmic microwave background and axion dark matter experiments.

Signal strength

- Power from the cavity is

$$P = 4 \cdot 10^{-22}\ \mathrm{W} \left(\frac{V}{200\ \ell}\right) \left(\frac{B_0}{8\ \mathrm{Tesla}}\right)^2 C_{nl} \left(\frac{g_\gamma}{0.97}\right)^2 \cdot \left(\frac{\rho_\mathrm{a}}{0.5 \cdot 10^{-24}\ \mathrm{g/cm}^3}\right) \left(\frac{m_\mathrm{a}}{1\ \mathrm{GHz}}\right) \left(\frac{\min(Q_\mathrm{L}, Q_\mathrm{a})}{1 \times 10^5}\right)$$

- Where C_{nl} is form factor, ρ_a is the halo density, m_a the axion mass, and
- $Q_L \sim 70000(\mathrm{GHz}/f)^{2/3}$ (ASE); $Q_a \sim 10^6$ are quality factors
- $g_\gamma \sim 0.97$ (KSVZ); $g_\gamma \sim 0.36$ (DFSZ) are coupling strengths

ORGAN Pathfinder

- Cavity dimensions:
- ~1 cm radius
- ~5 cm length
- TM_{020} Mode frequency ~26.5 GHz
- First “path-finding run” complete
- Stationary frequency, single cavity
- Traditional HEMT amplification
- 4 K
- 7 T
- Commercial Vector Signal Analyzer
- Successful test of entire system, ready for tunable run
- Scale up sensitivity

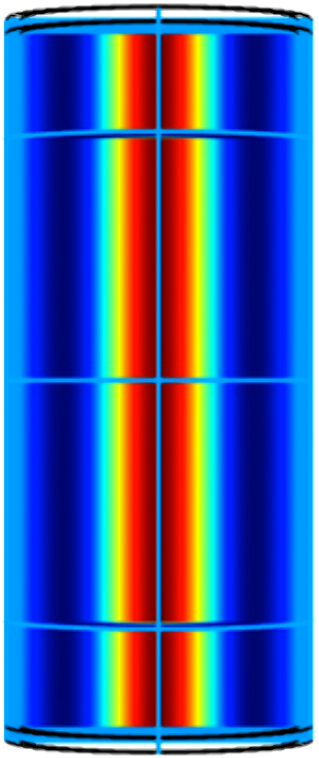

THE ORGAN CONCEPT

Brute force solution: Compensate for loss in volume at high frequencies by looking at multiple frequencies simultaneously (Like an Organ!).

Alternative to power-summing at one frequency and dealing with keeping all the cavities frequency-tuned / locked

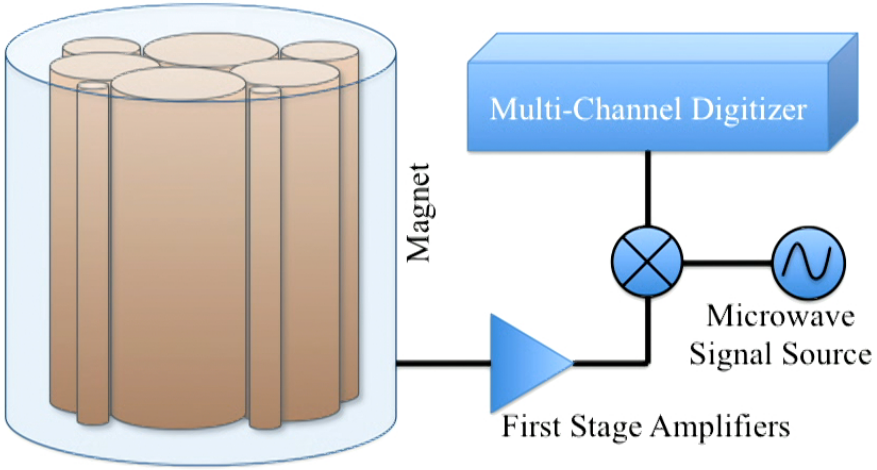

THE ORGAN CONCEPT

Brute force solution: Compensate for loss in volume at high frequencies by looking at multiple frequencies simultaneously (Like an Organ!).

Alternative to power-summing at one frequency and dealing with keeping all the cavities frequency-tuned / locked

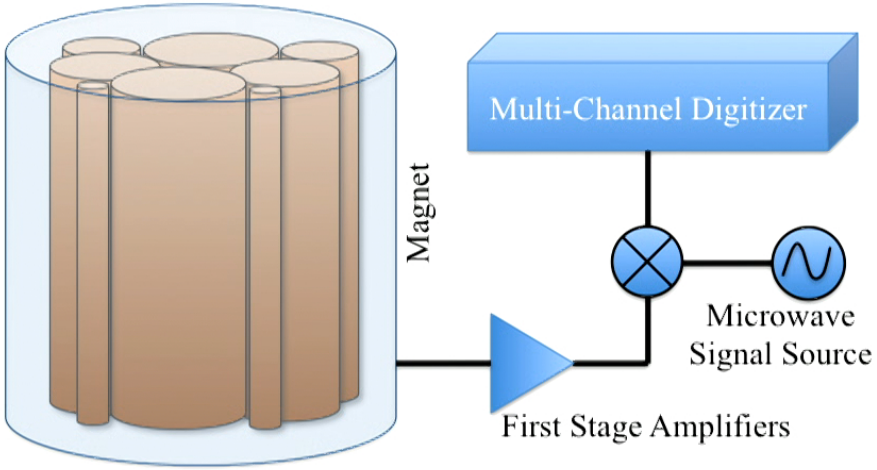

ORGAN

Oscillating **R**esonator **G**roup **A**xion co**N**vertor: Australian consortium
Project funded by the ARC CoE for Engineered Quantum Systems

-> ARC LIEF Application 14 Tesla Magnet (~ B^2) plus dedicated Dil Fridge for multiple year operation etc.

ORGAN

Oscillating **R**esonator **G**roup **A**xion co**N**vertor: Australian consortium
Project funded by the ARC CoE for Engineered Quantum Systems

-> ARC LIEF Application 14 Tesla Magnet (~ B^2) plus dedicated Dil Fridge for multiple year operation etc.

Oscillating **R**esonator **G**roup **A**xion co**N**vertor **P**athf**I**nder **P**roj**E**ct (ORGAN PIPE)

ORGAN

Oscillating **R**esonator **G**roup **A**xion co**N**vertor: Australian consortium
Project funded by the ARC CoE for Engineered Quantum Systems

-> ARC LIEF Application 14 Tesla Magnet (~ B^2) plus dedicated Dil Fridge for multiple year operation etc.

Oscillating **R**esonator **G**roup **A**xion co**N**vertor **P**athf**I**nder **P**roj**E**ct (ORGAN PIPE)

Start with 1 cavity…

1) Check Detection Claim
2) Show proof of concept at higher masses
3) Test novel noise reduction and signal enhancing techniques

ORGAN

Oscillating **R**esonator **G**roup **A**xion co**N**vertor: Australian consortium
Project funded by the ARC CoE for Engineered Quantum Systems

-> ARC LIEF Application 14 Tesla Magnet (~ B^2) plus dedicated Dil Fridge for multiple year operation etc.

Oscillating **R**esonator **G**roup **A**xion co**N**vertor **P**athf**I**nder **P**roj**E**ct (ORGAN PIPE)

Start with 1 cavity…

1) Check Detection Claim
2) Show proof of concept at higher masses
3) Test novel noise reduction and signal enhancing techniques

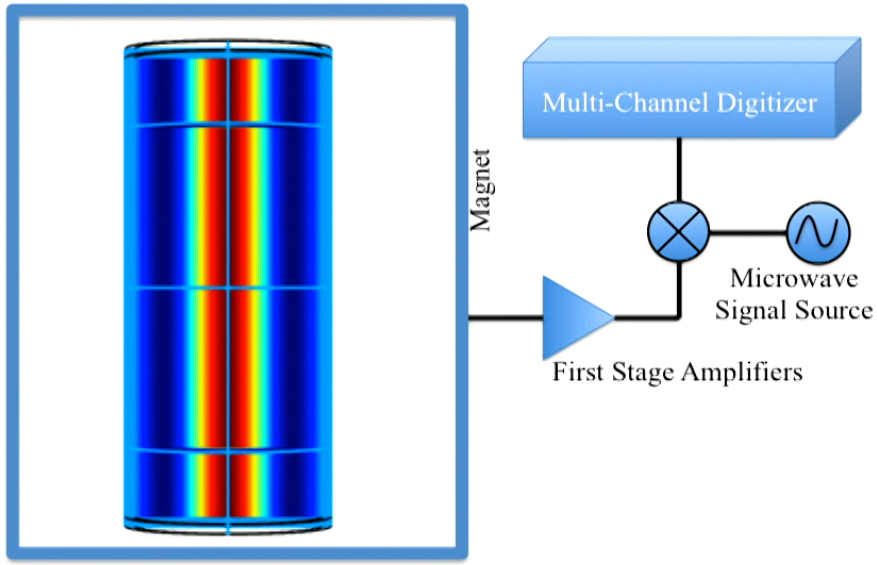

ORGAN Pathfinder

Mode	C	V (cm^3)	G
TM010	0.69	1.45	386.5
TM020	0.13	7.783	744.6
TM030	0.053	18.87	1244.3

- Mode crowding gets worse, but there is a trade off to consider
- More on higher order modes later

First run complete

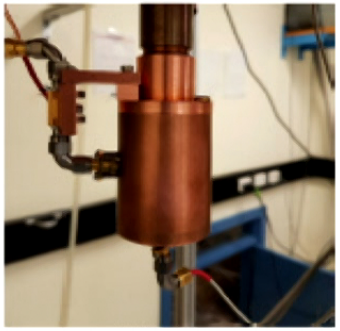

TM_{020} mode

sampling frequency of the digitizer is 1GHz, the 26.54GHz

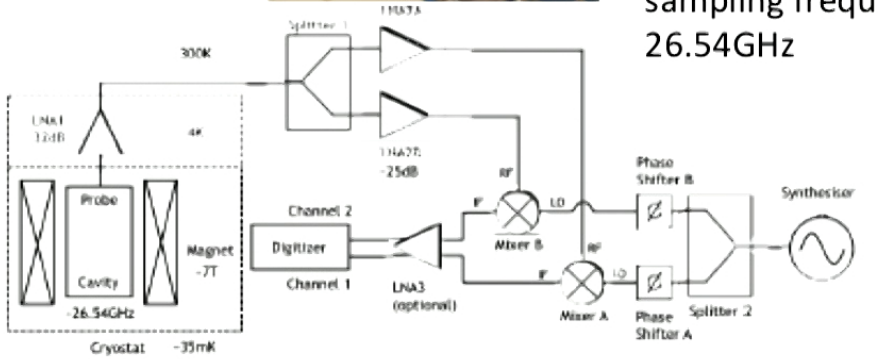

Figure 3.1: **ORGAN configuration.** The copper microwave cavity being used in the initial experiment (top) and a current ORGAN hardware diagram (bottom).

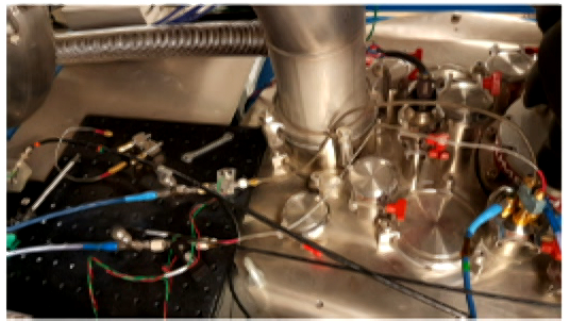

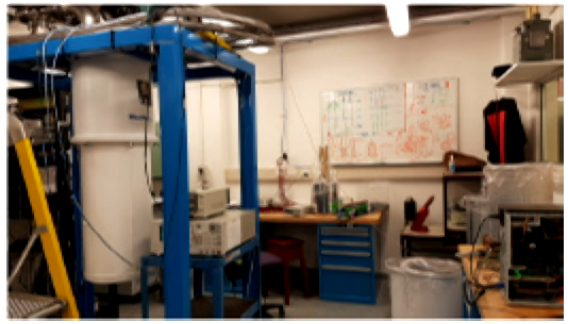

First run complete

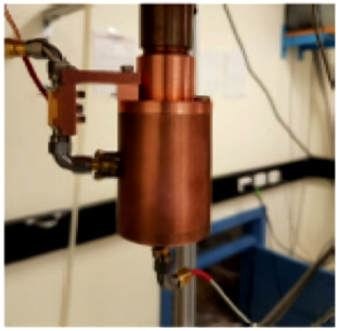

TM_{020} mode

sampling frequency of the digitizer is 1GHz, the 26.54GHz

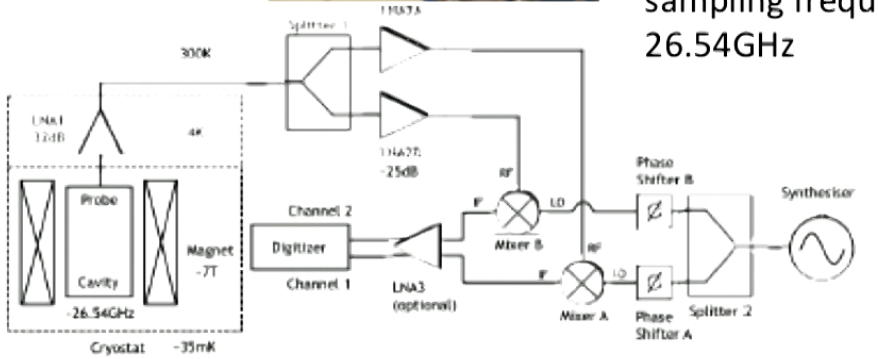

Figure 3.1: **ORGAN configuration.** The copper microwave cavity being used in the initial experiment (top) and a current ORGAN hardware diagram (bottom).

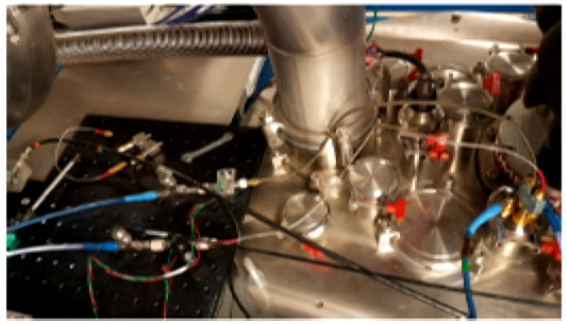

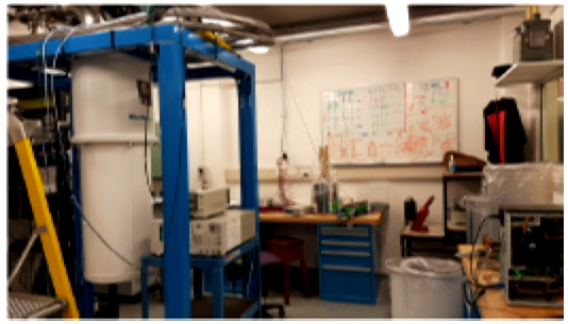

Magnet & readout

ARC CENTRE OF EXCELLENCE FOR
ENGINEERED QUANTUM SYSTEMS

7 T Magnet (10 cm bore)

LNF Cryo HEMTS
~10 K Noise temp (15 – 29 GHz)
Need to develop JPA's at high frequency

2-channel digitizer
Keysight U5303A

ORGAN

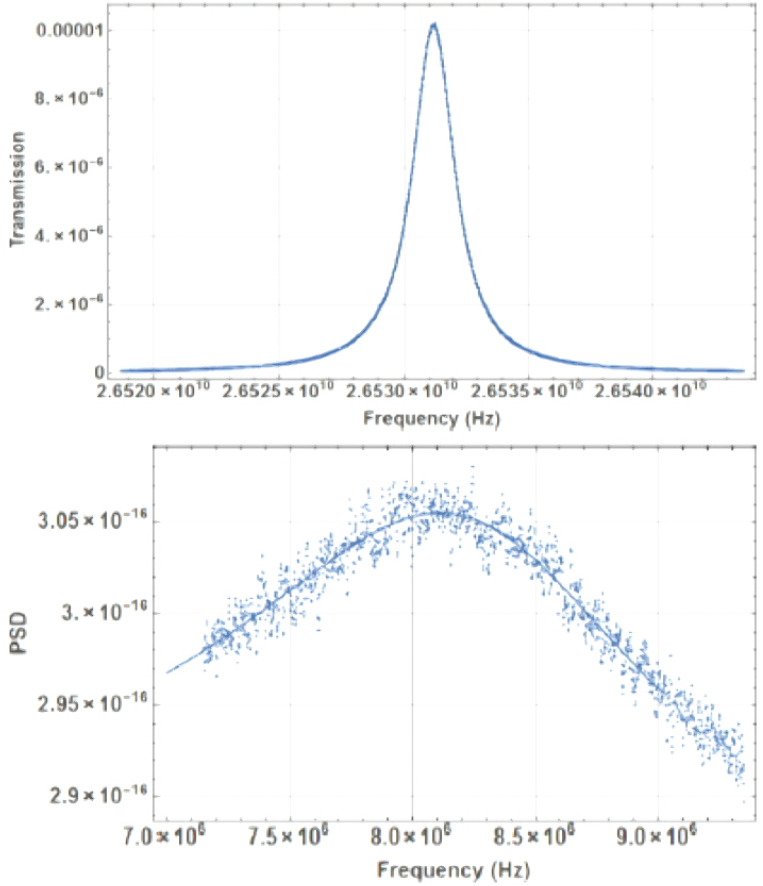
0.00001
8. × 10⁻⁶
6. × 10⁻⁶
4. × 10⁻⁶
2. × 10⁻⁶
0
Transmission
2.6520 × 10¹⁰
2.6525 × 10¹⁰
2.6530 × 10¹⁰
2.6535 × 10¹⁰
2.6540 × 10¹⁰
Frequency (Hz)
3.05 × 10⁻¹⁶
3. × 10⁻¹⁶
2.95 × 10⁻¹⁶
2.9 × 10⁻¹⁶
PSD
7.0 × 10⁶
7.5 × 10⁶
8.0 × 10⁶
8.5 × 10⁶
9.0 × 10⁶
Frequency (Hz)

ORGAN Pathfinder

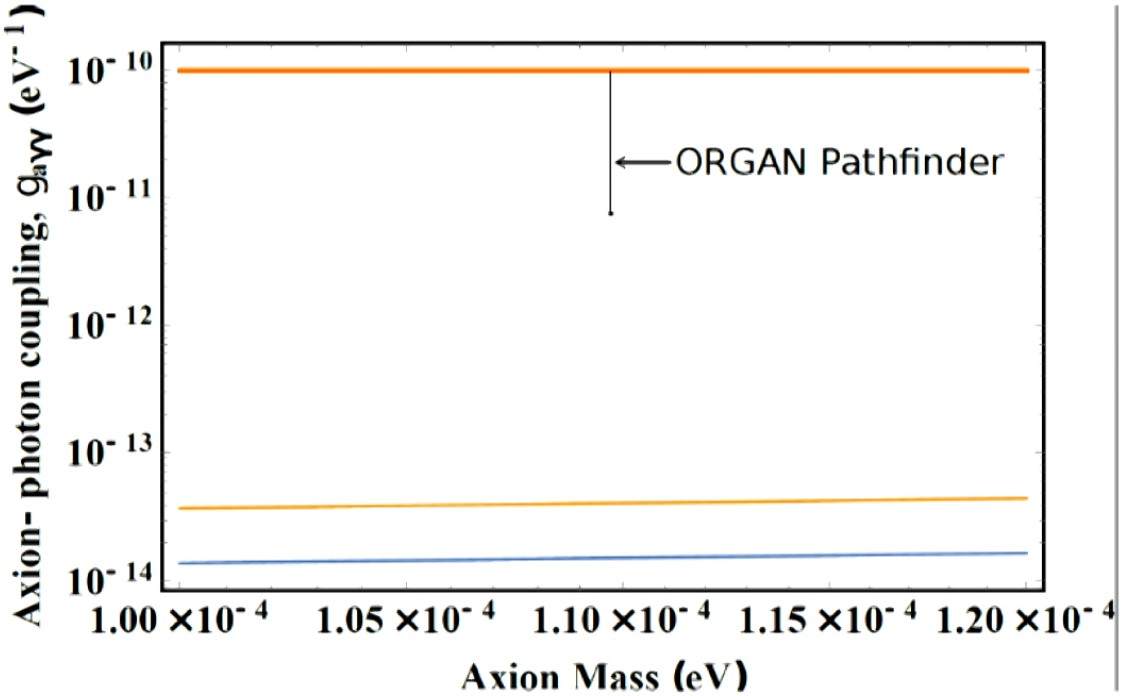

- Set and forget
- Very narrow limits (no tuning to cavity)

Dielectric Disks

- Two dielectric short cylinders, or disks located together
- Gap between them increases, mode tunes
- "Supermodes", symmetric and anti-symmetric

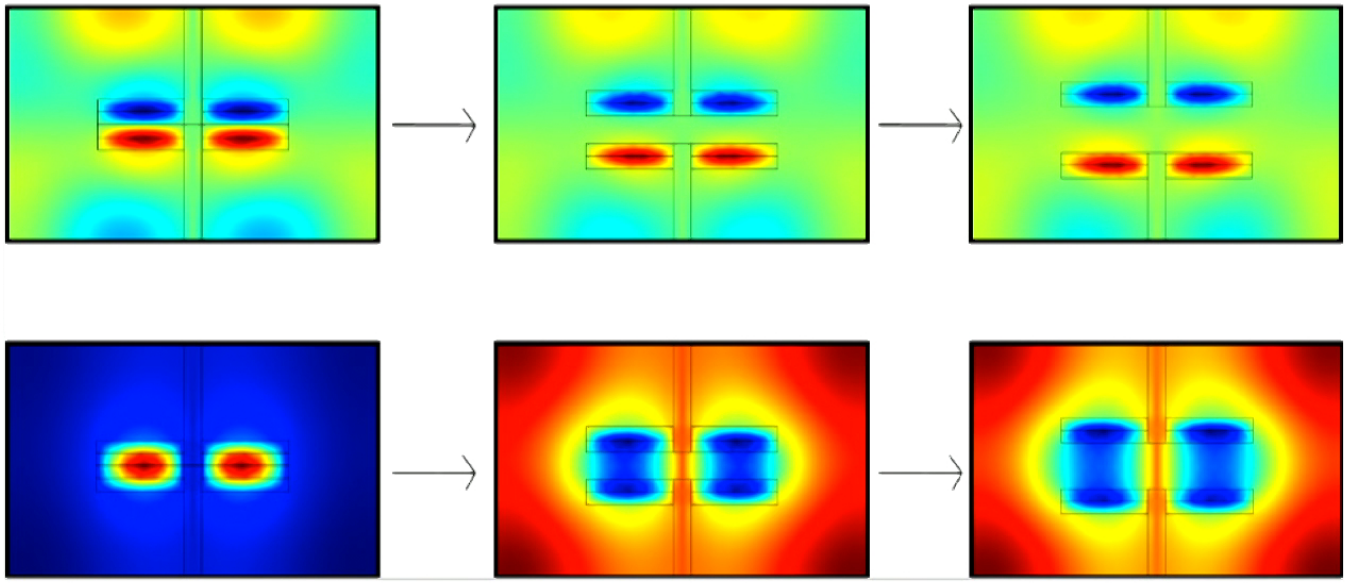

Haloscope Resonator Design

THE UNIVERSITY OF WESTERN AUSTRALIA

- Scan rate of a haloscope

$$\frac{df}{dt} \propto \frac{1}{SNR_{goal}^2} \frac{g_{a\gamma\gamma}^4 B^4 C^2 V^2 \rho_a^2 Q_L Q_a}{m_a^2 (k_B T_n)^2}$$

- We use $C^2\ V^2\ G$ as a figure of merit for resonator
- G is geometry factor, proportional to Q

ORGAN Pathfinder

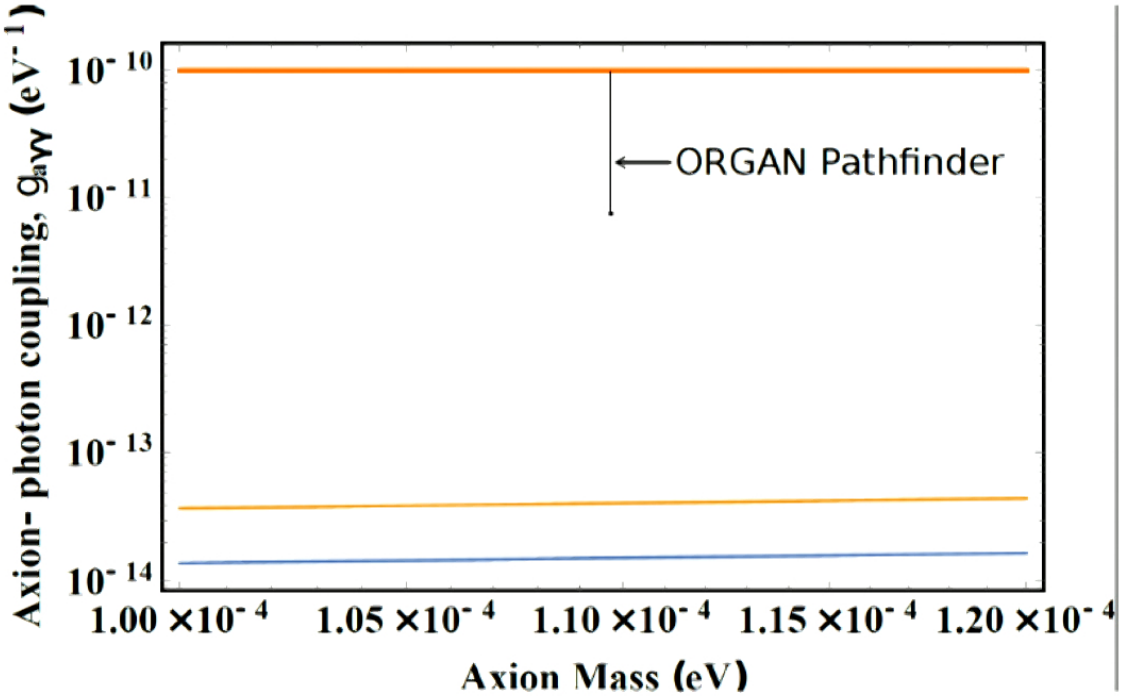

- Set and forget
- Very narrow limits (no tuning to cavity)

Lief Grant to gain infrastructure necessary to test well known Axion models

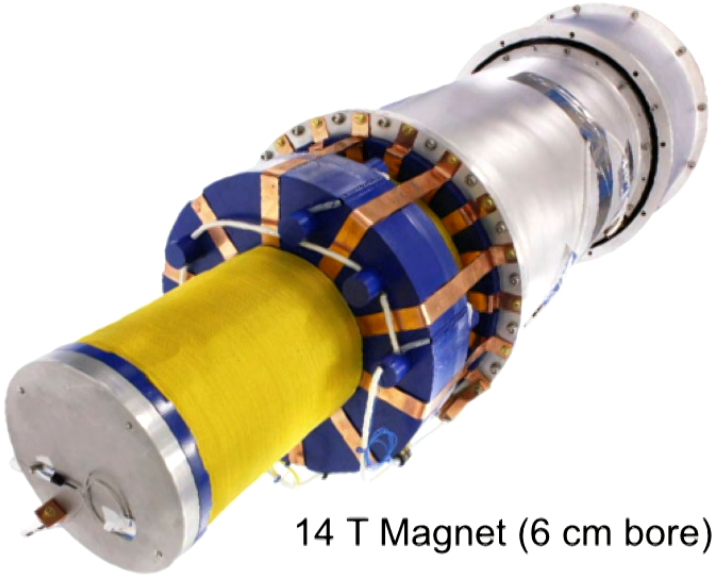

14 T Magnet (6 cm bore)

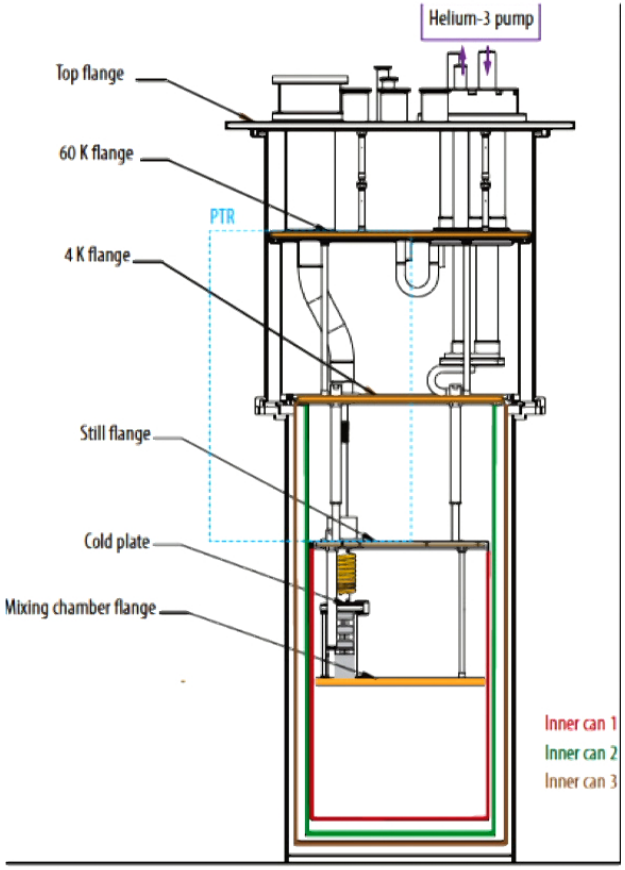

Dedicated dilution Fridge

Sensitivity Projections

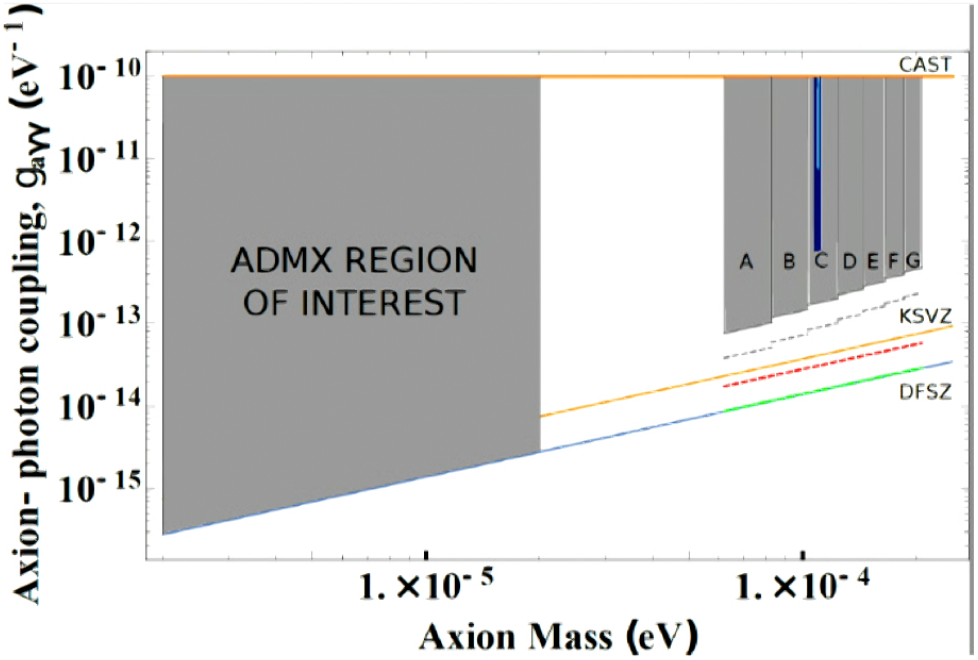

- Narrow aqua bar is pathfinder result
- Wider navy bar is 2018 run, 26-27 GHz
- A→G are the 2018-2025 runs, with 14 T magnet and SQL Amps
- Dashed limits depend on new technology and R&D ie Squeezed vacuum to beat SQL, upgrade magnet again to 28 T

Dielectric Resonators

- Dielectric resonators have been proposed before
- Boost in axion form factor with careful placement

$$\mathrm{C} = \frac{\left| \int dV_c \vec{E}_c \cdot \vec{\hat{z}} \right|^2}{V \int dV_c \epsilon_r \mid E_c \mid^2}.$$

- Some proposals and experiments, ie MADMAX, Electric Tiger
- Two schemes proposed – Dielectric Disks and Rings
- Tuning mechanisms naturally included in both

Dielectric Disks

- Two dielectric short cylinders, or disks located together
- Gap between them increases, mode tunes
- "Supermodes", symmetric and anti-symmetric

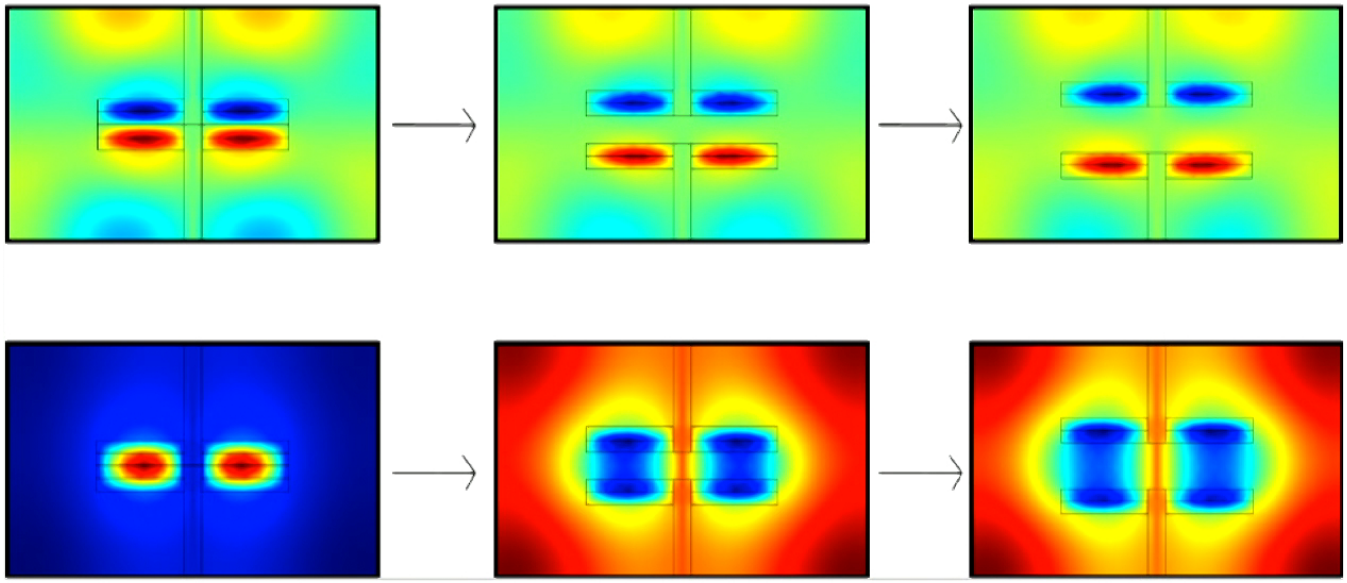

Dielectric Disks

- Decided to try other numbers of disks
- Nothing appears to be gained
- G may go down due to proximity of disks to cavity walls

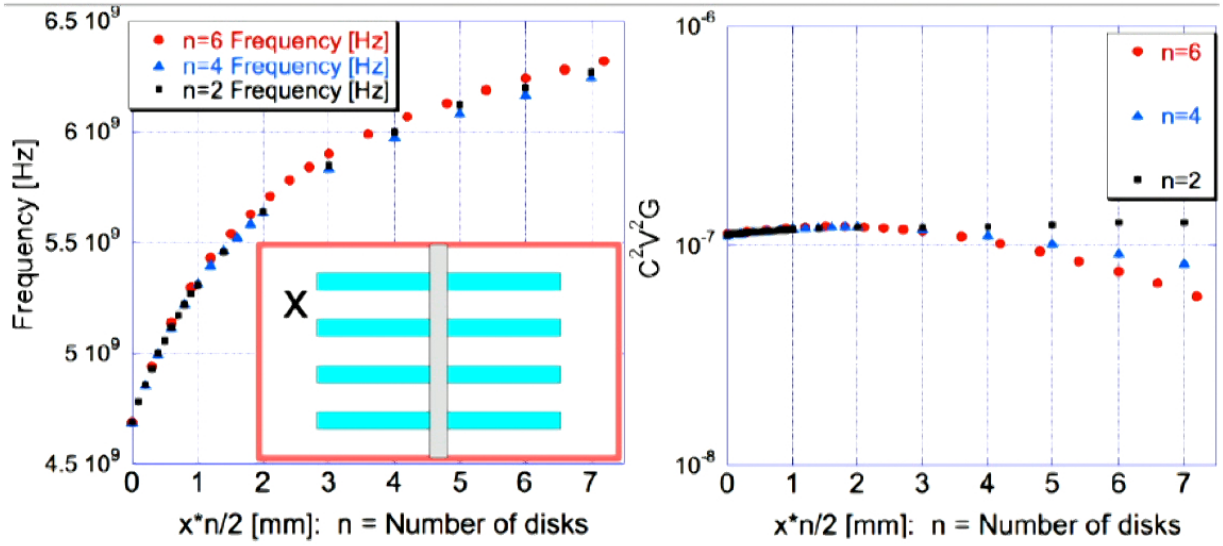

Further Work Since Jan 2017

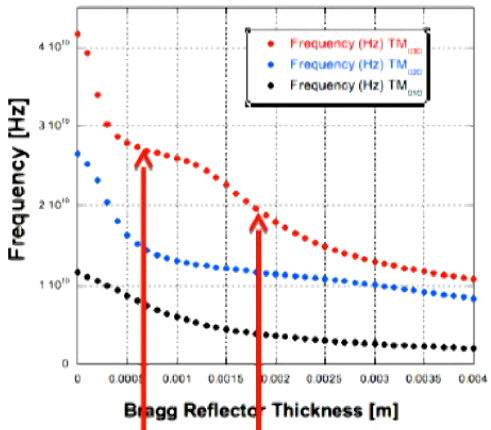

Bragg Condition

Braxion Condition

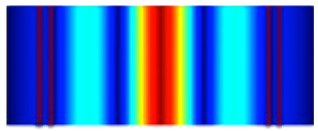

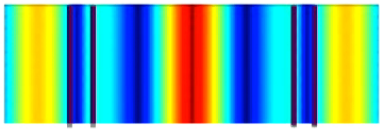

Bragg Condition

Braxion Condition

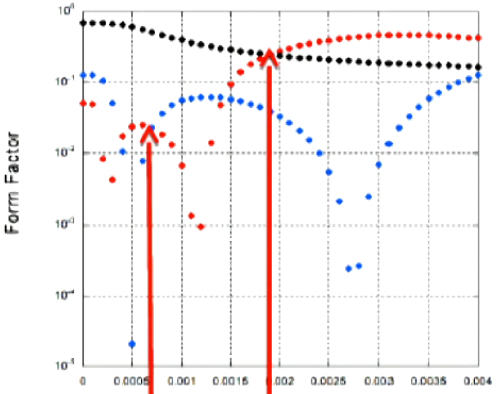

Bragg

Braxion

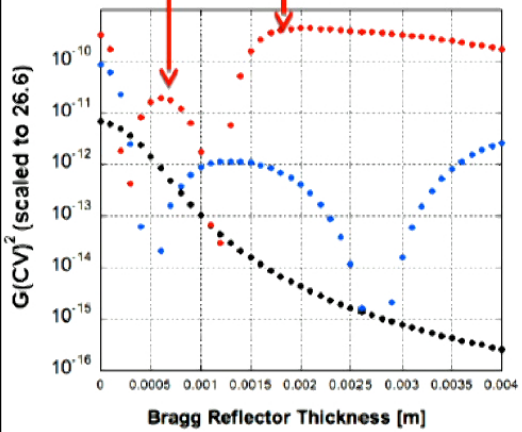

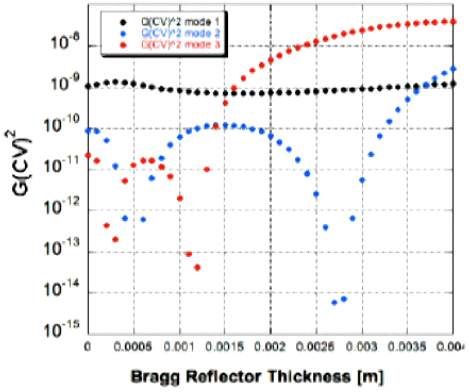

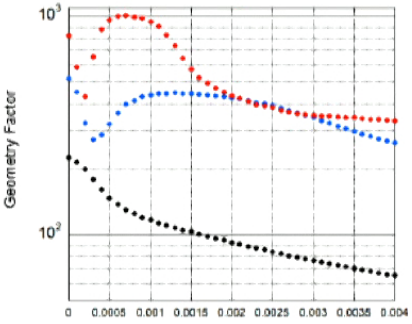

Axion-Bragg Resonator

- We can tune this structure, similar to the disk structure
- Axial "supermodes"
- TM030 and TM031 modes

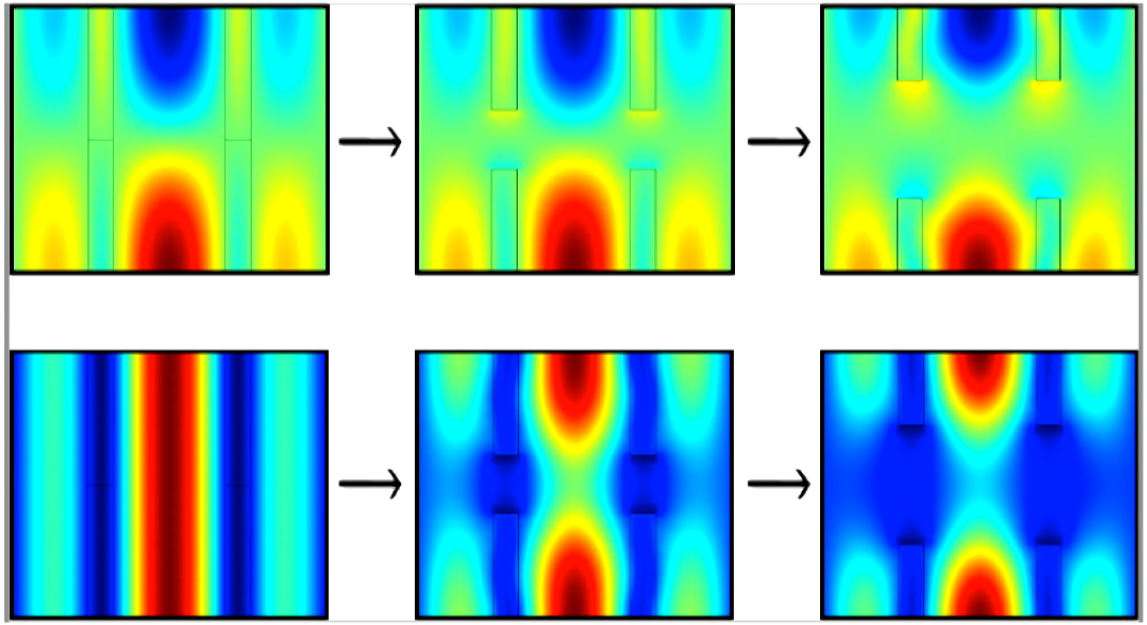

Axion-Bragg Resonator

THE UNIVERSITY OF WESTERN AUSTRALIA

•When these conditions are met we get the following field structure

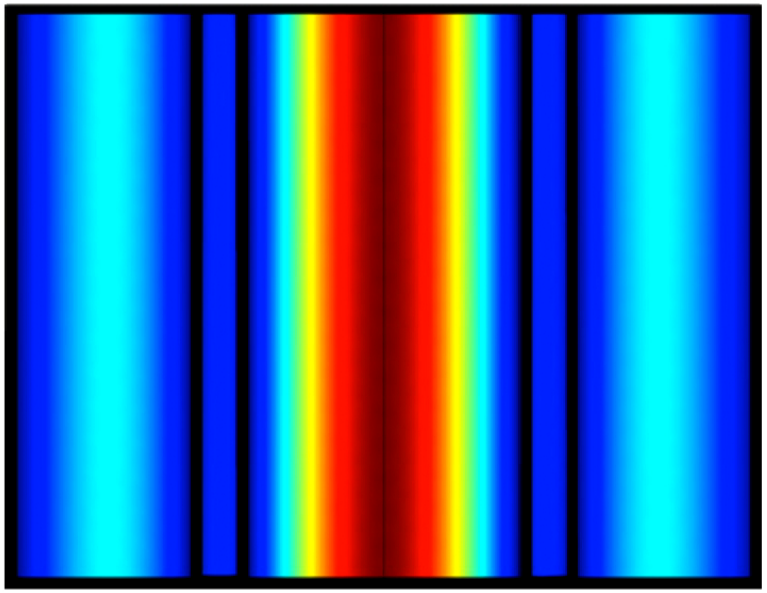

•Finite element simulations → Form factor ~0.45, improved from 0.053

Sensitivity comparison

Axion-Bragg resonator →

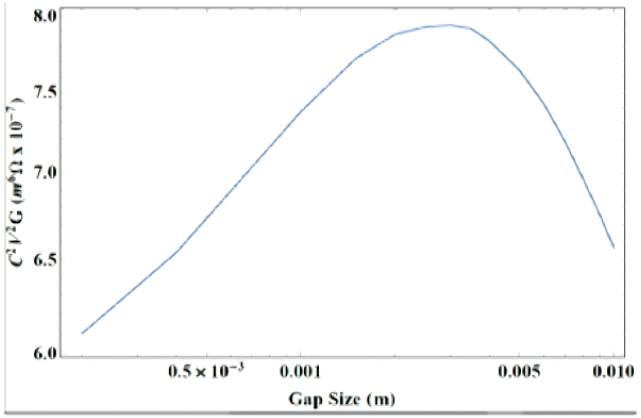

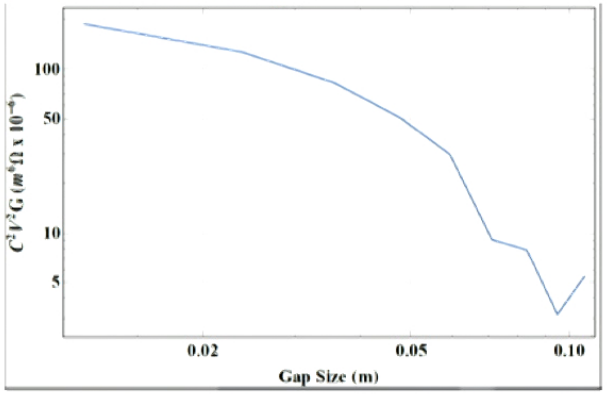

← Disk tuning resonator

Tuning rod→